LANDSCAPE AND BIOTIC EVOLUTION OF THE KOCHKOR BASIN, KYRGYZSTAN

by

WIN NADIA FRANCIS MCLAUGHLIN

A DISSERTATION

Presented to the Department of Earth Sciences
and the Graduate School of the University of Oregon
in partial fulfillment of the requirements
for the degree of
Doctor of Philosophy

June 2018

DISSERTATION APPROVAL PAGE

Student: Win Nadia Francis McLaughlin

Title: Landscape and Biotic Evolution of the Kochkor Basin, Kyrgyzstan

This dissertation has been accepted and approved in partial fulfillment of the requirements for the Doctor of Philosophy degree in the Department of Earth Sciences by:

Samantha Hopkins	Chairperson
Edward Davis	Core Member
Stephen Frost	Core Member
Ray Weldon	Core Member
Stephen Dueppen	Institutional Representative

and

Sara D. Hodges	Interim Vice Provost and Dean of the Graduate School

Original approval signatures are on file with the University of Oregon Graduate School.

Degree awarded June 2018

DISSERTATION ABSTRACT

Win Nadia Francis McLaughlin

Doctor of Philosophy

Department of Earth Sciences

June 2018

Title: Landscape and Biotic Evolution of the Kochkor Basin, Kyrgyzstan

Kyrgyzstan is the single most seismically active country in the world. Accessing the past, and therefore future hazard of faults, necessitates a high-resolution understanding of the timing of different geologic events. With no radiometrically datable rocks from the Neogene of Kyrgyzstan, I herein present the first work formally describing Neogene vertebrate faunas from the Kochkor Basin of Kyrgyzstan. I utilize a combination of biostratigraphy and magnetostratigraphy to constrain the timing of when the vertebrate assemblages were emplaced, and have dated the three bone beds to all fall in the latest Miocene, spanning 9-5 million years ago. All four bone beds represent mass death assemblages, inferred to be from drought-caused mortality. The timing of the deposits corresponds to uplift in the Pamirs, Himalayan, and greater Tibetan Plateau, which would have blocked the Indian monsoon from reaching Central Asia, forever altering the climate and biota of the region. This change is reflected in the shifting mammals faunas, as evidenced by the novel rhinocerotid I describe in a phylogeographic context.

CURRICULUM VITAE

NAME OF AUTHOR: Win Nadia Francis McLaughlin

GRADUATE AND UNDERGRADUATE SCHOOLS ATTENDED:

University of Oregon, Eugene
University of the Pacific, Stockton, California

DEGREES AWARDED:

Doctor of Philosophy, Earth Sciences, 2018, University of Oregon
Master of Science, Geology, 2012, University of Oregon
Bachelor of Science, Environmental Science, 2010, University of the Pacific

AREAS OF SPECIAL INTEREST:

Vertebrate Paleontology
Neotectonics
Field Geology
Biogeography

PROFESSIONAL EXPERIENCE:

Instructor, University of Oregon, 2016-2017

Teaching Assistant, University of Oregon, 2012-2018

Condon Collections Curator, Museum of Natural and Cultural History, University of Oregon, 2012-2017

English Language Instructor, American Corners, U.S. Embassy Bishkek, Kyrgyzstan, February-October 2015

Osteological Consultant, SWCA Environmental Consultants, July-August 2012

GRANTS, AWARDS, AND HONORS:

Jackson Travel Grant, Society of Vertebrate Paleontology, 2017

Mountain Research Grant, American Alpine Club, 2017

Student Research Award, Geological Society of America, 2016

Ewart Baldwin Scholarship, University of Oregon, 2001, 2012, 2014, 2016

Best Student Proposal, Paleontological Society, 2015

Student Researcher Grant, Fulbright, 2014

1st in the 3-Minute Thesis, University of Oregon, 2014

Condon Scholarship, University of Oregon, 2014

Student Research Grant, Society of Sedimentary Geology, 2014

Welles Fund Travel and Research Grant, University of California Berkeley, 2013

Student Travel Grant, Geological Society of America, 2013

Theodore Roosevelt Grant, American Museum of Natural History, 2013

Student Research Grant, Department of Geological Sciences, UO, 2013

Research Grant, Evolving Earth, 2012

PUBLICATIONS:

McLaughlin, W.N.F., S.S.B. Hopkins, and M.D. Schmitz. 2016. A new Late Hemingfordian vertebrate fauna from Hawk Rim, Oregon, with implications for biostratigraphy and geochronology. Journal of Vertebrate Paleontology, 35(5); e1201095.

ACKNOWLEDGMENTS

I wish to express sincere appreciation to my adviser Samantha Hopkins and to Ray Weldon for becoming my bonus adviser. Thanks is also needed for all the rest of my committee for their advice, insight, and support throughout my graduate school education. Kanatbek Abdrakhmatov, my Kyrgyz collaborator, for both scientific advice and facilitating nearly all the fieldwork presented on herein. Thank you to all the collections managers who provided me with access to comparative specimens and great scientific discussions, such as P. Holroyd at the UCMP, Chris Conroy at the UCMVZ, Amanda Millhouse at the NMNH, Jan Ove R. Ebbestad at the Uppsala Universitat Museum of Evolution, and Judy Galkin at the AMNH. Pat Ward prepared the rhino skull and jaws featured in Chapter 4 and the juvenile *Hipparion* mandible in Chapter 2, and without his painstaking artistry reconstructing the fossils, much of this work would have been impossible. Liz White illustrated the rhinoceros in a beautiful reconstruction, and helped facilitate all opportunities thus far to display Kyrgyz mammal fossils to the public. A huge "thank you" is needed to all of my past and current lab mates for the support and scientific discussions, including John Orcutt, Meaghan Wetherell, John Jacisin, Kristen MacKenzie, Dana Reuter, Genevieve Perdue, Paul Barrett, Nick Famoso, Leonard Finkelstein, Kellum Tate Jones, Holley Flora. Thank you to the students whom I have had the privilege of helping advise, and especially for all of the too many hours you have spent gluing broken Kyrgyz fossils back together or stripping the flesh from roadkill, including Márti May, Selina Robson, Eva Bierdron, Caitlyn Boatman, Julien Royer, Adi Chainey, Rafael Newman, Dylan Carlini, Holley Flora. My family and friends are also deserving of thanks, especially my parents who encouraged me to pick up dead birds and poke dead things on the beach. A ginormous thank you to all the people who have assisted me in fieldwork including Meaghan Wetherell, Ryan Seward, Zach Buehler, Brian Meyers, Michael Elizabeth, Kyle Haggart, Azat Moldobaev, Kyle Olsen, Rebecca Cramerus, Win Francis, Alana Francis, Ben Alldritt, Dylan Colón. Thank you to Azis Kubanychbek Uulu and Nazgul Ibraimova for help locating sites, and translation, as well as Elin Irgistseva and David Zakharov for translation. Thanks (I think) to Falling Sky, for opening a brewery across from my office and providing the writing and editing "fuel" needed to finish. The investigation was supported in part by a Fulbright Student Research Grant to the Kyrgyz Republic, a Sedimentary Geology Student Research Grant, the Paleontological Society Best Student Research Proposal, and significant funding from the Department of Earth Sciences at University of Oregon.

To Killian, who is just a cat, and that’s all he has to be.

TABLE OF CONTENTS

Chapter Page

Chapter Page

LIST OF FIGURES

CHAPTER IV

A NEW CHILOTHERE (MAMMALIA, RHINOCEROTIDAE) FROM THE NEOGENE OF KYRGYZSTAN, WITH IMPLICATIONS FOR PHYLOGENY AND BIOGEOGRAPHY OF THE RHINOCEROTID FAMILY

Introduction

While today herd behavior in rhinoceroses is limited, rhinoceros are presumed to exhibit herd behavior far back into the fossil record (Prothero, 2005, Milhbachler, 2005). Modern white rhinoceros (*Ceratotherium simum*) travel in mixed sex herds of up to 14 individuals (Shrader & Owen-Smith, 2002), while modern Indian rhinoceros (*Rhinoceros unicornis*) form female herds and sub-adult male herds (Laurie, 1982), although some historical accounts suggests most modern species were more gregarious before crippling population declines (Hutchins & Kreger, 2006). Fossil rhinocerotids are conclusively shown to travel in even larger herds, thanks to catastrophic mass death assemblages such as the *Teleoceras* herds of Ash Fall Fossil Beds National Monument (Prothero, 2005). While behavior can be hard to establish in the fossil record, the overabundance of rhinocerotids in all Kyrgyz bone beds examined in this study at least suggests that these large-bodied ungulates were both one of the more common organisms and were likely traveling in large groups. Additionally, rhinoceros' material comes from a wide age range of individuals, and tusks suggest the presence of both male and females, further indicating the presence of some sort of social structure.

The Kyrgyz rhinocerotid material is produced from two Neogene formations, the Chu and Shamsi groups, spanning the latest Miocene into the Pliocene (Figure 39). Both

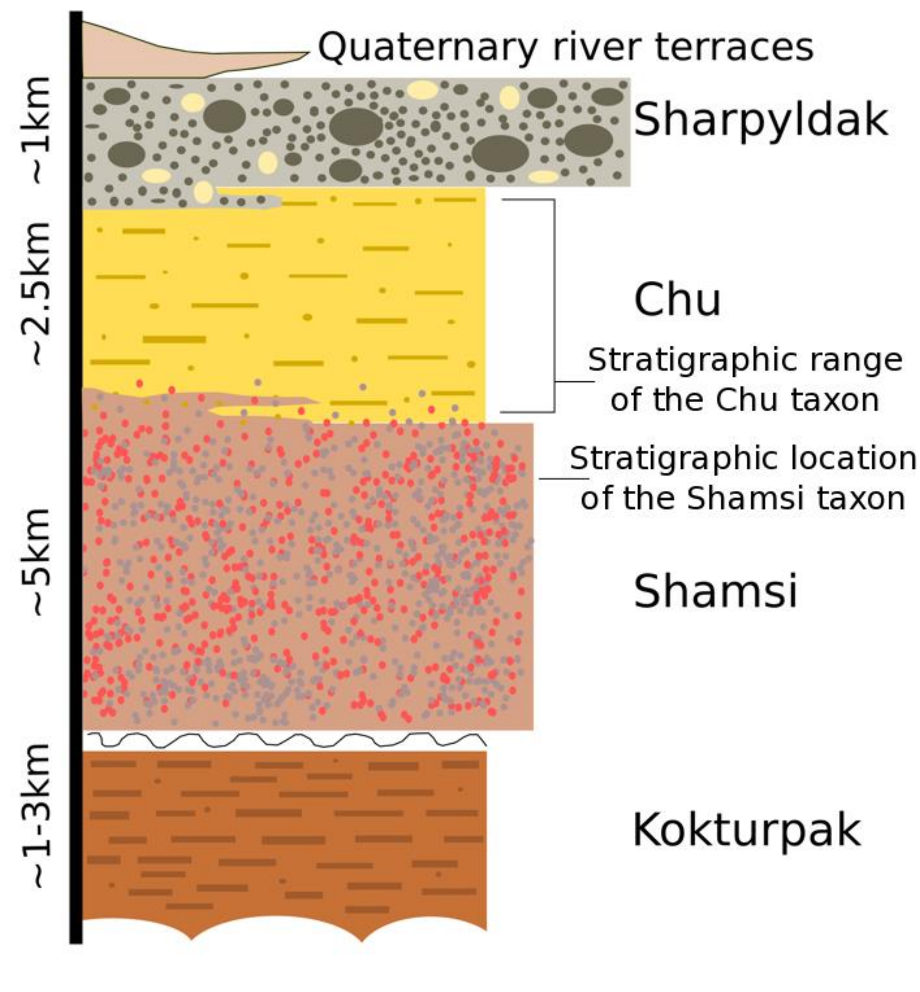

Figure 39: Composite stratigraphic column of Neogene sediments in the Kochkor Basin, Kyrgyzstan, showing the stratigraphic ranges of rhinocerotid fossils. The Kokturpak contains one dated basalt, placing the formation across the Eocene. The Shamsi and Chu formations are syntectonic, and generally finning upwards with a gradational contact. Capping the Neogene section is the Sharpyldak, a thick conglomerate presumed to be Pleistocene in origin. Rhinoceros included in this study span the upper Shamsi and throughout the Chu, although only the Shamsi rhinocerotid is described in detail.

formations are syntectonic basin filling sequences, primarily composed of fluvial and alluvial sediments, with a general fining upwards. Regional geologic and paleoclimatic data suggests Central Asia underwent uplift and climatic shifts in the late Miocene-Pleistocene to reach the semi-arid steppe ecosystems of today. Climate became both drier and colder as the monsoon effect ceased to reach Central Asia (Wang et al., 2006). As topography and climate remodeled, corresponding faunal turnovers resulted in the evolution of both ice age and modern cold-adapted faunas (Deng et al., 2011).

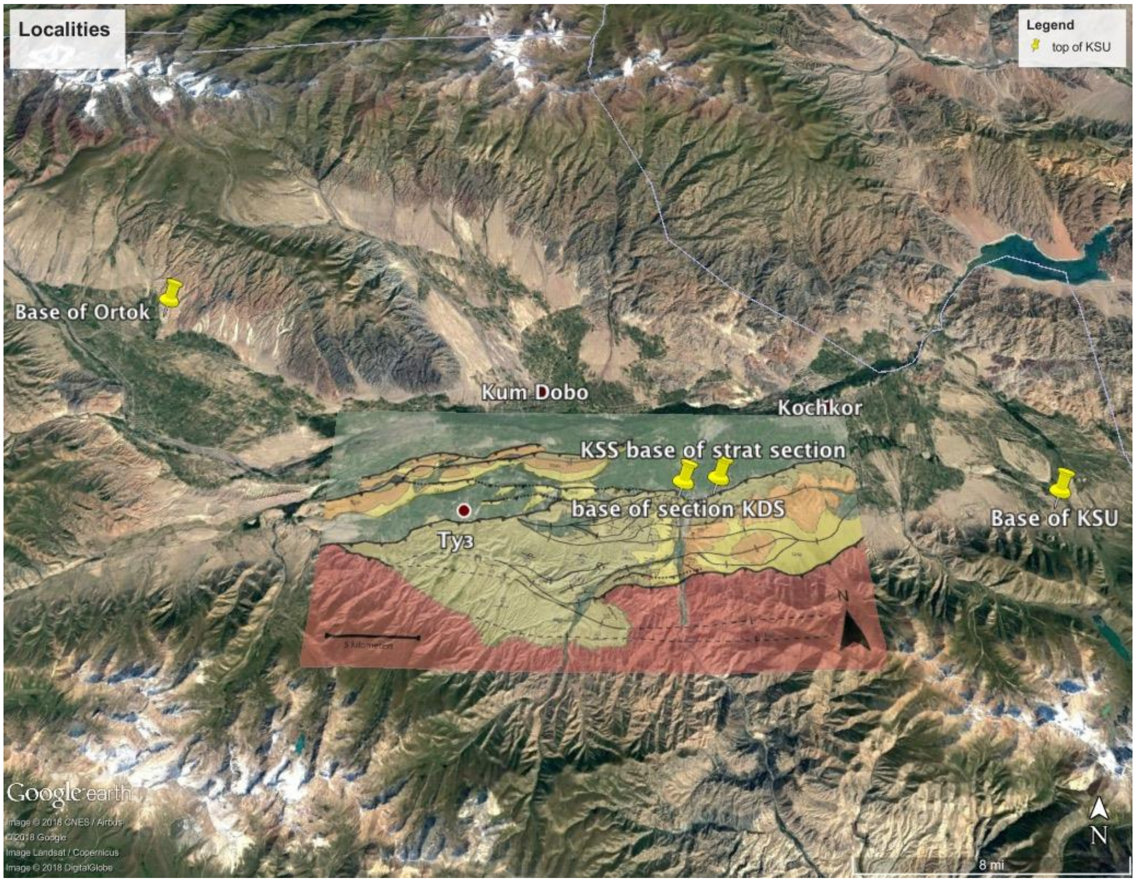

Figure 40: Google Earth imagery (accessed January 2018) of the Kochkor Basin Kyrgyzstan, with an overlay of some geologic mapping (Paulson, 2013). Pin represent bone bed localities, all of which produce rhinocerotid material. The novel taxon described in this work is from the KSU section on the far east of the map. Rhinocerotid material is produced throughout the section and is not confined to the bone beds, although all of the specimens included in coding characters for the phylogenetic analysis are from the four labeled bone beds.

Located in the heart of Central Asia (Figure 40), Kyrgyz fossil deposits therefore offer a unique opportunity to observe rhinoceros evolution over not only several million years, but at a key location for geographically and temporally understanding the paleobiogeography and phylogeny of this family (Figure 41). While the family evolved in

North America, previous authors suggest significant faunal interchange between North America and Eurasia, throughout the Cenozoic history of the family (Prothero, 2005, Lu, 2012). While this study concentrates on two species from Kyrgyzstan, the inclusion of North American Neogene taxa suggests strong phylogeographic connections between Asia and North America in the Miocene.

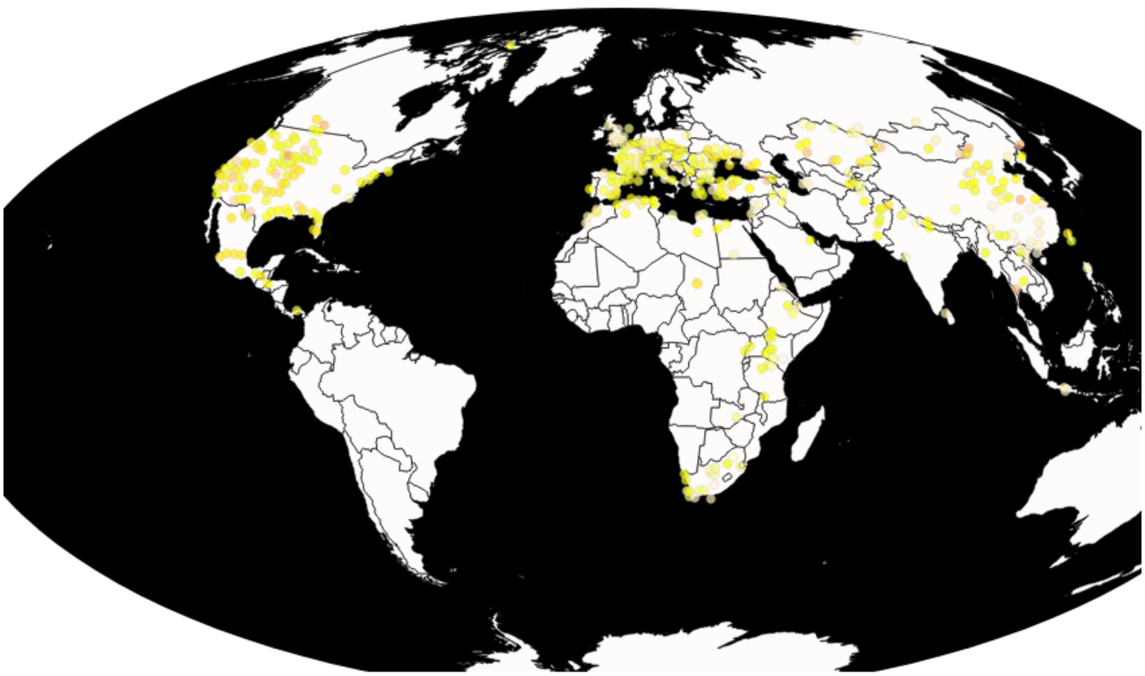

Figure 41: Distribution, both temporally and geographically, of Rhinocerotidae fossils. Data and graphic taken from the Paleobiology Database, search <Rhinocerotidae> on January 6th, 2018. Peach colors are Paleogene fossil localities publishing the occurrences of rhinocerotids, while the Neogene localities are shown in yellows. Rhinocerotids are first found in the Eocene of North America, but appear to have quickly spread to Asia, as evidenced my numerous Eocene localities in China. The PBDB search returns 2,347 localities with rhinocerotids, illustrating the wide-spread nature of this family throughout the Cenozoic.

Materials and Methods

Paleontology: The rhinoceros fossils described herein are all from a single bone bed outcrop, Vodka UO-4603, located along the southeastern margin of the Kochkor Basin, Kyrgyzstan (Figure 42). Locally, the larger drainage containing the fossil locality is called the Kara Suu valley, as the closest village draws the name (meaning “black water” in Kyrgyz) from the numerous springs along the fault scarp. South of the South Kochkor Fault trace, the sediment packages are Neogene sequences in turn underlying the over-thrust Mesozoic basement rocks.

Figure 42: Google Earth view of the Kara Suu Valley denoting where the stratigraphic section was measured as well as the location of the Vodka bone bed. Inset image is looking south, from just north of the bone bed. The fossil bearing stratum outcrops in the dry wash.

The locality was discovered in 2012 by E.S. Przhiyalgovskiy and E.V. Laurushina of the Geological Institute of the Russian Academy of Sciences, two structural geologists who were conducting geologic mapping of the area. Initial collection was limited to fragmentary material weathered into the dry wash below the cut bank exposing the fossiliferous stratum. In 2014, the outcrop was excavated by a field crew from the University of Oregon, producing most of the postcranial material. Again in 2015 the outcrop was quarried by a joint expedition from University of Oregon and the Kyrgyz Institute of Seismology, this time producing both the skull and complete mandibles (Figure 43).

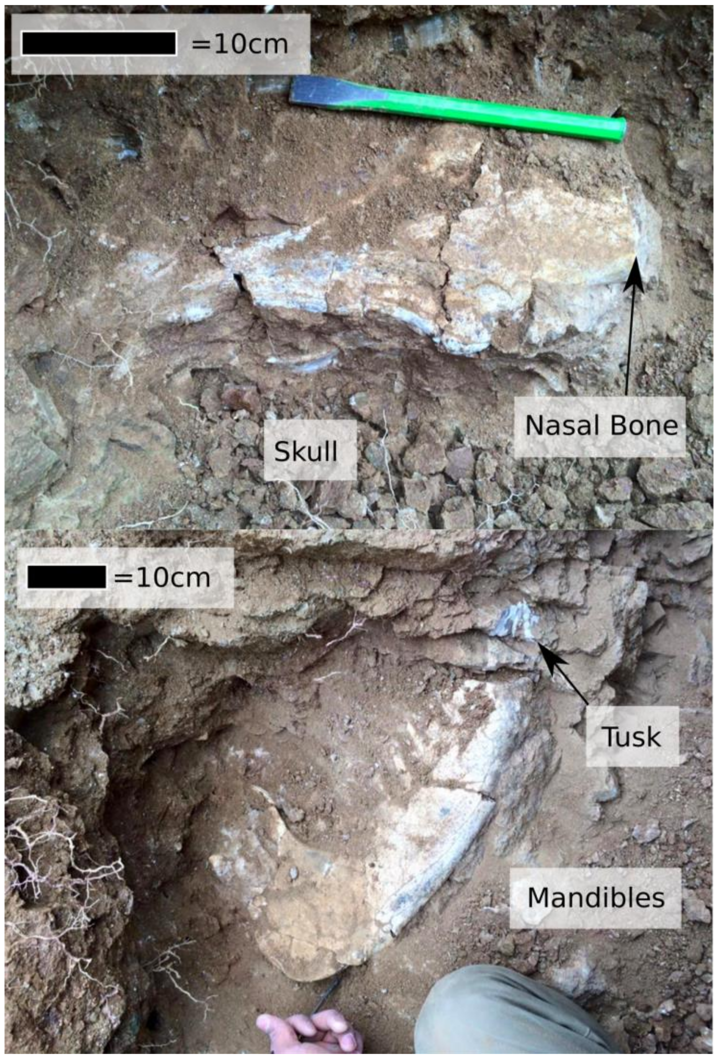

Figure 43: Top, dorsal view of the Vodka taxon skull in situ, after the projecting nasals had been removed (far right of image). Bottom, Left mandible exposed after the removal of the right mandible, in situ. Less than 1.5 meters separates the two specimens, and they lie at the same stratigraphic level.

A stratigraphic section and palaeomagnetic samples were also collected at the locality; however, stratigraphic and geochronologic placement will be discussed in another work (Chapter 3). Most of the exposure in the Kara Suu valley appears to belong to the Shamsi Group, and gradationally changes to the younger and finer grained Chu Group. This geologic assignment places the locality in the mid to late Miocene. The aforementioned work currently estimates the Vodka bone bed to be 8.6 Ma (although biostratigraphically it could range from 9.6-5.3 Ma).

The specimens were compared with the only previously attributed rhinocerotid species in Kyrgyzstan, *Chilotherium* cf. *chabereri* (Sotnikova, 1997), although the previous material is attributed to the presumably younger locality of Ortok, and is not reposited in an extant collection for comparison. Complicating comparisons is the high diversity of rhinocerotids in the late Miocene. Thus far, the Kyrgyz faunas share the most faunal similarities with the Hipparion faunas of China, which have the highest diversity of rhinocerotids in the Late Miocene (MN 9-12) over any other time period (Deng, 2006), with over two dozen species. In the Chinese to Mongolian Late Miocene, *Chilotherium wimani* is the dominant species (Deng, 2006).

Phylogenetic Analysis: I performed a cladistic analysis to evaluate the phylogenetic placement of the Kyrgyz rhinocerotid craniodental material. Taxa included in the analysis followed the published matrix of Pandolfi et al. (2015), which is based on characters developed in Lu (2013) and Antoine (2002, 2003, 2010). Pandolfi (2015) significantly expanded the number of included taxa, although narrowed the taxonomic breadth as compared to Antoine (2010). I include all taxa used in the Pandolfi (2015) analysis, as well as incorporate several novel taxa. I also recoded the basal North American rhinocerotid *Subhyracodon occidentalis*, as a check on coding the characters. This taxon is already included in the Pandolfi (2015) phylogeny, and my recoding serves to check my interpretation of characters as similar to the previously published matrix. I also used different, more complete, specimens to code the species than those used by Pandolfi (2015), with both a male and female skull from the NMNH. The basal North American rhinocerotid *Trigonias osborni* was retained as the outgroup in the study. New taxa added to the analysis included both rhinoceros taxa from Kyrgyz Neogene fossil deposits, three additional species of *Chilotherium*, and several more North American rhinocerotids, notably three species of *Aphelops* and two of *Teleoceras* from the Neogene. Previous work suggests significant dispersal events in the history of the family, yet little work addresses the timing and exact nature of these relationships (Prothero, 2005). We therefore included North American rhinocerotids, North American temporal contemporaries of the Kyrgyz rhinos with similar “barrel bodied” morphologies, as a test if the morphology in the overall body shape is derived from relatedness or convergence. New taxa (see SI T1 for full list of taxa and morphological sources) were primarily coded from museum-reposited specimens at University of Oregon, Uppsala University, and the Smithsonian National Museum of Natural History, although some morphological data, including all juvenile dentition except for the Chu rhino, were coded from the literature (also in Apendix K).

Characters were coded into Mesquite (http://mesquiteproject.org/), and the full character matrix is available in the Apendix L. Detailed descriptions of each character are also available in the Apendix L. Trees were generated using “Tree analysis using New Tecnology” (TNT) (Goloboff &Catalano, 2016) using a normal run, although other run types were tested and did not yield reduced numbers of trees or improved resolution. We completed 10,000 runs of the matrix, generating 5 most parsimonious trees using the entire character list of Pandolfi (2015), which is primarily taken from the character list of Lu (2013) and Antoine (2002). Characters were not weighted, but were designated as single vs. multistate, and ordered and non-ordered multistate. There were 53 ordered multistate characters, and an additional ten multistate, but not ordered, characters. Owing to poor resolution in some aspects of the tree, possibly derived from uninformative characters, we propose conducting future analyses with a pruned set of characters, as well as the future inclusion of postcranial characters.

Systematic Paleontology

Order PERISSODACTYLA Owen, 1848

FAMILY RHINOCEROTIDAE Owen, 1845

Tribe ACERATHERIINI Dollo, 1885

CHILOTHERIUM Ringström, 1924

CHILOTHERIUM sp. nov.

Holotype—UOMNH F-64557 skull, missing premaxillary bones and part of the maxillary bones.

Paratypes—UOMNH F-70507 mandible with m3-i2 both left and right, UOMNH F-64522 distal lateral metapodial, UOMNH F-64523 tibia, UOMNH F-64527 carpal, UOMNH F-64537 astragalus, UOMNH F-64552 distal humerus, UOMNH F-64555 radius, UOMNH F-64577 fibula, UOMNH F-70305 calcaneum, UOMNH F-70314 metapodial.

Referred material— UOMNCH-64514 distal radius, UOMNCH-64515 distal radius, UOMNCH-64554 bascranium, UOMNCH-64575 tibia.

Type locality—UO-4603 Vodka.

Diagnosis—Chilotherium sp. nov. is a medium sized, barrel-bodied rhinocerotid, but with more gracile limb proportions than other members of the genus. Like other members of the genus, it possesses a concave ventral surface in the mandibular symphysis, an anteroposterior widened symphysis, and two large lower tusks projecting laterally and formed from the i2. The nasal notch is broad, with horizontally projecting blunt-tipped nasals and lacking a nasal horn. The skull profile is slightly concave in the posterior portion of the skull. The posttympanic process and postglenoid process are in contact, but not fully fused into a pseudomeatus, although are separated ventrally, with the postglenoid process curving anteriorly. The teeth lack cementum, and the occlusal shape of the M3 is trapezoidal.

Description

Skull

The skull is largely complete (Figure 44), although lacking the premaxilla and much of the maxilla. Only the left and right M3 and partial left M2 are present for the upper dentition (See Figure 45). The nasals are widest posterior and narrow anteriorly, ending in a blunt tip. The ventral surface of the nasals is flat rather than vaulted. The anterior portion of the nasal bones is not notched and is fully sutured. The entire dorsal surface of the nasal bone and into the frontal bones is smooth, with no surface roughening, indicating a lack of any horns. The nasal septum is not ossified and the dorsal profile is slightly very slightly curved downwards, with the anterior portion of the nasals almost parallel to the plane of the upper dentition. This profile continues back into the unvaulted frontal bones, which are nearly flat in profile until extending dorsally into the parietals. The posterior-most portion of the nasal notch opening is broad and U-shaped, with the nasal notch relatively posterior, leaving a small distance from the posterior-most portion of the opening to the orbits. The nasal notch is dorsal to the M2, making the nasal notch set relatively posterior in the skull and the unattached portion of the nasals moderately long as compared to other rhinocerotids.

Figure 44: Skull of the Shamsi taxon, left lateral view. Note the missing premaxillary bone and most of the upper dentition.

The skull narrows gradually posterior to the orbits, which are somewhat projecting with dorsal boney “hoods” over the orbits. When viewed dorsally, the zygomatic arches project directly posteriorly until the anteroposterior midpoint where they extend slightly laterally in a gently convex shape while also increasing in thickness and height. The parietal crests do not connect, but converge briefly before immediately diverging again, forming a split “X”, and failing to make a distinct sagittal crest. Throughout the extent of the parietal crests they are low in profile. Viewed dorsally (Figure 46), the occipital crest makes a gentle “M” shape, with the parietal crests connecting into the lateral limbs of the “M”. Viewed from the posterior, the occipital crest and the occipital surface are trapezoidal. The occipital surface forms a plane roughly vertically, with the surface inclined posteriorly through the occipital crest, which forms a rounded knob shape in profile, where the posterior edge of the occipital crest overhangs the occipital condyles.

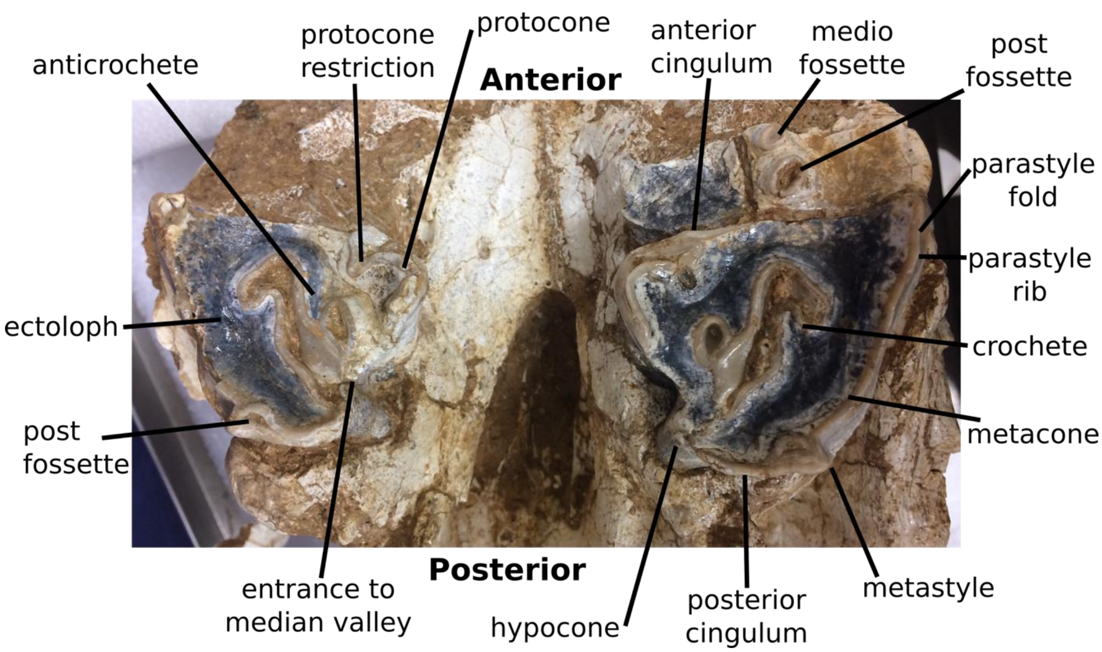

Figure 45: Ventral view of the dentition, showing the upper M3s and partial left M2. Major dental features visible in the Vodka taxon labeled.

Figure 46: Dorsal view of the skull with character 48 highlighted. The skull is widest across the posterior portion of the zygomatic arches, and the brain box is relatively narrow. Also note the gentle “M” shape of the paraoccipitals. Additionally, the nasals are fully fused and lacking any rugosity.

The posttympanic and postglenoid processes are in contact but not fused, before separating again ventrally, but form a pseudomeatus (Figure 47). The posttympanic process is enlarged and is of equal length as the postglenoid process, and as in other tapirids and all rhinocerotids, the paraoccital process and posttympanic process are completely and fully fused (Parker & Haswell, 1910). The postglenoid process is ovate in cross section and hooks anteriorly. Both the posttympanic and the postglenoid processes terminate ventrally before becoming even with the most ventral extent of the occipital condyles. On the ventral side of the skull, the anterior border of the choanae is rounded, but much more laterally constricted than other aceratheres. While the palatine spine is not well preserved, it also appears to be a weakly developed feature and does not continue significantly posterior in the palate. The pterygoids are also damaged, but appear to project horizontally, or at least nearly horizontally.

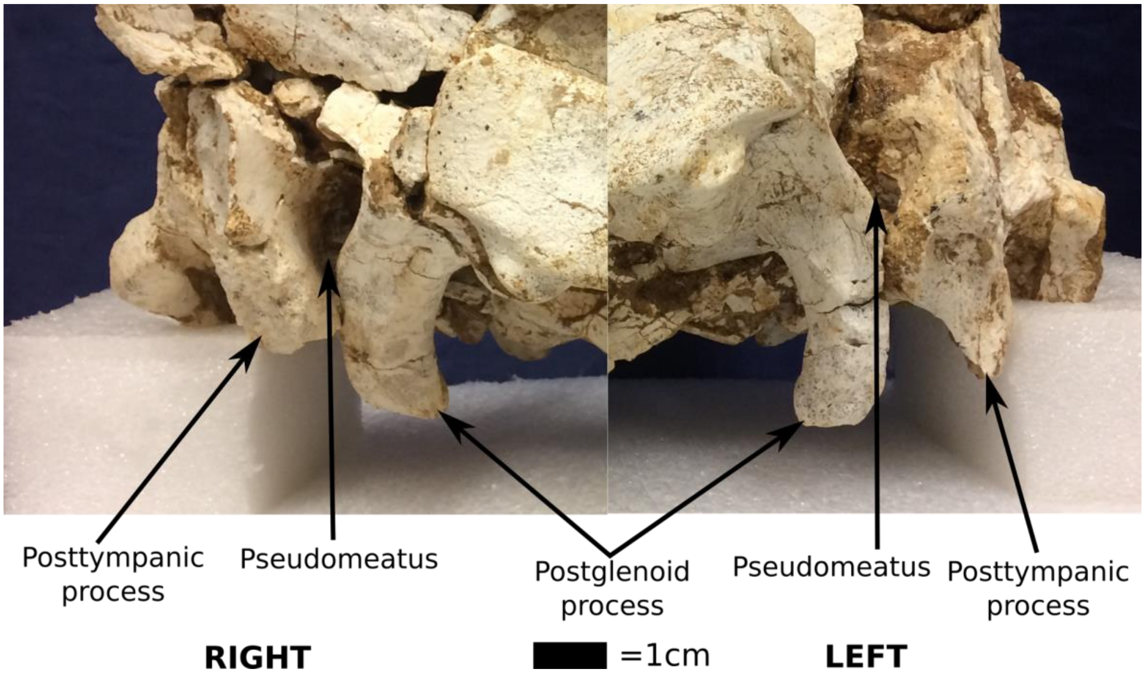

Figure 47: Lateral views of the posterior-most portion of the skull highlighting several important features. Because of diagenic deformation, combined with structural damage that occurred during excavation, the degree of closure on the pseudomeatus is variable between sides. Clearly there was not a complete suture, although contact can be clearly seen on the left side, and alteration of the surface of the postglenoid where contact previously occurred can be seen just to the right of arrow head on the right side. This character is touted as a defining character of Chilotherium, although is not coded on many species, including the several most basal. Note that in rhinocerotid and tapirids, the posttympanic process and paraoccipital process are completely fused together (Parker & Haswell, 1910).

The orbits are placed high in the skull, directly posterior to the posterior of the nasal notch. Both the supraorbital tubercle and postorbital tubercles are present and robust, with the surpraorbital process being slightly rugose. The orbits themselves are circular and slightly forward facing. Compared to other rhinocerotids, the orbits are moderate in size. The infraorbital foramina are not visible with the degree of damage and bone alteration displayed in the specimen.

Little remains of the upper dentition, other than the M3 on both sides and the posterior portion of the M2 on the left side (see Figure 45 for occlusal view of dentition). The teeth are very worn, indicating an old individual and an abrasive diet. The labial edge of the molars is wavy and complicated, even worn to less than one centimeter of enamel. No evidence of cementum is present in preserved teeth. In occlusal view, the shape of the M3 is trapezoidal. The M3 retains a paracone rib and parastyle fold (see Figure 45) on the labial surface. The protocone is strongly restricted, and a medifossette is present. There is also a strong antecrochet on both M3. Interestingly, the paracone rib and parastyle fold are characters considered basal in *Chilotherium*, while the restricted protocone, midifossette, and antecrochet are all considered derived characteristics in the genus. The M3, where not worn below the enamel-dentine junction, also have a strong lingual cingulum, although no labial cingulum is present.

Mandibles

The mandibles are robust and connected via a stout symphysis. The symphysis is anteroposteriorly thickened, with the dorsoposterior surface angling upwards at an intermediate angle. Anteriorly to the premolars, the mandibles constrict and have indented dimples on the ventral most portion of the lateral surface directly posterior to the base of the tusks. The tusks project laterally on an angle not in line with the tooth row. They are quite circular in cross section, with wear facets spanning the exposed length of the tusk. While worn, the tusks do not show evidence of a medial flange at the base. The smaller size in length and diameter, as well as the cross-sectional shape implies the preserved individual to be female (Mihlbachler, 2005, Chen et al., 2010), a character noted in another *Chilotherium* species, *Chilotherium wimani*. All species of *Chilotherium* with sufficient sample size are sexually dimorphic in tusk cross-sectional shape, and no other taxa have circular cross sections (Chen et al., 2010).

The ventral surface of the mandibles is relatively flat, and only projects upwards immediately posterior to the base of the tusks. The mandible is robust both in thickness and in height. Within the mandible, the tooth row is offset on an angle compared to the axis of the mandible. Despite some diagenic deformation to the fossil, the ascending rami are both vertical, and therefore it looks to be a true character of the specimen.

The teeth are extremely worn and exhibit wear commonly associated with drought (Kaiser et al., 2013). While premolars wear before molars, from a combination of the chewing pattern and eruption pattern (Prothero, 2009, Kaiser et al., 2013), the molars are typically worn more progressively from the m3 forward. Other than fragmentary labial scraps of enamel, all premolars are worn below the enamel dentine junction. All remaining enamel lacks cementum on any surface. As the bone is somewhat eroded perimortem around the roots of the teeth, splaying double roots are visible for all teeth, except for the possibly single rooted p2. While the mandible does not appear to have an alveolus anterior to the remaining portion of the p2, the bone is worn, and this disappearance of presumably previously occupied alveola is present in several of the *Teleoceras* mandibles examined in this study. The degree of root formation and splay angle of the roots suggests that while an aged individual, the teeth were likely never approaching hypsodont. In the molars, particularly the m3 as it is least worn, the ectoconid and metaconid are well developed, with the m3 metaconid larger and extending lingually more than the metaconid (Figure 48). Only the m3 preserved the talonid basin, and therefore gives an accurate estimate of relative cusp extent internal to the tooth margin. The p3-m1 are wider than they are long, indicating some degree of shortening in the tooth row.

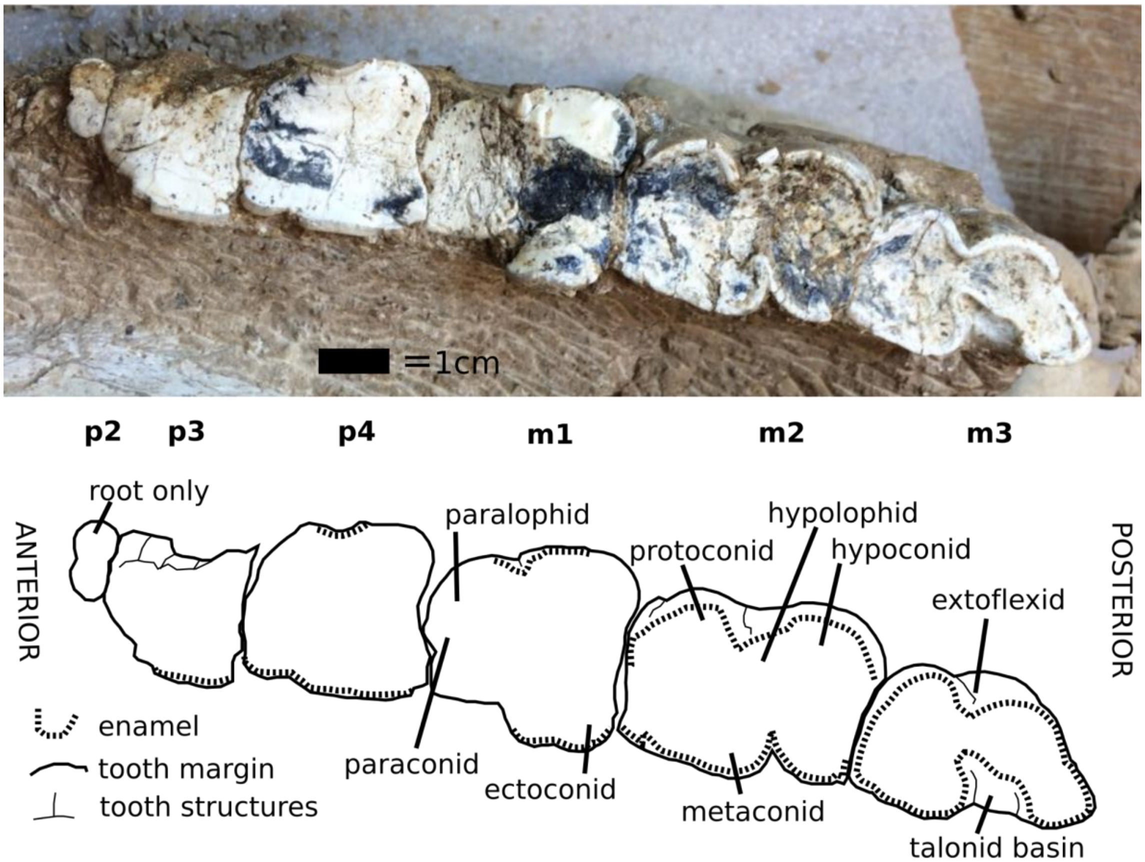

Figure 48: Occlusal view of the better preserved right lower dentition. While extremely worn, the chewing surface is not broken or otherwise diagenically altered. The m3 is least worn and preserves the best estimate of the relationship of interior cusps. Internal part of each tooth is dentine, while cross-sections of enamel are shown with a dashed line.

Radius

The radius is relatively elongate compared to other *Chilotherium* (see Figure 49), although limb length may respond more plastically than many other features. Some previous studies have associated more gracile distal limb elements with adaptation to open steppe environment (Deng, 2006, Guérin, 1980, Ringström, 1924). There is some dorsoventral flattening, with an ovate cross-section. Still robust compared to a modern white rhinoceros (UOMNH B-8701), the radius is also more curved, another feature seen in “barrel-bodied” rhinocerotids (Prothero, 2009).

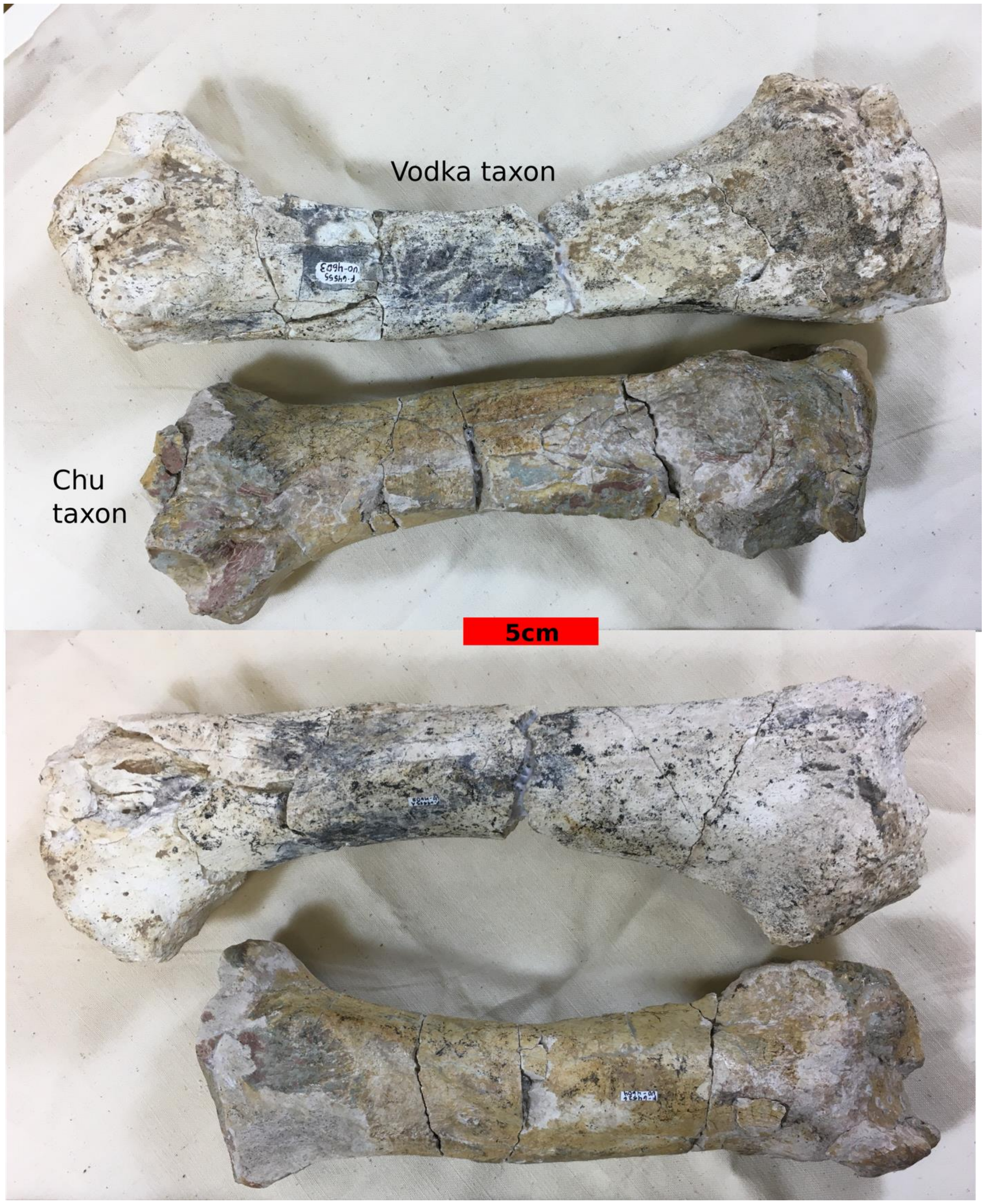

Figure 49: Side by side comparison of the radia from the Vodka taxon (top in both images) and the Chu taxon (lower in both images). Both are robust; however the older Vodka taxon is proportionately longer.

Astragalus

The astragalus is more strongly keeled than either *Teleoceras* or *Aphelops*. Wider than long, the astragalus also has a pronounced medial bulge. The articular surface constricts around the groove between trochlea, although the groove itself is shallow. Some of the head is damaged, but the head overall projects out from the trochlea more than modern white rhinoceros (UOMNH B-8701).

Metacarpal III

While the majority of the third metacarpal is preserved, the proximal surface is broken and missing. The bone exhibits good symmetry across a central axis, and is slightly curved dorsally at the distal-most end. Ovate in cross section, the metapodial is quite compressed dorsoventrally. The distal end is robust, with a very pronounced trochlear keel that is also narrow in lateral extent. The dorsal surface has a thin ridge projecting towards the proximal end of the bone and extending from the trochlear keel. Limited cysting (Stilson, 2017) is present just proximal to the joint surface.

Tibia and fibula

The tibia is shortened and robust compared to a modern white rhinoceros (UOMNH B-8701). The proximal end is mediolaterally wider than it is antioposteriorly, with 0.5 centimeter depression in each articular surface for the distal condyles of the femur. The articular surface is heart shaped, with a medial projection. Some evidence of “lipping” (Stilson, 2017) is shown on the lateral and posterior edges of the proximal articular surface. The distal end is strongly keeled, with deeper keels than seen in comparatives. The cross section is slightly tear-drop shaped, with a pronounced ridge forming the anterior edge. The radius only preserves the distal end, but it is also quite robust in form.

Discussion

Assignment to *Chilotherium*

In the skull, the fused posttympanic and postglenoid processes are seen in all other species of *Chilotherium*, but are lacking in more basal aceratheres (Deng, 2006). While this character is unfortunately on a gradient (Fortelius et al., 2003), the Shamsi specimen has closure of the opening, although the sutured fusion between the posttympanic process and postglenoid process is lacking. This could place the Shamsi taxon just outside of *Chilotherium*, or as a more basal member of the taxon. However, the nasals project outwards, rather than curving ventrally, and there is no evidence of a horn on the nasals or frontal (Ringström, 1924). In the mandibles, the ventral surface of the symphysis is concave, and the symphysis in general is robust and thickened anteroposterior (Deng, 2006). The limb length, while longer than some *Chilotherium* species, is still proportionately short and robust compared to the overall body size. The metapodials are also dorsoventrally flattened (Prothero, 2009).

Comparison to other *Chilotherium* species

Chilotherium wimani is a similarly medium-sized rhinoceros, with a trapezoidal occipital; however, the occipital ridge possesses a prominent notch unlike the Shamsi taxon. Additionally, the dorsal profile of the frontal and parietal is almost perfectly horizontal, with only a slightly concave profile in *C. wimani*, whereas the Shamsi taxon is upturned sharply through the posterior portion of the parietal. *Chilotherium wimani* is one of the only *Chilotherium* species with a prominent supraorbital tubercle (Deng, 2006); however, this does illustrate the possible presence of this feature in the genus, as it is also seen the Shamsi taxon. This taxon also shows sexual dimorphism in both size and cross-sectional shape of the i2 tusks (Chen et al., 2010), which we believe the Shamsi taxon shows, as no non-sexually dimorphic rhinocerotids have circular cross-sections to the tusks (Chen et al., 2010)\.

Chilotherium anderssoni was originally diagnosed largely by the broadly separated parietal crests (Ringström, 1924), however Deng (2001) showed this character is variable in several Chilotherium species and can also be impacted by ontogenetic development, with older individuals displaying greater distance between the parietal crests. The Shamsi specimen has widely separated parietal crests, but is also clearly an old individual given the wear stage on the teeth, so if that character is impacted by ontogenetic development it may be a poor method for comparison. *Chilotherium anderssoni* also has a nearly flat labial surface to the molars and lacks a lingual cingulum in the molars (Deng, 2006), while the Shamsi skull has a complicated labial profile on the M3 and partial M2 and a strong lingual cingulum.

Chilotherium persiae has a well-developed antecrochet on the upper molars (Pandolfi, 2015), like that seen in the Shamsi taxon. However, the nasals on C. persiae are quite short. *Chilotherium killasi*, a taxon not included in the phylogenetic analysis at this time, has a far more refined mandible where the ventral surface curves upwards and lacks the robusticity seen in the Shamsi taxon, or any other *Chilotherium* species (Fortelius et al., 2003).

Not included in previous discussion or phylogenies is *Chilotherium orlovi*. While an extremely limited number of specimens are attributed to this species, a comparison is needed, as the taxon is known from and described from southeast Kazakhstan (Bayshashov, 1982). The dorsal profile of the skull is quite different, with a more gradual slope angled anteriorly from the elevated paraoccipital ridge and a slightly ventrally projecting nasal (Bayshashov, 1982). Additionally, the nasals are quite short, similar to *C. persiae*.

Chilotherium habereri, the only rhinocerotid previously attributed to the Kyrgyz Neogene (Sotnikova, 2001) has a more level profile to the skull, with less dorsoposterior extension to the occipital crest. This taxon also has very short nasals compared to the Shamsi taxon or any other species of *Chilotherium* examined. While Sotnikova (2001) lists *C. chabereri* instead of *C. habereri*, this difference is presumed to be a translation error, as no other record of *C. chabereri* exists. If the nasals are indeed the most differentiating feature, the misattribution could have resulted from the sole figured skull in Tarosov (1970) lacking any of the dorsal portion of the skull. While the Shamsi specimen has extremely worn dentition, the degree of root formation and angle of the roots suggests the taxon was not particularly hyposodont, while *C. habereri* is reported to be one of the most hypsodont species of *Chilotherium* (Fortelius et al., 2003). The lower dentition also differs in the p4-m1 being much longer than they are wide (Fortelius et al., 2003), a character lacking in the Shamsi taxon.

Comparisons to other rhinocerotids

Within the previously proposed tribe or subtribe "Chilotheriini" (Qiu, Xie & Yan, 1987), although more appropriately assigned to Acerarthiini, *Acerorhinus hezhengensis* is another common large-bodied Asian rhinoceros present in *Hipparion* faunas (Deng, 2006). However, unlike the Shamsi taxon, *A. hezhengensis* has a posttympanic process projecting ventrally to the condyles. Another species in the Late Miocene of China is *Acerorhinus yuanmousensis* from the Yuanmou Basin, although the genus is known across Eurasia in the Late Miocene (Lu, 2013). *Acerorhinus yuanmousensis* has a nasal notch only extending to the M1, and has an undulating profile to the extremely short nasals (Lu, 2013). All Acerorhinus species have a prominent supraorbital tubercle like the Shamsi taxon and unlike most *Chilotherium* species, and the feature is considered more primitive (Deng, 2006). Additionally, *Acerorhinus* has vaulted ventral surfaces to the nasals with drooping lateral margins. *Acerorhinus* is also typically larger than the medium-sized Shamsi taxon, and the outline of the skull quickly constricts posterior to the orbits, unlike the more gradual narrowing seen in most *Chilotherium* species and the Shamsi taxon.

One of the more basal members of the Aceratheriini, *Persiatherium rodleri*, is also a medium-sized rhinocerotid from the edges of Central Asia (Iran). Like the Shamsi taxon, it also lacks a labial cingulum on the upper molars, but contrasting in the absence of cristae and absence of the antecrochet on the upper molars (Pandolfi, 2015). The lingual cingula are only present on the M1-M2 in *P. rodleri*, whereas it continues to the M3 in the Shamsi taxon. Lastly, the M3 on *P. rodleri* is triangular is shape (Pandolfi, 2015), unlike the trapezoidal form in the Shamsi taxon.

Within the Elasmotheriini, *Hispanotherium matritense* is another middle to late Miocene rhinocerotid known from Chinese *Hipparion* faunas, although more common in Iberian Peninsula sites. However, *H. matritense* is a small-bodied rhinocerotid with a nasal horn and significant amounts of cement in the upper molars (Deng, 2006). Like the Shamsi rhinocerotid, the limb proportions are more gracile, and the protocone of the upper molars is highly constricted (Deng, 2006). *Parelasmotherium simplum* and *Parelasmotherium schansiense* are additional Miocene rhinocerotids documented in correlative sites in China. Both taxa have only rudimentary crista in the upper molars, unlike the well-developed crista remaining even in advanced wear in the Shamsi taxon. *Parelasmotherium simplum* is also a small rhinocerotid, while *P. schansiense* is closer in size to the Shamsi taxon. *Parelasmotherium* (including *Paralasmotherium linxiaense*, another Chinese species of the genus) also have strong anterior and posterior cingula on the lower molars, a feature lacking in the Shamsi mandibles. An additional related candidate is *Sinotherium*; however, this taxon has lower molars angled anteriorly, and premolars angled posteriorly, so that the teeth wear in a bevel (Deng, 2006). *Sinotherium* also has a large frontal horn.

Also within the Elasmotheriini is *Iranotherium morgani*. Initial runs of the phylogeny, before cleaning and checking some of the character coding, placed the Shamsi taxon as sister to *I. morgani* in two out of 12 returned trees. However, this is more of an argument for reanalyzing the characters, as we have done, than actual phylogenetic affiliation, as the two taxa are quite different in gross morphology. *Iranotherium morgani* is quite large bodied, although body size is a potentially quickly evolving character, and hardly grounds for exclusion. Notably, *I. morgani* has a huge nasal horn, and presence/absence of horns and relative position of horns is a more constrained feature within lineages (Prothero, 2005). The skull is also a very different shape in dorsal profile, with much of the skull forming a significantly convex profile and the nasals dipping ventrally sharply (Deng, 2006, Deng, 2005). The occipital crest, when viewed dorsally, is strongly "V" shaped, with the notch pointing anteriorly and is indented along the axis when viewing the occipital surface (Deng, 2005). Male *I. morgani* have roughened posterolateral zygomatic arches, indicating a degree of sexual dimorphism. The orbits are placed far posterior relative to the posterior portion of the nasal notch. In the mandible, *I. morgani* has a narrow mandibular symphysis. All teeth, both lowers and uppers, have significant amounts of cement (Deng, 2005, Pandolfi, 2015), a trait lacking in the Shamsi rhinocerotid. In the upper M3 the crochet is still strong on the Shamsi taxon, while weak on *I. morgani*, and the occlusal surface of the M3 is triangular-shaped (Deng, 2005). In the lower dentition, the premolars are more reduced in total tooth row portion in *I. morgani* and are overlapping in the p2-p4, and there are no enlarged tusks, as are prominently featured in the robust symphysis of the Shamsi taxon. *Iranotherium morgani* is also inferred to have evolved in Northwest China and dispersed through what would now be Kyrgyzstan to get to western Central Asia (Deng, 2005, 2006).

Within the Rhinocerotini, *Dicerorhinus* is one of the most frequent Asian genera from the Miocene. The nasal bones are much longer and wider than the Shamsi taxon, and contain a well-developed horn boss. The nasal notch extends only as far as the P3-4 making the distance from the orbit to the nasal notch also much greater than seen in the Shamsi taxon. The skull roof is concave, with a barely raised occipital, and the frontal is quite concave, differing from the level to slightly concave surface of the Shamsi taxon. In the occipital, *Dicerorhinus* has an anteriorly inclined occipital surface, as opposed to the upright surface in the Shamsi skull, and the occipital crest has a strong notch at the median point. The M3 occlusal surface in *Dicerorhinus* is triangular, as opposed to the trapezoidal shape seen in the Shamsi taxon's M3s. *Dicerorhinus ringstromi* is very large in body size, far larger than the Shamsi taxon, but is notable in that it had cursorial limb bones, similar in degree of gracility, to those seen in the Vodka bone bed. Ringström (1924), Guérin (1980), and Deng (2006) propose a correlation between open steppe habitat and these more gracile limb proportions. All members of Rhinocerotini are characterized by the presence of at least one horn, nasal or frontal (Antoine, 2002, Pandolfi, 2015), ruling out less common members of this tribe as well.

All European members of Teleoceratini included in this study (the genus Brachypotherium) lack lingual cingula on the upper molars and have a pronounced labial cingulum on the upper molars (Pandolfi, 2015). The Shamsi taxon is the opposite of this, with lingual, but not labial cingula on the M2-M3.

Phylogenetic Analysis: Our analysis in TNT returned 5 most parsimonious trees from the cladistic analysis. Our preferred tree, the consensus tree, is shown in Figure 49. We retain the same definitions and included taxa for Aceratheriini as Pandolfi (2015), although we find a more complicated and possibly nested relationship between *Chilotherium* and *Acerorhinus* than Pandolfi (2015). In all trees returned, not just the consensus tree, *Chilotherium* is not returned as a monophyletic genus. Several authors, notably Fortelius (et al., 2003), imply many of the characteristics used to unite

Chilotherium may be pleisiomorphic traits. Not only were both new Kyrgyz taxa included within the *Chilotherium* clade, but also *Teleoceras*, *Aphelops*, and consistently *Aceratherium porpani*. While the preserved material for the Chu rhinocerotid was limited, and therefore limited the characters that could be coded, the taxon still consistently nested with *C. kowalevskii* and *C. schlosseri*. Likely, the entire tribe Aceratheriini is in need of taxonomic revision, although future alalyses should include postcranial characters and a revised set of craniodental characters.

Our inclusion of Neogene North American rhinocerotids is novel compared to previous studies. As proposed in Prothero (2005), both *Teleoceras* and *Aphelops* are supported in having an Asian origin. We retain Prothero's (2005) assignment of *Aphelops* to Aceratheriini, as the taxon nests well within the clade. Against the Prothero (2005) assignment however, we also find *Teleoceras* to nest well within the Aceratheriini in all trees, and not with the tribe Teleocerini, despite that tribe being named for the North American genus. This suggests some of the gross morphological similarities used for the inclusion of Eurasian taxa are more likely to be environmentally plastic characters, rather than phylogenetically informative characters. Teleoceratini (as used in Pandolfi, 2015), or Teleoceratina in Antoine (2002), are characterized by a shortening of the skull and distal leg segments (Heissig, 1999, Prothero, 2005). However, this shortening of distal limb elements is also strongly shown in *Chilotherium*, as well as several other members of the Aceratheriini. Prothero (2005) further describes the metapodials as flattened, but as no postcranial elements were included in this study, this character is harder to discuss in the context of the Asian rhinocerotids. This character was also present in the Asian Shamsi taxon, and several species of *Chilotherium*. Prothero (2005) also lists a "U-shaped" nasal

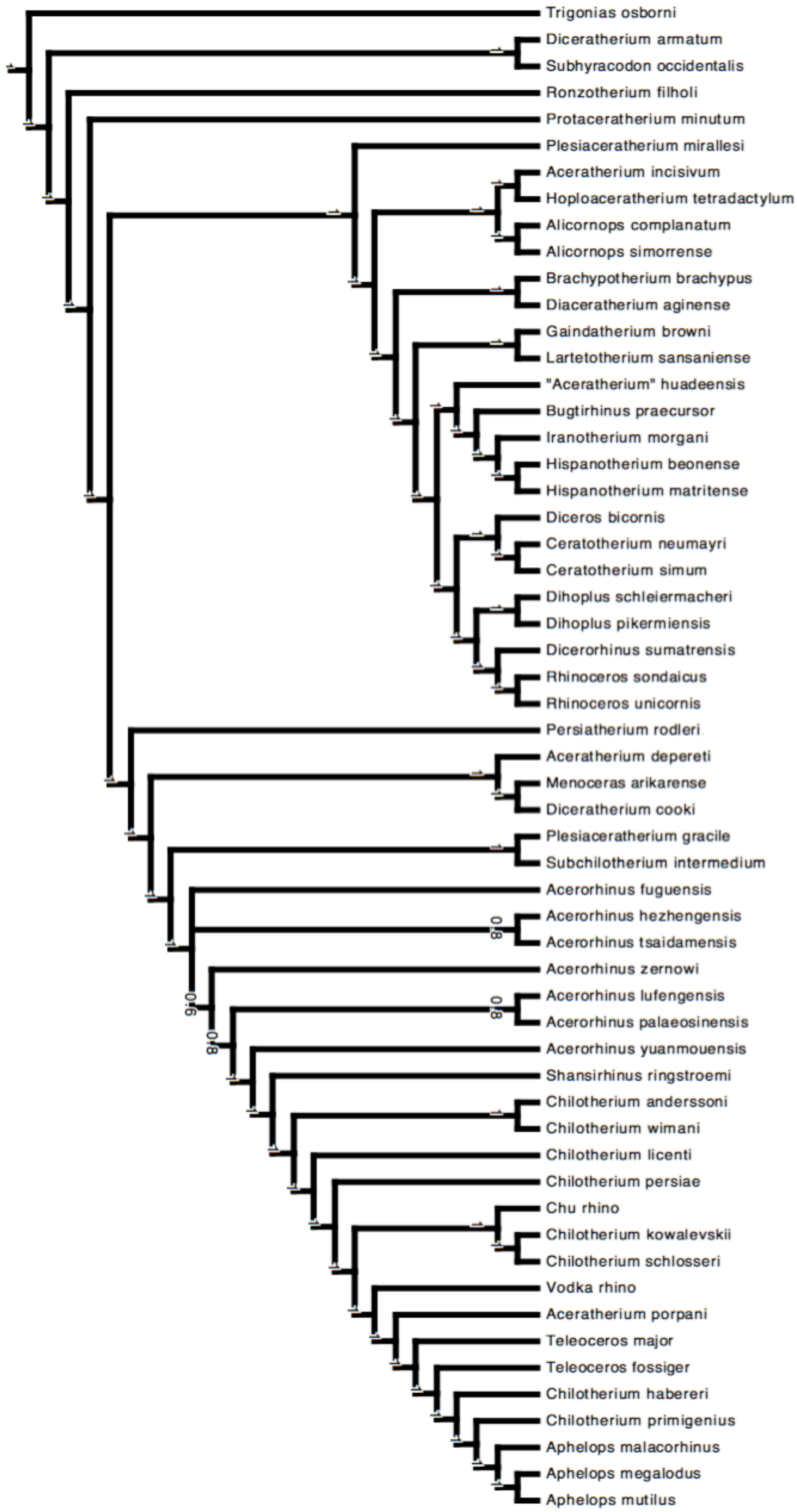

Figure 50: Consensus tree, of five returned trees. Numerical values on nodes are values that split was returned in the analysis. Note the non-monophyletic nature of both *Acerorhinus* and *Chilotherium*.

notch as a synapamorphy of the Teleoceratini, however this character is extremely common in Eurasian Aceratheres, yet again highlighting the need to examine rhinocerotids on a broader scale than single continents. Limb proportions change within genera, and thus may be more indicative of ecology than phylogeny as a result. The degree of skull shortening is also not more than seen *Chilotherium habereri*, and thus again may not be a synapamorphy.

I found the new Shamsi taxon distinct in enough characters to justify the description of a new taxon, although as this is a dissertation, designation of novel nomenclature will be left for the subsequent publication stemming from this work. The Shamsi taxon consistently nested with the genus *Chilotherium*, although the validity or organization of this genus is now questionable. Some previous authors (Qiu, Xie & Yan, 1987) have proposed the tribe Chilotheriini, with others following this assignment (Deng, 2006). However, the inclusion of *Acerorhinus* in any monophyletic group containing *Chilotherium* leads us to reject Chilotheriini as a tribe within Rhinocerotidae, and retain the assignment of *Chilotherium* to the tribe Aceratheriini as done by Pandolfi (2015). Our new taxon from the Vodka locality is therefore assigned to the tribe Aceratheriini, as it is included within the genus *Chilotherium* as it currently stands.

Despite incomplete character coding for the Chu Formation Kyrgyz rhinoceros (see Chapter 2 for description of material), the Chu taxon consistently nests near or with the Shamsi taxon within our analysis, although closer to two species of *Chilotherium*, *C. kowalevskii* and *C. schlosseri*. As the Chu Formation overlies the Shamsi Formation, the Chu taxon is undoubtedly younger, and therefore may represent a descendant of the Shamsi taxon. It is possible the Chu taxon may also represent a new species given its placement in many of the analyses; however, the craniodental material is too incomplete and therefore prohibits a definitive assessment of the taxon. The Chu rhinoceros does not nest outside of *Chilotherium*, and therefore is retained as *Chilotherium* sp. in our phylogeny.

Paleoecology: The Shamsi taxon is a medium sized rhinocerotid, making the species certainly one of the larger taxa present in the Kyrgyz Miocene. While larger giraffids and pachyderms are possible, none have thus far been produced by the Vodka bone bed. By element representation (see McLaughlin Chapter 2) the Shamsi *Chilotherium* is the dominant taxon, represented by a MNI of three individuals. While this is not a sufficient sample to make substantial claims about behavior, the relative elemental abundance of the rhinocerotid taxon at least opens the possibility of herd behavior, as demonstrated in fossil rhinocerotids like *Teleoceras* (Prothero, 2005). Fossil rhinocerotids were likely more social than modern rhinocerotids, even exhibiting behaviors with no modern analogue (Milhbachler, 2005), although habitat fragmentation and decimated populations in modern rhinoceros make establishing possible ancestral behavioral traits more difficult. Tusked modern rhinoceros, like *Rhinoceros unicornis*, use their sexually dimorphic tusks in male-male displays (Laurie, 1982), which may have also been part of the function of tusks in the fossil taxa. The combination of the large body size and possible herding behavior made the Shamsi taxon potentially one of the dominant organisms in its ancient ecosystem (Figure 51).

While the dental material present at Vodka belonged to a presumably quite elderly individual, and therefore crown height could not be assessed, the teeth lack cementum, a dental characteristic more commonly associated with grazing rhinoceros (Prothero, 2005). The wear pattern on the lower teeth is also very uneven, consistent with browsing or at least mixed-feeding. This jagged macrowear indicative of browsing was also present in the associated Hipparion horse teeth and the unidentified cervid. While the Kochkor Basin was lower elevation 8-9 million years ago than today, the initiation of uplift in the Oligocene-Miocene (Abdrakhmatov et al., 2001) implies the region was already quite mountainous by the late Miocene. Even in the intermontane basins, the habitat was likely lacking in dense vegetation and semi-open, consistent with browsing taxa as the predominant ungulates.

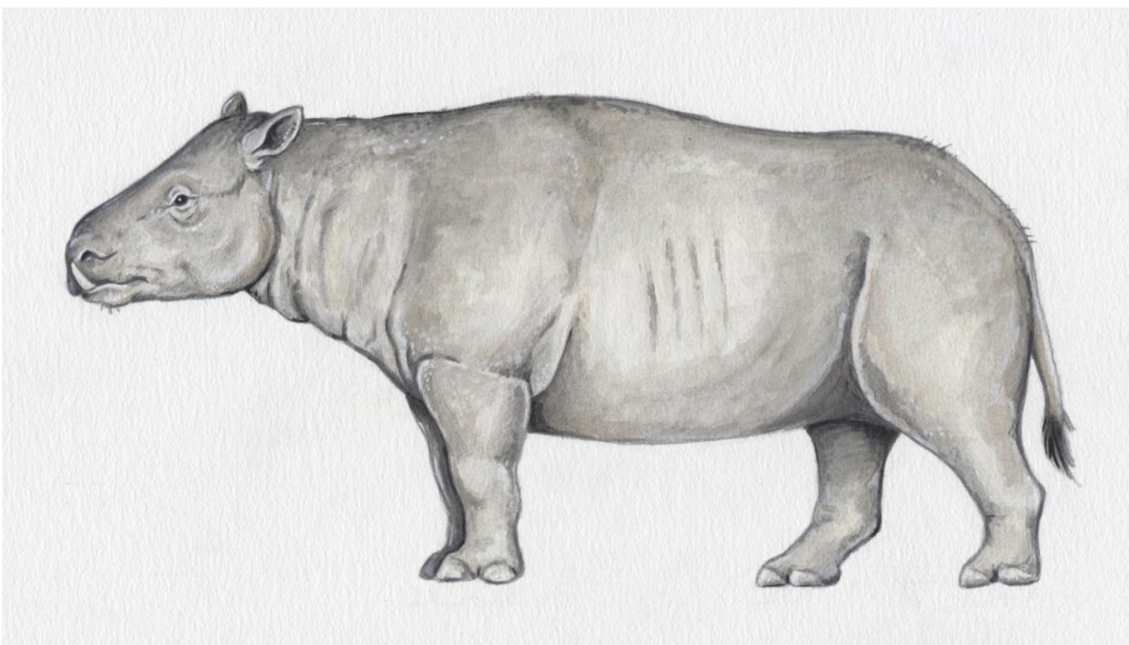

Figure 51: Life reconstruction of the Shamsi *Chilotherium*. Note the lack of horn, tusks, large body, and relatively gracile limbs.

The Shamsi rhinocerotid is produced from a fluvial sandstone to conglomerate. The clasts are subangular to subrounded, and frequently imbricate, with extensive cross bedding. Those sedimentary characteristics are consistent with braided river channels emptying out of the uplifting mountain range to the south. The basin floor may have been wider in the past (Sobel et al., 2006), with high energy material being deposited in the valley floor, resulting in quick burial of carcasses. The rhinocerotids could have inhabited ranges throughout of the river profile, as discussed in the transport section of Chapter 2, ranging from the valley floors to foothills and even sub-alpine habitats. While significant uplift occurs from aproxematly 7 Ma to modern times, the Tien Shan were already at moderate elevations, with the Kochkor Basin likely greater than 700 m by the late Miocene (Chapter 3).

Conclusions

The Shamsi taxon is herein assigned to the genus *Chilotherium*, and represents a new species. This moderate sized, hornless and tusked rhinocerotid may have lived in moderately open habitats and been an abundant member of Late Miocene Central Asian endemic faunas. As the Greater Tibetan Plateau was already an area of moderately high elevation by 9 Ma (Sobel et al., 2006), this endemic taxon could reflect early sub-alpine to steppe habitats. Central Asia represents the obvious corridor for biotic interchange between much of Europe and Asia, yet transitional endemic faunas have received little attention previously. The new taxon, and its placement in a novel phylogenetic analysis, highlight the importance of Central Asia in both biogeographic and phylogenetic studies. While *Chilotherium* was previously reported from younger fossil beds (the Chu Formation) in Kyrgyzstan, we find the older Shamsi taxon to be distinctly different than the Chu Formation rhinocerotid.

The inclusion of North American taxa in the phylogenetic analysis displays the need for careful evaluation of what characters are taxonomically informative, rather than environmentally driven phenotypic response. Additionally, characters (like the shape of the nasal notch) may be consistent on a continent level, but not at an intercontinental level. *Teleoceras* and *Aphelops* are clearly derived from Asian taxa, as previously proposed, and further drive home the need to address taxonomic assignments and phylogenetic analyses on an intercontinental scale to truly sample biotic interchange and relatedness. Additional older North American and Eurasian taxa should be included in future analyses to establish the degree of interchange between North American rhinocerotids and Eurasian and African taxa, as well as examining the timing of intercontinental biotic interchange.

CHAPTER V

CONCLUSION

The fossils of Kyrgyzstan offer a wealth of information about changing landscapes, climate, and the biota inhabiting Central Asia. From ancient bones alone I can reconstruct an ancient ecosystem, full of a diversity of megafauna. This fauna changes through time in response to changing climate, much as the organisms of Kyrgyzstan are responding to modern climate change today. The climate change was driven by uplift, both locally in the Tien Shan, but also in the broader region in the Pamir, Himalayas, and the Greater Tibetan Plateau. Rapid uplift changed global atmospheric circulation, and regionally blocked the Indian monsoon from reaching Central Asia. Without the monsoonal signal, Kyrgyzstan became drier, forcing changes in the fauna.

Via magnetostratigraphy and biostratigraphy I have dated this tectonically driven climatic change to have occurred between 9-7 million years ago. This aligns with similar data from China, Pakistan, India, and Kazakhstan, suggesting uplift in the region reached a level sufficient to block the monsoon by the latest Miocene. In contrast to some other geologic work, I find that the modern uplift and shortening rates seem to be consistent throughout the history of Neogene uplift of the Tien Shan. The Tien Shan, and many of the specific geologic formations, are younger than some studies suggested.

On an evolutionary perspective, Central Asia lies at an important boundary between Europe and Asia, yet despite the importance to dispersal events, or the evolution of endemic faunas, little paleontological work in the region concentrates on the Neogene. I begin to tackle this issue by investigating the taxonomy, phylogeny, and biogeography of the most common fossil animal of Kyrgyzstan’s Neogene: a rhinoceros. I find there to be two species in the two different age formations included in this work, both of which are likely new species. The older species I find to be a new member of the genus *Chilotherium*, a barrel-bodied, hornless, tusked rhinocerotid. Importantly, this taxon shares phylogenetic similarities with several North American rhinocerotids, suggesting significant biotic interchange in the late Miocene.

Together the faunas and their geochronologic placement illustrate a time of rapid change, both biologically and physically, to the ecosystems of ancient Kyrgyzstan. As the geologic processes remain the same today, Kochkor Basin’s ancient past can be an analogue for the future, both in terms of changing landscapes, but also the changes faced by a biota we are now part of.

APPENDIX A

VODKA BONE BED (UO-4603)

Specimen #	Locality #	Order	Family	Genus	element	L1	L2	L3
64560	UO-4603	Artiodactyla	Bovidae	Gazella?	mandible fragment with first two premolars (p2-3?)	22.62	14.99	5.82
64520	UO-4603	Artiodactyla	Cervidae		P4-M1	22.51	21.99	12.97
64532	UO-4603	Artiodactyla	Cervidae		1.5 teeth in jaw fragment of unknown cervid, m1-m2 or m2-m3	36.43	23.4	9.47
64533	UO-4603	Artiodactyla	Cervidae		mandible, p3-m3	80.49	36.4	13.5
64534	UO-4603	Artiodactyla	Cervidae		scapula	89.78	24.7	11.02
64535	UO-4603	Artiodactyla	Cervidae		metapodial	128.77	20.99	12.46
64536	UO-4603	Artiodactyla	Cervidae		phalanx	25.15	14.3	8.91
64537	UO-4603	Artiodactyla	Cervidae		proximal scapula	47.37	24.11	14
64538	UO-4603	Artiodactyla	Cervidae		proximal femur and partially articulated pelvis	46.93	23.87	21.57
64539	UO-4603	Artiodactyla	Cervidae		distal tibia	58.78	27.61	19.4
64517	UO-4603	Artiodactyla			distal radio/ulna	110.56	47.15	19.94
64524	UO-4603	Artiodactyla			skull bit, horn core	72.68	69.05	49.86
64553	UO-4603	Artiodactyla			sesamoid	16.69	10.35	5.69
64492	UO-4603	Perissodactyla	Equidae	Hipparion	R upper cheek tooth	46.37	22.97	20.55
64493	UO-4603	Perissodactyla	Equidae	Hipparion	mandible, w/ incisors and 6 cheek teeth	235	66.34	59.82
64521	UO-4603	Perissodactyla	Equidae		carpal sesamoid	40.81	27.08	10.79
70316	UO-4603	Perissodactyla	Equidae		tooth frag	11.71	10.8	1.19
64514	UO-4603	Perissodactyla	Rhinoceratidae		distal radius	111.77	82.55	30.9
64515	UO-4603	Perissodactyla	Rhinoceratidae		distal radius	105.76	80.54	38.39
64522	UO-4603	Perissodactyla	Rhinoceratidae		distal lateral metapodial	55.05	34.77	28.44
64523	UO-4603	Perissodactyla	Rhinoceratidae		tibia (whole)	282	103.09	40.45
64527	UO-4603	Perissodactyla	Rhinoceratidae		carpal	44	34.24	23.45
64529	UO-4603	Perissodactyla	Rhinoceratidae		tibia mid shaft	65.31	41	30.82
64530	UO-4603	Perissodactyla	Rhinoceratidae		calc frag	68.77	44.85	29.12

64534	UO-4603	Perissodactyla	Rhinoceratidae		thing	94.17	49.18	41.78
64537	UO-4603	Perissodactyla	Rhinoceratidae		astragalus	80.66	70.09	40.32
64551	UO-4603	Perissodactyla	Rhinoceratidae		tarsal	42.58	37.02	19.22
64552	UO-4603	Perissodactyla	Rhinoceratidae		distal humerus	146.18	124.08	55.31
64553	UO-4603	Perissodactyla	Rhinoceratidae		partial pelvis	152.86	84.41	37.83
64554	UO-4603	Perissodactyla	Rhinoceratidae		basacranium	101.57	65.4	16.74
64555	UO-4603	Perissodactyla	Rhinoceratidae	Chilotherium	complete radius, plus some little bits and pieces.	322	87.75	56.26
64556	UO-4603	Perissodactyla	Rhinoceratidae		proximal left tibia and associated frag	101.21	100.44	45.97
64557	UO-4603	Perissodactyla	Rhinoceratidae	Chilotherium	skull			
64558	UO-4603	Perissodactyla	Rhinoceratidae		acetabulum	83.29	60.6	27.91
64559	UO-4603	Perissodactyla	Rhinoceratidae	Chilotherium	distal lateral metapodial	54.05	33.09	27.19
64560	UO-4603	Perissodactyla	Rhinoceratidae		carpal	31.66	21.09	15.38
64561	UO-4603	Perissodactyla	Rhinoceratidae		carpal			
64562	UO-4603	Perissodactyla	Rhinoceratidae		tarsal, 1/2	38.04	25.68	24.87
64563	UO-4603	Perissodactyla	Rhinoceratidae		tarsal sesamoid	37.29	28.56	19.5
64564	UO-4603	Perissodactyla	Rhinoceratidae		sesamoid	29.57	26	23
64565	UO-4603	Perissodactyla	Rhinoceratidae		proximal meta tarsal			
64566	UO-4603	Perissodactyla	Rhinoceratidae		mid shaft of tibia	67.95	51	40.87
64567	UO-4603	Perissodactyla	Rhinoceratidae		distal metapodial	42.78	28.12	26.58
64568	UO-4603	Perissodactyla	Rhinoceratidae		carpal	69.63	55.14	34.64
64569	UO-4603	Perissodactyla	Rhinoceratidae		vertebra fragment	52.5	30.74	21.33
64570	UO-4603	Perissodactyla	Rhinoceratidae		fragment of humerus mid shaft, other fragment (?)	53.99	37.57	28.45
64571	UO-4603	Perissodactyla	Rhinoceratidae		pelvis fragments			
64572	UO-4603	Perissodactyla	Rhinoceratidae		ungal	42.51	38.81	19.07
64573	UO-4603	Perissodactyla	Rhinoceratidae		metapodial fragments	24.11	24.1	10.42
64574	UO-4603	Perissodactyla	Rhinoceratidae		metapodial, 3rd			
64575	UO-4603	Perissodactyla	Rhinoceratidae		tibia (whole)	275	119.59	44.1
64576	UO-4603	Perissodactyla	Rhinoceratidae		complete tarsal	47.46	46.61	17.52
64577	UO-4603	Perissodactyla	Rhinoceratidae		left fibula	148.89	34.68	19.42
64578	UO-4603	Perissodactyla	Rhinoceratidae		atlas fragment	60.04	47.07	28.88

64579	UO-4603	Perissodactyla	Rhinoceratidae	sesamoid	37.21	18.87	16.9
64580	UO-4603	Perissodactyla	Rhinoceratidae	tooth fragments	26.35	22.04	17.17
64581	UO-4603	Perissodactyla	Rhinoceratidae	thoracic vertebra process	65.75	34.85	32.77
70303	UO-4603	Perissodactyla	Rhinoceratidae	carpal	35.08	25.48	20.71
70304	UO-4603	Perissodactyla	Rhinoceratidae		86.91	38.05	36.26
70305	UO-4603	Perissodactyla	Rhinoceratidae	calcaneum	56.92	42.52	26.88
70306	UO-4603	Perissodactyla	Rhinoceratidae	calcaneum and other stuff	69.35	29.88	8.35
70307	UO-4603	Perissodactyla	Rhinoceratidae	5 bone scraps	20.87	12.02	7.25
70312	UO-4603	Perissodactyla	Rhinoceratidae	carpal	60.42	39.37	17.91
70314	UO-4603	Perissodactyla	Rhinoceratidae	whole metapodial	108.99	46.94	20.53
70318	UO-4603	Rodentia	Cricetidae	incisor	7.21	1.95	1.49
70319	UO-4603	Testudines		shell frag	30.19	16.43	8.46
64518	UO-4603			pelvis thing?	152.25	51.99	18.67
64519	UO-4603			small carpal fragment	31.5	16.47	8.16
64557	UO-4603			little rib bits, smaller animal	35.32	15.31	14.46
64558	UO-4603			crap	60.36	48.63	22.29
64559	UO-4603			bone frag	58.01	25.76	13.58
64560	UO-4603			bone frags	33.34	23.45	20.96
64561	UO-4603			frags of God only knows what	40.31	20.2	16.38
64562	UO-4603			pelvis frag? Maybe?	73.14	32.92	17.37
64563	UO-4603			proximal toe	14.77	12.92	10.95
64564	UO-4603			two complete podials, NOT rhino, smaller, shape doesn't seem to match	28.72	22.15	19.95
64565	UO-4603			rib fragment, not rhino, medium animal size			
64566	UO-4603			rib	77.28	15.55	14.97
64567	UO-4603			carpal?	30.9	29	20.73
64568	UO-4603			ribs?	54	8.12	4.19
64569	UO-4603			rib	85.25	36.47	32.55
64570	UO-4603			sesamoid?	28.75	20.06	19.62
64571	UO-4603			bone frags	15.05	11.94	9.04
64572	UO-4603			smallish animal bone bit?	20.43	17.44	11.47
70308	UO-4603			bone frag	17.96	10.03	7.37
70309	UO-4603			scapula	71.95	63.86	16.57

70310	UO-4603	pelvis	102.62	67.78	20.44
70311	UO-4603	bits	44.28	24.76	8.98
70313	UO-4603	frag	42.72	24.69	20.55
70315	UO-4603	frags	41.6	29.96	17.78
70317	UO-4603	indet	62.47	29.54	14.01
70319	UO-4603	frag	21.31	4.74	0.9

APPENDIX B

ORTOK BONE BED (UO-4605)

Specimen #	Locality #	Order	Family	Genus	element	L1	L2	L3
70325	UO-4605	Artiodactyla	Bovidae		distal metapodial	23.53	15.05	7.72
70327	UO-4605	Artiodactyla	Bovidae		right astragalus, small bovid munjack sized	22.42	12.03	11
70328	UO-4605	Artiodactyla	Bovidae		right astragalus, small bovid munjack sized	20.23	12.56	11.35
70329	UO-4605	Artiodactyla	Bovidae		distal 1st phalanx	20.45	8.51	6
70339	UO-4605	Artiodactyla	Bovidae	Gazella	horn core	50.79	24.7	20.45
70346	UO-4605	Artiodactyla	Bovidae		distal calcaneum, from very small bovid, muntjac in size	17.26	10.4	8.63
71406	UO-4605	Artiodactyla	Bovidae	Gazella	horn core	72.48	24.9	18.58
71407	UO-4605	Artiodactyla	Bovidae	Gazella	horn core	42.21	24.66	22.73
71408	UO-4605	Artiodactyla	Bovidae	Gazella	horn core	24.48	19.17	12.84
71409	UO-4605	Artiodactyla	Bovidae	Gazella	horn core	52.19	23.31	18.69
71410	UO-4605	Artiodactyla	Bovidae	Gazella	horn core	107.23	27.03	17.83
71411	UO-4605	Artiodactyla	Bovidae	Gazella	horn core	37.16	21.02	18.77
70333	UO-4605	Artiodactyla	Cervidae		two antler fragments	40.04	27.72	16.38
70334	UO-4605	Artiodactyla	Cervidae		antler pedicle	63.54	36.43	21.61
70356	UO-4605	Artiodactyla	Cervidae		antler fragment, base of branching tine	26.88	23.48	14.53
70380	UO-4605	Artiodactyla	Cervidae		antler fragments	62	22.67	16.68
70390	UO-4605	Artiodactyla	Cervidae		antler fragment	33.26	22.23	17.61
70423	UO-4605	Artiodactyla	Cervidae		radius	92	37.39	25.48

64478	UO-4605	Artiodactyla	Giraffidae	Samotherium	3 teeth	31.41	18.99	7.74
64481	UO-4605	Artiodactyla	Giraffidae	Samotherium	metapodial, articulating cubonavicular and other podial, associated distal tibia, other podial bits	366	62.29	35.33
67907	UO-4605	Artiodactyla	Giraffidae		ossicone frag	38.53	19.17	18.16
70341	UO-4605	Artiodactyla	Giraffidae		celene on tooth	12.03	9.97	7.84
70382	UO-4605	Artiodactyla	Giraffidae		distal metapodial frag	35.77	30.3	19.37
70400	UO-4605	Artiodactyla	Palaeomerycidae	palate	137.87	99.91	35.73	
70343	UO-4605	Artiodactyla			tooth frags	13.16	8.9	2.22
70364	UO-4605	Artiodactyla			calcaneum fragment	14.76	12.53	8.92
70372	UO-4605	Artiodactyla			distal toe frag	16.47	11.39	5.68
70384	UO-4605	Artiodactyla			astragalus fragment	24.43	17.49	16.29
	UO-4605	Perissodactyla	Equidae	Hipparion	complete mandible			
64481	UO-4605	Perissodactyla	Equidae	Hipparion	tooth frag	47.12	14.4	8.92
64482	UO-4605	Perissodactyla	Equidae	Hipparion	partial upper molar	29.2	19.91	9.27
64483	UO-4605	Perissodactyla	Equidae	Hipparion	1/2 astragalus	59.65	41.42	24.71
70323	UO-4605	Perissodactyla	Equidae		distal metapodial frag	33.3	18.46	13.72
70334	UO-4605	Perissodactyla	Equidae	Hipparion	distal metapodial frag	26.1	19.72	16.69
70338	UO-4605	Perissodactyla	Equidae	Hipparion	tooth frag	21.85	16.91	8.04
70355	UO-4605	Perissodactyla	Equidae		distal femur fragment	40.73	31.1	23.12
70373	UO-4605	Perissodactyla	Equidae		tooth frags	28.85	10.73	4.61
70381	UO-4605	Perissodactyla	Equidae	Hipparion	upper cheek tooth fragment	39.62	12.58	11.94
70396	UO-4605	Perissodactyla	Equidae	Hipparion	upper tooth row	90	25.16	17.59
70398	UO-4605	Perissodactyla	Equidae		incissors and frags	21.81	14.48	6.37

70424	UO-4605	Perissodactyla	Equidae		tooth frag	23.74	10.27	5.69
64479	UO-4605	Perissodactyla	Rhinoceratidae	Chilotherium	1 astragalus fragment	36.25	31.65	13.44
64480	UO-4605	Perissodactyla	Rhinoceratidae	Chilotherium	podial	75.61	38.59	21.77
64481	UO-4605	Perissodactyla	Rhinoceratidae	Chilotherium	tooth fragments	33.2	9.4	3.57
64482	UO-4605	Perissodactyla	Rhinoceratidae	Chilotherium	astragalus fragment	44.45	38.45	32.86
64483	UO-4605	Perissodactyla	Rhinoceratidae	Chilotherium	carpal?	46.6	35.95	32
64484	UO-4605	Perissodactyla	Rhinoceratidae	Chilotherium	tooth frag	34.82	20.18	4.75
64485	UO-4605	Perissodactyla	Rhinoceratidae	Chilotherium	1/2 astragalus	79.7	42.58	29.15
64486	UO-4605	Perissodactyla	Rhinoceratidae	Chilotherium	tooth bit	31.39	17.14	4.01
64487	UO-4605	Perissodactyla	Rhinoceratidae	Chilotherium	unworn tooth fragments	36.72	17.8	12.23
64488	UO-4605	Perissodactyla	Rhinoceratidae	Chilotherium	distal tibia fragment	37.5	23.06	13.06
64489	UO-4605	Perissodactyla	Rhinoceratidae	Chilotherium	tooth frags	21.29	9.56	1.98
70324	UO-4605	Perissodactyla	Rhinoceratidae	tooth frag	36.63	12.91	5.7	
70335	UO-4605	Perissodactyla	Rhinoceratidae	Chilotherium	humerus	281	101.03	64.85
70337	UO-4605	Perissodactyla	Rhinoceratidae	tooth frag	18.73	9.37	2.33	
70342	UO-4605	Perissodactyla	Rhinoceratidae	tooth frags	23.16	14.86	2.14	
70345	UO-4605	Perissodactyla	Rhinoceratidae	tooth frags	18.47	16.97	7.88	
70347	UO-4605	Perissodactyla	Rhinoceratidae	tooth frags	26.3	12.8	7.07	
70348	UO-4605	Perissodactyla	Rhinoceratidae	astragalus fragment	59.08	40.11	29.8	
70349	UO-4605	Perissodactyla	Rhinoceratidae	distal femur fragment	42.44	24.08	20.63	
70350	UO-4605	Perissodactyla	Rhinoceratidae	distal metapodial frag	34.26	27.2	19.83	
70351	UO-4605	Perissodactyla	Rhinoceratidae	carpal	39.75	27.18	15.31	
70354	UO-4605	Perissodactyla	Rhinoceratidae	astragalus fragment	31.22	29.78	22.53	

70357	UO-4605	Perissodactyla	Rhinoceratidae	proximal humerus fragent		44.08	27.67	22.73	
70359	UO-4605	Perissodactyla	Rhinoceratidae	tooth fragments		43.62	19.8	7.65	
70360	UO-4605	Perissodactyla	Rhinoceratidae	Chilotherium	radius		70.09	68.93	42.4
70362	UO-4605	Perissodactyla	Rhinoceratidae	ooth fragment		9.22	4.09	2.2	
70363	UO-4605	Perissodactyla	Rhinoceratidae	tooth frag		27.69	11.84	3.47	
70365	UO-4605	Perissodactyla	Rhinoceratidae	tooth frags		20.07	9.99	3.68	
70374	UO-4605	Perissodactyla	Rhinoceratidae	astragalus fragment		58.42	49.46	26.7	
70375	UO-4605	Perissodactyla	Rhinoceratidae	tooth frags		26.73	15.1	5.15	
70385	UO-4605	Perissodactyla	Rhinoceratidae	tooth fragments		34.23	13.58	4.69	
70386	UO-4605	Perissodactyla	Rhinoceratidae	proximal humerus fragent		60.54	42	38.31	
70387	UO-4605	Perissodactyla	Rhinoceratidae	bone frag		49.36	40.68	30.83	
70388	UO-4605	Perissodactyla	Rhinoceratidae	distal femur fragment		50.19	35.57	23.14	
70389	UO-4605	Perissodactyla	Rhinoceratidae	tooth frag		42.65	15.51	3.16	
70391	UO-4605	Perissodactyla	Rhinoceratidae	tooth frags		23.05	13.6	6.6	
70394	UO-4605	Perissodactyla	Rhinoceratidae	tooth fragments		30.37	13.78	6.84	
70395	UO-4605	Perissodactyla	Rhinoceratidae	radius		70.01	66.9	26.89	
70397	UO-4605	Perissodactyla	Rhinoceratidae	tooth frags		21.71	8.68	3.27	
70399	UO-4605	Perissodactyla	Rhinoceratidae	tooth fragments		16	6.4	2.96	
70401	UO-4605	Perissodactyla	Rhinoceratidae	tooth frag		23.54	9.41	4.59	
70402	UO-4605	Perissodactyla	Rhinoceratidae	distal femur frag		49.86	41.27	22.62	
70403	UO-4605	Perissodactyla	Rhinoceratidae	proximal femur frag		46.5	28.68	24.93	
70404	UO-4605	Perissodactyla	Rhinoceratidae	patella		68.89	46.86	29.89	
70405	UO-4605	Perissodactyla	Rhinoceratidae	calcaneum		81.74	55.66	36.89	

70406	UO-4605	Perissodactyla	Rhinoceratidae	podial		37.68	23.55	19.98	
70407	UO-4605	Perissodactyla	Rhinoceratidae	podial		70.55	48.82	34.25	
70425	UO-4605	Perissodactyla	Rhinoceratidae	tooth frags		22.06	10.3	3.18	
70427	UO-4605	Perissodactyla	Rhinoceratidae	tooth frag		42.99	23.39	8.08	
70344	UO-4605	Perissodactyla		tooth scraps		11.67	10.16	5.49	
70353	UO-4605	Perissodactyla		distal tibia fragment		30.23	22.45	18.22	
70368	UO-4605	Perissodactyla		carpal		31.55	21.06	10.78	
70377	UO-4605	Perissodactyla		tooth frag		23.24	5.96	2.33	
64482	UO-4605				bone frags				
64483	UO-4605				unidentified piece		46.87	46.26	21.41
64484	UO-4605				small mandible fragment		23.21	12.51	4.74
70330	UO-4605				carpal fragment		27.81	16.76	10.72
70331	UO-4605				periotic capsul fragment		20.68	17.03	9.8
70332	UO-4605				fragment		35.13	30.57	22.49
70336	UO-4605						62.29	31.45	14.03
70352	UO-4605				bone		33.32	20.75	12.7
70358	UO-4605				bone frag		50.57	30.23	17.51
70361	UO-4605				tooth scraps		18.18	14.61	6.7
70366	UO-4605				frag		29.35	22.52	12.18
70367	UO-4605				frag		35.54	27.62	7.31
70369	UO-4605				frag		31.95	17.24	17.01
70370	UO-4605				frag		28.74	23.12	15.49
70371	UO-4605				frag		31.49	22.86	11.96
70376	UO-4605				proximal metapodial		28.62	18.89	11.05
70378	UO-4605				proximal metapodial frag		21.6	14.04	9.22
70379	UO-4605				carpal fragment		19.44	13.39	12.34
70383	UO-4605				podial frag		24.9	22.92	19.42
70392	UO-4605				periotic capsul fragment		20.08	12.42	9.54

70393	UO-4605			43.18	31.93	21.71
70408	UO-4605		frag	38.61	30.39	18.51
70409	UO-4605		frag	55.54	38.88	30.93
70410	UO-4605		frag	38.24	25.37	15.63
70411	UO-4605		frag	51.48	38.6	26.17
70412	UO-4605		frag	39.75	38.81	17.25
70413	UO-4605		frag	65.17	52.44	27.14
70414	UO-4605		frag	38.88	33.84	24.33
70415	UO-4605		frag	34.61	27	17.25
70416	UO-4605		frag	53.97	29.43	19.79
70417	UO-4605		frag	28.25	19.25	10.25
70418	UO-4605		frag	49.42	28.18	17.65
70419	UO-4605		frag	36.75	21.08	12.38
70420	UO-4605		frag	46.05	38.67	27.85
70421	UO-4605		frag	51.61	22.02	8.65
70422	UO-4605		frag	20.09	16.76	13.96
70426	UO-4605		frag	61.71	24.62	13.9
70428	UO-4605		frag	48.82	40.34	31.28
70429	UO-4605		frag	46.37	28.57	16.44
70430	UO-4605		frag	31.3	21.54	17.83
67906	UO-4605	Carnivora	canine tooth	28.16	13.58	8.76

APPENDIX C

BONE HILL BONE BED (UO-4601)

Specimen #	Locality #	Order	Family	Genus	element	L1	L2	L3
64376	UO-4601	Artiodactyla	Bovidae			10.41	6.41	3.75
64384	UO-4601	Artiodactyla	Bovidae		"Ryan's area"	39.97	31.75	6.05
64373	UO-4601	Artiodactyla	Bovidae			48.02	25.99	6.54
70451	UO-4601	Artiodactyla	Cervidae		was with F-64372, but bone not near each other, so association unknown	17.61	14.89	9.16
64565	UO-4601	Artiodactyla	Cervidae			18.32	7.18	5.38
70458	UO-4601	Artiodactyla	Cervidae		was with 64484, no direct evidence of association	18.89	16.96	14.92
64443	UO-4601	Artiodactyla	Cervidae			20.86	20.36	8.53
70456	UO-4601	Artiodactyla	Cervidae			20.97	9.89	8.63
70471	UO-4601	Artiodactyla	Cervidae			25	16.77	14.13
64353	UO-4601	Artiodactyla	Cervidae			25.84	18.54	8.56
64445	UO-4601	Artiodactyla	Cervidae		"ankle Logan"	31	25.08	18.26
64402	UO-4601	Artiodactyla	Cervidae			32.09	16.86	12.2
70446	UO-4601	Artiodactyla	Cervidae		"toes from Ryan 9/18/14"	34.97	23.51	12.82
64372	UO-4601	Artiodactyla	Cervidae			35.33	14.66	8.54

64441	UO-4601	Artiodactyla	Cervidae		"Meaghan's tooth row"	35.72	32.33	20.29
70452	UO-4601	Artiodactyla	Cervidae		was with 64392, split because not associated	37.77	30.89	17.34
70463	UO-4601	Artiodactyla	Cervidae		"Ryan's gazelle jaw :(9/18/14"	39	23.28	9.6
70439	UO-4601	Artiodactyla	Cervidae		"box 2 of 3"	39.04	30.99	12.04
70457	UO-4601	Artiodactyla	Cervidae		was with 64484, no direct evidence of association	42.15	32.05	10.7
64392	UO-4601	Artiodactyla	Cervidae			44.08	24.67	16.47
64375	UO-4601	Artiodactyla	Cervidae		base of cervid antler	44.9	38.52	28.52
64346	UO-4601	Artiodactyla	Cervidae			49.7	14.17	8.63
64484	UO-4601	Artiodactyla	Cervidae		tooth impression Ryan's area	55.67	53.45	5
64488	UO-4601	Artiodactyla	Cervidae			61.16	19.18	16.08
64545	UO-4601	Artiodactyla	Cervidae			61.7	25.6	10.91
70454	UO-4601	Artiodactyla	Cervidae		artiodactyl metapodial	69.44	20.19	10.91
70443	UO-4601	Artiodactyla	Cervidae		"Logan sept 11"	76.76	24.93	12.28
64368	UO-4601	Artiodactyla	Cervidae		"Ryan's jaw 3"	90.31	30.09	9.73
64348	UO-4601	Artiodactyla	Cervidae			134	23.16	13.18
70432	UO-4601	Artiodactyla	Cervidae		"WNFM-K-o814-08 Box 3 of 3"	153	20.45	16.46
70474	UO-4601	Artiodactyla			same batch as X1 below	14.24	8.23	2.58
70482	UO-4601	Artiodactyla			X1	15.77	9.09	8.58

64350	UO-4601	Artiodactyla			Kyle bovid horn	136	22.07	17.27
70472	UO-4601	Perissodactyla	Equidae	Hipparion	kyles horse tooth bits 9/18/19	19	16.77	13.89
64548	UO-4601	Perissodactyla	Equidae	Hipparion		24.57	16.35	10.92
64538	UO-4601	Perissodactyla	Equidae	Hipparion		36.49	16.86	10.05
64608	UO-4601	Perissodactyla	Equidae	Hipparion		37.43	21.18	15.57
64609	UO-4601	Perissodactyla	Equidae	Hipparion	"horse jaw" from Bone Hill	93.73	45.15	17.82
70460	UO-4601	Perissodactyla	Equidae	Hipparion	all teeth by m3 erupted and in wear	190	73.87	63.75
64463	UO-4601	Perissodactyla	Equidae	Hipparion		238	21.82	6.21
64393	UO-4601	Perissodactyla	Equidae			18.05	7.23	4.46
70467	UO-4601	Perissodactyla	Equidae			19.41	18.43	9.22
64379	UO-4601	Perissodactyla	Equidae		"Ryan's podials"	31.72	23.58	16.08
70495	UO-4601	Perissodactyla	Equidae		"Kyle's pawny toof" 9/18/11	32.01	22.88	21.29
70465	UO-4601	Perissodactyla	Equidae			46.94	37.89	21.84
70492	UO-4601	Perissodactyla	Equidae			68.13	49.75	33.52
70444	UO-4601	Perissodactyla	Equidae		"Logan sept 11"	82.07	48.67	39.17
64425	UO-4601	Perissodactyla	Rhinoceratidae	Chilotherium		23.29	9.58	8.13
64428	UO-4601	Perissodactyla	Rhinoceratidae	Chilotherium		38.62	37.05	19.03
64493	UO-4601	Perissodactyla	Rhinoceratidae	Chilotherium		73.44	62.02	35.73

70503	UO-4601	Perissodactyla	Rhinoceratidae	Chilotherium	split off of 64554		79.28	58.86	52.59
70500	UO-4601	Perissodactyla	Rhinoceratidae	Chilotherium	split off of 64554		105.09	54.9	32.42
64614	UO-4601	Perissodactyla	Rhinoceratidae	Chilotherium			109.36	88.07	38.29
64554	UO-4601	Perissodactyla	Rhinoceratidae	Chilotherium			195	130.7	110.98
64371	UO-4601	Perissodactyla	Rhinoceratidae			13.8	12.26	7.1	
64397	UO-4601	Perissodactyla	Rhinoceratidae			19.56	10.29	7.44	
70447	UO-4601	Perissodactyla	Rhinoceratidae	"toes from Ryan 9/18/14"		22.4	8.32	4.4	
70499	UO-4601	Perissodactyla	Rhinoceratidae			23.29	16.26	8.41	
70469	UO-4601	Perissodactyla	Rhinoceratidae			29.02	19.92	13.66	
70466	UO-4601	Perissodactyla	Rhinoceratidae			29.16	17.43	15.77	
70478	UO-4601	Perissodactyla	Rhinoceratidae	X1		29.19	16.32	7.42	
70438	UO-4601	Perissodactyla	Rhinoceratidae	"Zack=h's rhino tooth w/ horse tooth"		36.89	31.99	27.37	
70433	UO-4601	Perissodactyla	Rhinoceratidae	"WNFM-K-o814-08 Box 3 of 3"		38.93	37.31	25.35	
64499	UO-4601	Perissodactyla	Rhinoceratidae			54.17	44.28	21.38	
70437	UO-4601	Perissodactyla	Rhinoceratidae	" o814-08 Box 3 of 3"		55.05	33.09	20.26	
70464	UO-4601	Perissodactyla	Rhinoceratidae	"9/18/14"		69.52	39.95	39.83	

70468	UO-4601	Perissodactyla	Rhinoceratidae			74.81	46.7	39.17	
70502	UO-4601	Perissodactyla	Rhinoceratidae	"tibia in five pieces"		153.53	70.42	45.96	
70442	UO-4601	Perissodactyla		"Logan sept 11"		280	55.57	25.52	
70498	UO-4601						2.74	2.59	0.2
70449	UO-4601				"toes from Ryan 9/18/14"		8.75	6.76	3.91
64439	UO-4601						9.52	5.8	3.94
70448	UO-4601				"toes from Ryan 9/18/14"		10.64	8.56	7.37
70487	UO-4601				X1		10.79	10.18	5.21
70485	UO-4601				X1		11.16	9.03	2
70486	UO-4601				X1		11.55	7.69	7.32
70481	UO-4601				X1		11.93	7.09	3.97
70488	UO-4601				X1		13.13	9.73	4.77
70483	UO-4601				X1		14.03	11.54	9.78
70484	UO-4601				X1		16.26	10.96	6.16
70470	UO-4601						18.21	15.31	7.24
70455	UO-4601				was with F-64402		20.86	13.69	8.16
70480	UO-4601				X1		21.13	16	14.12
70479	UO-4601				X1		22.01	20.7	12.93

70475	UO-4601	X1	22.2	14.24	11.36
70453	UO-4601	was with F-64350	24.12	9.3	3.92
70450	UO-4601	"toes from Ryan 9/18/14"	24.21	11.48	9.95
70493	UO-4601		25.57	24.3	11.54
64349	UO-4601		25.96	20.46	8.73
70496	UO-4601		29.57	18.35	8.67
70473	UO-4601	was with F-70472, not associated	30.07	17.82	8.13
70445	UO-4601	"Logan sept 11"	33.37	32.07	25.47
70494	UO-4601		33.91	24.68	23.64
70436	UO-4601	"WNFM-K-o814-08 Box 3 of 3"	35.06	23.43	13.07
70477	UO-4601	X1	35.55	31.04	9.16
70434	UO-4601	"WNFM-K-o814-08 Box 3 of 3"	35.65	26.53	17.88
70491	UO-4601	with last F#	39.01	38.67	17.34
70489	UO-4601	new batch	42.43	34.42	24.95
70435	UO-4601	"WNFM-K-o814-08 Box 3 of 3"	46.11	33.11	19.48
70490	UO-4601	with last F#	47.75	27.59	22.74
70497	UO-4601		55.36	40.12	19.51
70476	UO-4601	X1	60.97	46.52	26.94

70440	UO-4601				"box 2 of 3"	67.15	35.77	31.89
70441	UO-4601					142.59	69.65	17.5
64341	UO-4601	Squamata	Varanidae	Varanus	mandible	30.7	6.28	5.38

APPENDIX D

DAM SITE BONE BED (UO-4604)

Specimen #	Locality #	Order	Family	Genus	element	L1	L2	L3
64509	UO-4604	Artiodactyla	Bovidae	Gazella	base of horn core	31.88	24.71	21.33
64639	UO-4604	Artiodactyla	Bovidae	Gazella	partial jaw with 1 partial tooth	34.93	25.06	10.24
64618	UO-4604	Artiodactyla	Bovidae	Gazella	basal horn core	36.3	24.76	18.2
64457	UO-4604	Artiodactyla	Bovidae	Gazella	horn core	67.08	25.96	19.75
71402	UO-4604	Artiodactyla	Bovidae	Gazella	horn core	68.01	25.89	21.28
70340	UO-4604	Artiodactyla	Bovidae	Gazella	two horn cores and associated imprint. From bag “rhino radius and stuff”	69.8	24.01	20.5
64539	UO-4604	Artiodactyla	Bovidae	Gazella	two horn cores and associated imprint. From bag “rhino radius and stuff”	102.25	25.03	18.61
71404	UO-4604	Artiodactyla	Bovidae	Gazella	horn core	102.28	25.58	18.25
71403	UO-4604	Artiodactyla	Bovidae	Gazella	horn core	104.07	23.89	19.2
71405	UO-4604	Artiodactyla	Bovidae	Gazella	horn core	119.79	21.28	18.85
64462	UO-4604	Artiodactyla	Bovidae	Gazella	horn core	127.08	26.65	17.81
64463	UO-4604	Artiodactyla	Bovidae		tooth frag	8.52	6.93	3.58
70326	UO-4604	Artiodactyla	Bovidae		partial jaw w/ m3-m1	44.98	23.51	8.46

64542	UO-4604	Lagomorpha		tooth frag	5.49	3.03	2.01	
70321	UO-4604	Lagomorpha		incissors	10.93	3.2	2.67	
70320	UO-4604	Lagomorpha		partial skull, front w/incissors. Pika.	14.6	7.2	2.38	
64363	UO-4604	Lagomorpha		bunny jaw	16.99	15.43	5.31	
64460	UO-4604	Lagomorpha		two distal humeri, calcaneous, other bone bits	20.83	10.63	5.04	
64452	UO-4604	Lagomorpha		small bones, mostly rabbit, but I think there is some rodent mixed in	77.12	14.28	4.36	
64453	UO-4604	Perissodactyla	Equidae	Hipparion	jaw fragment with 4 teeth	99.98	56.92	13.48
64504	UO-4604	Perissodactyla	Equidae		distal tibia	59.39	36.87	28.44
64423	UO-4604	Perissodactyla	Rhinoceratidae	Chilotherium	rhino tooth bit	38.68	19.5	14.91
64540	UO-4604	Perissodactyla	Rhinoceratidae	Chilotherium	metacarpal bit and other bit	39.49	33.71	30.04
64544	UO-4604	Perissodactyla	Rhinoceratidae	Chilotherium	distal metapodial from bag “rhino radius and shit”	53.98	41.77	31.32
70462	UO-4604	Perissodactyla	Rhinoceratidae	Chilotherium	patella	93.12	81.24	19.8
64617	UO-4604	Perissodactyla	Rhinoceratidae	Chilotherium	ulna thing?	95.68	75.9	71.38

70461	UO-4604	Perissodactyla	Rhinoceratidae	Chilotherium	proximal radius	99.77	81.56	38.18
64637	UO-4604	Perissodactyla	Rhinoceratidae	Chilotherium	proximal tibia	115.24	106.35	85.29
64489	UO-4604	Perissodactyla	Rhinoceratidae	Chilotherium	distal radius with articulated carpals	149.44	79.85	48.82
64624	UO-4604	Perissodactyla	Rhinoceratidae	Chilotherium	distal tibia and tiny bit of astragalus	170	88.06	45.45
64526	UO-4604	Perissodactyla	Rhinoceratidae	Chilotherium	whole radius	253	88.03	30.99
64638	UO-4604	Perissodactyla	Rhinoceratidae	Chilotherium	proximal radius and ulna	262	89.37	36.13
70501	UO-4604	Perissodactyla	Rhinoceratidae	astragalus	62.21	42.12	32.71	
70502	UO-4604	Perissodactyla	Rhinoceratidae	proximal radius	96.41	83.7	32.08	
64557	UO-4604				small thing… rodent?	10.12	6.54	5.69
64620	UO-4604				composite of a lot of crap	40.79	34.53	31.52
64619	UO-4604				proximal metapodial	55.19	27.36	19.28
70322	UO-4604				little things, will be sorted more….			

APPENDIX E

UNCORRECTED STRIKE AND SUN COMPASS READINGS

Sample #	**Azimuth**	**Sun compass**	**Difference**	**Average error by section**
KSS-001	no Brunton	139.3		
KSS-002	no Brunton	157.6		
KSS-003	no Brunton	113.6		
KSS-011	160	89.4	70.6	
KSS-022	194	136.8	57.2	
KSS-023	181	135.6	45.4	
KSS-024	219	108	111	
KSS-025	168	178.5	10.5	
KSS-026	186	152.2	33.8	
KSS-028	181	178.9	2.1	
KSS-029	159	198.9	39.9	
KSS-030	178	201.6	23.6	
KSS-032	177	189.6	12.6	
KSS-033	249	141.6	107.4	
KSS-034	264	125.7	138.3	
				54.36666667
KDS-001	238	239.3	1.3	
KDS-002	240	242.4	2.4	
KDS-003	285	208	77	
KDS-004	252	240.3	11.7	
KDS-005	274	226.1	47.9	
KDS-006	242	261.3	19.3	
KDS-007	200	314	114	
KDS-008	180	324.8	144.8	
KDS-009	218	295.8	77.8	
KDS-010	254	242.9	11.1	
KDS-011	213	269.3	56.3	
KDS-012	256	270.7	14.7	
KDS-013	255	287.4	32.4	

KDS-014	258	286.4	28.4	
KDS-015	277	275.7	1.3	
KDS-016	9	4.1	4.9	
KDS-017	21	341.1	39.9	
KDS-018	21	21.1	0.1	
KDS-019	356	17.6	21.6	
KDS-020	354	24	28	
KDS-021	9	17.3	8.3	
KDS-044	144	229.8	85.8	
KDS-045	165	248.6	83.6	
KDS-046	213	245.4	32.4	
KDS-047	182	239	57	
KDS-048	210	218.8	8.8	
KDS-049	174	260	86	
KDS-050	155	274.2	119.2	
KDS-051	156	276.1	120.1	
KDS-052	110	14.4	95.6	
KDS-054	111	10.2	100.8	
				49.43548387
KO-009	100	102.9	2.9	
KO-010	101	105	4	
KO-011	112	95.5	16.5	
KO-012	102	109.5	7.5	
KO-013	131	82.8	48.2	
KO-014	110	108.3	1.7	
				13.46666667
KSU-011	207	169.7	37.3	
KSU-012	187	182	5	
KSU-013	190	182.3	7.7	
KSU-100	140	87.8	52.2	
KSU-101	137	87.7	49.3	
KSU-102	164	74.3	89.7	
KSU-103	155	79.5	75.5	
KSU-104	160	78.4	81.6	
KSU-105	128	99	29	
KSU-106	155	87.9	67.1	
KSU-107	157	95.7	61.3	
KSU-108	25	328	57	
KSU-109	10	75.2	65.2	

KSU-110	20	77.4	57.4	
KSU-020	135	148.8	13.8	
KSU-021	140	84.7	55.3	
KSU-022	139	86.9	52.1	
KSU-026	351	-35.6	44.6	
KSU-027	355	331.5	23.5	
KSU-028	0	-37.6	37.6	
KSU-029	129	181.6	52.6	
KSU-030	134	175	41	
KSU-031	136	185.8	49.8	
KSU-111	91	61.2	29.8	
KSU-112	111	35.7	75.3	
KSU-113	135	199.5	64.5	
KSU-114	166	172.8	6.8	
KSU-115	156	186.5	30.5	
KSU-116	173	171.9	1.1	
KSU-050	32	327.1	64.9	
KSU-051	35	95	60	
KSU-052	49	125.6	76.6	
KSU-053	64	132.2	68.2	
KSU-054	64	127.2	63.2	
KSU-055	79	123.4	44.4	
KSU-056	74	144.1	70.1	
KSU-057	74	126.1	52.1	
KSU-058	79	127.5	48.5	
KSU-059	96	107.8	11.8	
KSU-060	125	78.4	46.6	
KSU-061	122	79.5	42.5	
KSU-062	42	356.7	45.3	
KSU-063	53	345.6	67.4	
KSU-064	89	130.6	41.6	
KSU-065	19	106.2	87.2	
KSU-066	33	21.6	11.4	
KSU-067	41	25.4	15.6	
				48.5

APPENDIX F

P-MAG SAMPLE COLLECTION FIELD DATA

LOCATION	SAMPLE #	ROTATION	STIKE	DIP	LITHOLOGY
KSS	KSS-001	+1			siltstone below red layer
	KSS-002	+5			siltstone below red layer
	KSS-003	+3			siltstone below red layer
	KSS004	-5	S51E	50°	reddish siltstone
	KSS005	+3	S65E	35°	reddish siltstone
	KSS006	0	S47E	36°	reddish siltstone
	KSS007	+4	S57.5E	40°	2m up from red
	KSS008	-3	S71E	42.5°	2m up from red
	KSS009	+12	S48E	43.5°	2m up from red
	KSS010	-1	S19E	46°	mud stone with yellow altered material
	KSS011	+2	S20E	51°	mud stone with yellow altered material
	KSS012	+2	S24E	53°	mud stone with yellow altered material
	KSS013	+14	S15E	43.5°	slightly sand grey siltstone
	KSS014	-3	S64E	45°	slightly sand grey siltstone
	KSS015	-3	N75E	39°	slightly sand grey siltstone
	KSS016	+11	S24E	56.5°	red claystone thin band
	KSS017	-7	S22W	46.5°	grey claystone
	KSS018	-4	S34E	50°	grey claystone
	KSS019	0	S38W	67.5°	brick red paleosol
	KSS020	+6	S1E	49°	brick red paleosol
	KSS021	-5	S62W	45°	brick red paleosol
	KSS022	+8	S14W	50°	tannish grey siltstone
	KSS023	+17	S1W	48°	tannish grey siltstone
	KSS024	+3	S39W	55°	tannish grey siltstone
	KSS025	+2	S12E	57.5°	sandy siltstone
	KSS026	+25	S6W	47°	sandy siltstone
	KSS027	+10	S8E	44°	sandy siltstone
	KSS028	+23	S1W	45°	greyish greenish siltstone
	KSS029	+7	S21E	35°	greyish greenish siltstone
	KSS030A	+20	S30E	35°	greyish greenish siltstone
	KSS030	-10	S2E	52.5°	red sandy claystone
	KSS031	-5	240E	53°	red sandy claystone
	KSS032	+3	S3E	47°	red sandy claystone
	KSS033	+5	S69W	44°	dark red siltstone

	KSS034	-7	S84W	55°	dark red siltstone
	KSS035	0	N58W	47°	dark red siltstone
	KSS036	+17	S18W	58.5	sandy greyish tan layer
	KSS037	-3	S42W	65°	sandy greyish tan layer
	KSS038	-2	S54W	65°	sandy greyish tan layer
KDS	KDS-001	-17	S58W	36°	brown shaley layer below sandstone
	KDS-002	-20	S60W	52°	brown shaley layer below sandstone
	KDS-003	-13	N75W	45°	brown shaley layer below sandstone
	KDS-004	-9	S72W	30°	brown shaley layer below sandstone
	KDS-005	-15	N86W	38°	brown shaley layer below sandstone
	KDS-006	-18	S62W	63°	brown shaley layer below sandstone
	KDS-007	+3	S20W	54°	brown shaley layer below sandstone
	KDS-008	+5	S0	44°	brown shaley layer below sandstone
	KDS-009	+6	S38W	38°	brown shaley layer below sandstone
	KDS-010	-32	S74W	40°	brown shaley layer below sandstone
	KDS-011	-6	S33W	46.5°	brown shaley layer below sandstone
	KDS-012	-10	S76W	50°	brown shaley layer below sandstone
	KDS-013	+5	S75W	44°	brown shaley layer below sandstone
	KDS-014	-8	S78W	44°	brown shaley layer below sandstone
	KDS-015	0	N83W	39°	brown shaley layer below sandstone
	KDS016	+14	S9W	55°	red paleosol
	KDS017	+10	S21W	49°	red paleosol
	KDS018	+4	S21W	45°	red paleosol
	KDS-019	+1	S4E	43°	red paleosol
	KDS-020	+3	S6E	28°	red paleosol
	KDS-021	-4	S9W	30°	red paleosol
	KDS-022	+7	S60W	47°	red paleosol
	KDS-023	+1	S68W	34°	red paleosol
	KDS-024	+1	S50W	43°	red paleosol
	KDS-025	+13	S60W	37°	red paleosol
	KDS-026	+8	S47W	42°	red paleosol
	KDS-027	+8	S65W	35°	red paleosol
	KDS-028	+5	S0	64°	grey paleosol below a thick sandstone
	KDS-029	+3	S11E	62°	grey paleosol below a thick sandstone
	KDS-030	0	S24W	70°	grey paleosol below a thick sandstone
	KDS-031	+10	S86W	52°	reddish brown paleosol
	KDS-032	0	S62W	63°	reddish brown paleosol
	KDS-033	+10	N64W	46°	reddish brown paleosol
	KDS-034	-18	S9W	51°	greenish siltstone, fossil bed layer
	KDS-035	-20	S12E	49°	greenish siltstone, fossil bed layer

	KDS-036	-20	S2W	50°	greenish siltstone, fossil bed layer
	KDS-037	-4	S25W	62°	reddish clayey siltstone
	KDS-038	-9	S15W	60°	reddish clayey siltstone
	KDS-039	-6	S39W	52°	reddish clayey siltstone
	KDS-040	+18	N73W	45°	silty sandstone
	KDS-041	-11	N43W	46°	silty sandstone
	KDS-042	-3	N44W	62°	silty sandstone
	KDS-043	-11	S12E	56°	dark brown clayey paleosol
	KDS-044	-3	S6E	64°	dark brown clayey paleosol
	KDS-045	+5	S15E	68°	dark brown clayey paleosol
	KDS-046	-8	S33W	59°	brown paleosol
	KDS-047	+5	S2W	65°	brown paleosol
	KDS-048	0	S30W	60°	brown paleosol
	KDS-049	-4	S6E	47°	red brown blocky paleosol
	KDS-050	-1	S25E	59°	red brown blocky paleosol
	KDS-051	0	S24E	60°	red brown blocky paleosol
	KDS-052	-12	S70E	35°	red brown blocky paleosol
	KDS-053	+1	S68E	38°	red brown blocky paleosol
	KDS-054	+3	S69E	29°	red brown blocky paleosol
	KDS-055	-15	S12W	33°	reddish paleosol
	KDS-056	-4	S8W	44°	reddish paleosol
	KDS-057	-3	S44W	43°	reddish paleosol
	KDS-058	-9	S17E	29°	sandy silt layer
	KDS-059	0	S17W	30°	sandy silt layer
	KDS-060	0	S13W	44°	sandstone
	KDS-061	-3	S25W	34°	sandstone
	KDS-062	+1	S27W	39°	sandstone
	KDS-063	0	N1W	39°	reddish brown paleosol above sandstone
	KDS-064	-5	N3W	35°	reddish brown paleosol above sandstone
	KDS-065	+9	N4E	29°	reddish brown paleosol above sandstone
	KDS-066	0	N55E	29°	brownish tan paleosol
	KDS-067	-3	S60W	27°	brownish tan paleosol
	KDS-068	0	S70W	22°	brownish tan paleosol
	KDS-068A	-5	S41W	45°	sandy silt layer
KO	KO-001	+9	N34E	24°	tan siltstone
	KO-002	-3	N60E	29°	tan siltstone
	KO-003	-4	N67E	17°	tan siltstone
	KO-004	+15	S75E	48°	siltstone with some bands of oxidized material
	KO-005	+4	S83E	54°	siltstone with some bands of oxidized material
	KO-006	+3	279E	46°	siltstone with some bands of oxidized material

KO-007	+4	S75E	57°	tan siltstone
KO-007A	+4	S75E	57°	tan siltstone
KO-008	-15	S88E	41°	tan siltstone
KO-009	+8	S80E	58°	tan/grey siltstone with oxidized bands
KO-010	-15	S79E	53°	tan/grey siltstone with oxidized bands
KO-010A	-15	S79E	53°	tan/grey siltstone with oxidized bands
KO-011	+10	S68E	51°	tan/grey siltstone with oxidized bands
KO-011A	+10	S68E	51°	tan/grey siltstone with oxidized bands
KO-012	+4	S78E	43°	tan/grey siltstone with oxidized bands
KO-013	-18	S49E	49°	tan/grey siltstone with oxidized bands
KO-014	0	S70E	48°	tan/grey siltstone with oxidized bands
KO-015	-10	S74E	53°	tan/grey siltstone with oxidized bands
KO-16	-10	S67E	49°	tan/grey siltstone with oxidized bands
KO-17	-10	S76E	40°	tan/grey siltstone with oxidized bands
KO-18	-20	S71E	44°	tan/grey siltstone with oxidized bands
KO-19	-5	S68E	59°	tan/grey siltstone with oxidized bands
KO-19A	-5	S68E	59°	tan/grey siltstone with oxidized bands
KO-20	0	S72E	50°	tan/grey siltstone with oxidized bands
KO-21	+17	S66E	53°	tan/grey siltstone with oxidized bands
KO-22	-10	S74E	44°	tan/grey siltstone with oxidized bands
KO-23	-8	S62E	41°	tan/grey siltstone with oxidized bands
KO-24	-5	S69E	63°	tan siltstone with orange oxidized banding, platier peds
KO-25	-10	S74E	50°	tan siltstone with orange oxidized banding, platier peds
KO-26	+4	S70E	49°	tan siltstone with orange oxidized banding, platier peds
KO-27	-16	S55E	45°	tan siltstone with some clastic material present
KO-28	+5	S67E	29°	tan siltstone with some clastic material present
KO-29	0	S70E	48°	tan siltstone with some clastic material present
KO-30	+5	S81E	58°	tan siltstone, platy peds
KO-31	-3	S72E	54°	tan siltstone, platy peds
KO-32	0	S68E	38°	tan siltstone, platy peds
KO-33	-12	S62E	64°	yellowish tan siltstone
KO-34	-10	S54E	32°	yellowish tan siltstone
KO-35	-4	S65E	47°	yellowish tan siltstone
KO-36	+3	S66E	61°	yellowish silts with oxidized bands
KO-37	0	S65E	54°	yellowish silts with oxidized bands
KO-38	-15	S64E	45°	yellowish silts with oxidized bands
KO-39	-9	S65E	48°	light brown siltstone
KO-40	+5	S46E	40°	light brown siltstone
KO-41	-10	S45E	46°	light brown siltstone

	KO-42	-6	S58E	44°	grey/tan/orange banded silts
	KO-43	-3	S69E	43°	grey/tan/orange banded silts
	KO-44	-4	S64E	68°	grey/tan/orange banded silts
	KO-45	-8	S51E	43°	grey/tan/orange banded silts
	KO-46	-5	S80E	44°	grey/tan/orange banded silts
	KO-47	-5	S81E	68°	grey/tan/orange banded silts
KU	KU-115	-2	S24E	38°	reddish siltstone
	KU-116	-2	S7E	37°	reddish siltstone
	KU-113	+13	S45E	37°	reddish siltstone
	KU-114	+1	S14E	33°	reddish siltstone
	KU-111	+10	S89E	39°	siltstone
	KU-112	-3	S69E	43°	siltstone
	KU-108	-3	N25E	56°	silt with granule sized clastic component
	KU-109	-5	N10E	54°	silt with granule sized clastic component
	KU-110	-10	N20E	45°	silt with granule sized clastic component
	KU-105	0	S52E	47°	sandy silt layer
	KU-106	+20	S25E	34°	sandy silt layer
	KU-107	0	S23E	36°	sandy silt layer
	KU-102	-8	S16E	48°	sandy silt layer
	KU-103	+8	S25E	50°	sandy silt layer
	KU-104	-10	S20E	42°	sandy silt layer
	KU-100	+9	S40E	41°	reddish sandy silt
	KU-101	0	S43E	40°	reddish sandy silt
	KU-101A	0	S43E	40°	reddish sandy silt
	KU-01	-10	N70W	58°	tan silt with abundant granule sized clastic material
	KU-02	-20	N43W	46°	tan silt with abundant granule sized clastic material
	KU-03	+8	N25W	48°	tan silt with abundant granule sized clastic material
	KU-04	-5	N29W	42°	tan silt with abundant granule sized clastic material
	KU-5	+5	S36W	48°	sandy silt inbetween two gravel layers
	KU-6	0	S6E	43°	sandy silt inbetween two gravel layers
	KU-7	-15	S16W	36°	sandy silt inbetween two gravel layers
	KU-8	+5	S12W	46°	sandy silt 1m above gravel layer
	KU-9	+10	S0	44°	sandy silt 1m above gravel layer
	KU-10	-15	S13W	47°	sandy silt 1m above gravel layer
	KU-11	+5	S27W	45°	sandy siltstone
	KU-12	-10	S7W	34°	sandy siltstone
	KU-13	+8	S10W	49°	sandy siltstone
	KU-14	+6	S24E	45°	sandy siltstone with some sand layers

	KU-15	-10	S10E	52°	sandy siltstone with some sand layers
	KU-16	-15	S25E	48°	sandy siltstone with some sand layers
	KU-20	0	S45E	36°	reddish sandy siltstone
	KU-21	-14	S40E	43°	reddish sandy siltstone
	KU-22	0	S41E	45°	reddish sandy siltstone
	KU-23	-18	N51E	55°	reddish paleosol
	KU-24	-10	N61E	50°	reddish paleosol
	KU-25	-20	N57E	45°	reddish paleosol
	KU-26	-20	N9W	57°	reddish paleosol
	KU-27	+8	N5W	49°	reddish paleosol
	KU-28	0	N	48°	reddish paleosol
	KU-29	+16	S51E	35°	siltstone at base of gravel
	KU-30	+6	S46E	34°	siltstone at base of gravel
	KU-31	0	S44E	28°	siltstone at base of gravel
	KU-50	+10	N32E	43°	reddish sandy siltstone
	KU-51	+8	N35E	57°	reddish sandy siltstone
	KU-52	0	N49E	78°	reddish sandy siltstone
	KU-53	-5	N64E	56°	brownish paleosol interbed
	KU-54	+3	N64E	57°	brownish paleosol interbed
	KU-55	+3	N74E	41°	brownish paleosol interbed
	KU-56	-2	N54E	41°	clayey silt, brown with green gley
	KU-57	+20	N74E	37°	clayey silt, brown with green gley
	KU-58	+3	N79E	48°	clayey silt, brown with green gley
	KU-59	+15	S84E	36°	sandy silts with carbonate nodules
	KU-60	-9	S55E	50°	sandy silts with carbonate nodules
	KU-61	+3	S58E	51°	sandy silts with carbonate nodules
	KU-62	+10	N42E	28°	poorly sorted orangish tan material with clay to sand
	KU-63	+25	N53E	31°	poorly sorted orangish tan material with clay to sand
	KU-64	+10	N89E	27°	poorly sorted orangish tan material with clay to sand
	KU-65	+17	N19E	39°	sandstone
	KU-66	+3	N33E	28°	sandstone
	KU-67	0	N41E	21°	sandstone
	KU-68	+2	N42E	46°	redish brown clay with metavolcanic components (Chu Like)
	KU-69	-3	N44E	50°	redish brown clay with metavolcanic components (Chu Like)
	KU-70	-5	N41E	58°	redish brown clay with metavolcanic components (Chu Like)
	KU-71	-13	N34E	48°	sandy siltstone
	KU-72	-30	N26E	40°	sandy siltstone

KU-73	-15	N31E	42°	sandy siltstone
KU-74	-1	N3E	34°	siltstone with clastic material
KU-75	+15	N24E	29°	siltstone with clastic material
KU-76	10	N52E	31°	siltstone with clastic material
KU-77	+8	N40E	32°	siltstone with clastic material
KU-78	+11	N34E	39°	siltstone with clastic material
KU-79	0	N30E	38°	siltstone with clastic material
KU-150	+20	S33W? 9wrong side)	42°	tan siltstone
KU-151	+15	N62E	37°	tan siltstone
KU-152	+6	N70E	38°	tan siltstone
KU-153	+15	N77E	30°	sandy siltstone
KU-154	+24	N84E	62°	sandy siltstone
KU-155	+15	N74E	33°	sandy siltstone
KU-156	+13	N40E	46°	red paleosol
KU-157	+17	N57E	34°	red paleosol
KU-158	+6	N73E	34°	red paleosol
KU-159	+15	N61E	32°	reddish sandy siltstone
KU-160	+8	N70E	48°	reddish sandy siltstone
KU-161	-10	N86E	31°	reddish sandy siltstone
KU-162	+30	N13E	22°	siltstone
KU-163	-13	N66E	26°	siltstone
KU-164	+15	N36E	33°	siltstone
KU-165	+17	N26W	39°	reddish brown paleosol
KU-166	+13	N9W	30°	reddish brown paleosol
KU-167	-11	N44E	30°	brown siltstone
KU-168	+13	N27E	29°	brown siltstone
KU-169	+20	N32E	31°	brown siltstone

APPENDIX G

SQR FILE FOR ORTOK WITH RATINGS

#	Sample		path							degree	180	Geo	RATING	N/R
37	KO-001	L	int	189.8	-48.3	202.8	-41.0	D-I	6	14	X	9.8		
38	KO-001	L	pri	167.7	-82.6	230.5	-73.3	I-N	6	14.3	X	347.7	A2	R
39	KO-001	L	ovr	187.4	-44.1	199.1	-37.3	B-I	8	13.8	X	7.4		
40	KO-002	L	int	356.4	49.3	11.9	44.7	B-H	7	10.6				
41	KO-002	L	ovr	357.4	49.6	12.9	44.8	BCE-H	6	10.6				
42	KO-002	L	vrm	180.4	-56.5	199.3	-50.6	AB	2	0				
43	KO-002	L	pri	18.1	66.4	38.9	56.3	H-N	7	9.1			A1	N
44	KO-001	L	vrm	343.5	59.6	7.9	57.3	AB	2	0				
45	KO-003	L	vrm	152.1	-72.6	197.8	-70.3	AB	2	0				
46	KO-003	L	ovr	2.8	71.0	33.7	63.1	B-H	7	11.3				
47	KO-003	L	pri	318.6	70.1	3.2	71.8	H-MN	7	7.5			A1	N
48	KO-004	L	vrm	344.4	37.7	356.0	36.8	AB	2	0	X	164.4		
49	KO-004	L	ovr	207.5	5.4	205.5	14.1	B-F	5	7.1	X	27.5		
50	KO-004	L	pri	174.8	-7.8	176.5	-5.6	G-N	8	4.8	X	354.8	A2	N
51	KO-005	L	vrm	176.9	-35.5	186.6	-31.6	AB	2	0				
52	KO-005	P	ovr	61.8	27.3	63.3	12.4	B-F	5	7.5				
53	KO-005	L	pri	350.5	66.5	20.3	61.6	G-N	8	3.1			A1	N
54	KO-006	L	vrm	187.2	-44.1	198.9	-37.5	AB	2	0				
55	KO-006	L	ovr	10.2	48.6	22.9	40.6	B-G	6	10.6				
56	KO-006	L	pri	5.3	55.4	22.6	48.5	G-N	8	4.5			A1	N
57	KO-008	L	vrm	168.2	-48.2	184.2	-45.7	AB	2	0				
58	KO-008	P	ovr	175.4	48.8	157.8	48.8	B-H	7	15.7				
59	KO-008	L	pri	0.2	57.0	19.4	51.1	I-N	6	11.1			A1	N
60	KO-010	L	vrm	174.5	-37.8	185.3	-34.5	AB	2	0				
61	KO-010	P	ovr	87.0	-17.4	88.2	-32.5	B-GN	7	15.8				
62	KO-010	L	pri	3.2	21.8	8.2	17.0	G-N	8	6			A2	N
63	KO-010A	L	vrm	187.8	-37.0	196.9	-30.5	AB	2	0				
64	KO-010A	L	ovr	43.6	17.6	45.2	5.6	B-G	6	12.8				
65	KO-010A	P	pri	181.0	67.2	145.5	66.0	H-N	7	10				
66	KO-011A	L	vrm	236.8	-31.3	239.0	-17.1	AB	2	0				
67	KO-011A	P	ovr	352.2	48.2	8.0	45.1	B-F	5	9.6				

68	KO-011A	P	pri	318.5	20.8	324.6	27.2	I-N	6	11.7			B2	N
69	KO-011A	L	int	18.5	21.7	22.4	13.3	F-I	4	6.6				
70	KO-012	L	vrm	177.7	-45.9	191.4	-41.3	AB	2	0				
71	KO-012	P	ovr	170.8	47.2	155.8	46.9	B-G	6	9.8				
72	KO-012	P	int	59.2	-20.1	236.8	34.2	G-K	5	10.4				
73	KO-012	P	pri	356.5	-8.2	353.9	-10.4	K-N	4	18.2			B2	N
74	KO-014	L	vrm	241.8	-32.0	243.5	-17.5	AB	2	0				
75	KO-014	L	ovr	74.7	25.6	74.9	10.6	B-I	8	7				
76	KO-014	L	pri	72.7	39.6	73.3	24.7	G-N	8	15			A2	N
77	KO-015	L	vrm	179.5	-36.0	189.2	-31.5	AB	2	0				
78	KO-015	P	ovr	128.8	14.1	127.0	4.2	B-G	6	19.4				
79	KO-015	L	pri	347.6	41.5	0.3	39.7	G-N	8	10.1			A1	N
80	KO-017	L	vrm	141.0	-34.3	151.6	-39.6	AB	2	0				
81	KO-017	L	ovr	11.8	42.2	21.5	34.7	B-E	4	10.6				
82	KO-017	L	pri	305.0	51.2	323.5	59.5	FGI-N	8	8.8			A2	N
83	KO-018	L	vrm	173.2	-42.4	185.9	-39.1	AB	2	0				
84	KO-018	P	ovr	50.6	-30.3	47.2	-43.8	B-F	5	16.5				
85	KO-018	L	pri	352.2	36.9	2.8	34.2	G-N	8	4.8			A1	N
86	KO-19A	L	vrm	206.3	-30.4	211.6	-20.3	AB	2	0				
87	KO-19A	L	ovr	325.9	67.7	3.9	68.4	B-F	5	9.1				
88	KO-19A	L	pri	45.5	36.1	49.7	23.0	G-M	7	10.6			A2	N
89	KO-020	L	vrm	172.4	-35.8	182.6	-33.0	AB	2	0				
90	KO-020	L	ovr	358.1	39.3	9.2	35.1	B-H	7	10				
91	KO-020	L	pri	344.8	39.6	357.0	38.5	H-N	7	10			A1	N
92	KO-021	L	vrm	4.4	32.8	12.5	27.3	AB	2	0	X	184.4		
93	KO-021	L	ovr	222.3	25.0	216.6	37.0	B-G	6	11.1	X	42.3		
94	KO-021	L	pri	184.5	-24.4	190.1	-19.2	H-N	7	13	X	4.5	A3	N
95	KO-022	L	vrm	183.0	-45.5	195.8	-39.7	AB	2	0				
96	KO-022	L	ovr	183.6	-45.9	196.6	-40.0	A-F	6	2.7				
97	KO-022	L	pri	7.9	52.5	23.2	45.3	G-N	8	14.5			A1	N
98	KO-023	L	vrm	190.1	-50.2	203.9	-42.5	AB	2	0				
99	KO-023	L	ovr	8.3	60.1	27.7	52.3	B-GN	7	8.2				
100	KO-023	L	pri	2.2	56.3	20.6	49.9	G-KMN	7	8.4			A1	N
101	KO-024	L	nrm	18.2	27.7	23.6	19.3	AB	2	0	x	x		
102	KO-024	P	ovr	41.1	78.6	61.9	65.3	B-F	5	10.4	x	x		
103	KO-024	L	pri	185.8	6.5	183.6	11.1	H-N	7	14.5	x	5.8	A2	N
104	KO-025	L	vrm	184.5	-40.2	195.1	-34.3	AB	2	0				

105	KO-025	P	ovr	335.5	-16.1	331.3	-13.5	B-F	5	9		
106	KO-025	L	pri	2.5	37.6	12.4	32.3	G-N	8	4.7	A1	N
107	KO-026	L	vrm	202.0	-40.7	210.5	-31.2	AB	2	0		
108	KO-026	P	ovr	134.3	6.3	132.9	-5.2	B-F	5	15.6		
109	KO-026	L	pri	21.0	35.1	28.1	25.9	G-N	8	3.9	A2	N
110	KO-028	L	vrm	167.9	-56.2	188.8	-53.1	AB	2	0		
111	KO-028	P	ovr	296.0	49.9	311.6	60.4	B-E	4	8.4		
112	KO-028	L	pri	341.6	50.9	359.9	49.9	F-N	9	7	A1	N
113	KO-029	L	vrm	173.8	-37.4	184.5	-34.2	AB	2	0		
114	KO-029	P	ovr	97.1	2.7	98.9	-11.9	B-E	4	17.3		
115	KO-029	L	pri	353.4	38.0	4.3	35.0	F-N	9	10.9	A1	N
116	KO-031	L	vrm	173.6	-31.0	182.0	-28.2	AB	2	0		
117	KO-031	P	ovr	116.8	73.6	98.3	60.2	B-F	5	18		
118	KO-031	L	pri	342.9	50.3	0.6	49.0	G-N	8	6.7	A1	N
119	KO-032	L	vrm	195.0	-50.6	208.0	-41.9	AB	2	0		
120	KO-032	P	ovr	4.6	-23.4	357.7	-28.5	B-E	4	15.4		
121	KO-032	L	pri	13.2	56.5	29.3	48.0	F-N	9	6.4	A1	N
122	KO-035	L	vrm	151.0	-22.0	157.5	-25.3	AB	2	0		
123	KO-035	P	ovr	91.5	-42.5	276.7	56.8	B-DF	4	3.7		
124	KO-037	L	vrm	179.5	-31.5	187.6	-27.1	AB	2	0		
125	KO-037	P	ovr	115.9	54.7	106.5	43.0	B-FN	6	14.6		
126	KO-037	L	pri	1.5	15.9	5.1	11.7	G-N	8	7.9	A2	N
127	KO-040	L	vrm	188.6	-42.1	199.4	-35.3	AB	2	0		
128	KO-040	L	pri	14.8	41.3	24.4	33.2	G-N	8	12	A1	N
129	KO-041	L	vrm	195.2	-34.2	202.7	-26.1	AB	2	0		
130	KO-041	L	ovr	88.7	-32.2	91.5	-47.0	B-F	5	9.6		
131	KO-041	P	pri	72.0	-25.1	71.2	-40.0	H-LN	6	15.8	B2	N

132	KO-043	L	vrm	347.1	38.1	358.5	36.6	AB	2	0				
133	KO-043	L	ovr	193.5	-18.1	196.9	-11.1	B-F	5	11.3				
134	KO-043	P	pri	95.8	-16.2	97.9	-30.2	G-N	8	21			B2	N
135	KO-044	L	vrm	245.9	-17.8	246.4	-3.0	AB	2	0				
136	KO-044	L	ovr	83.2	-6.5	83.7	-21.5	B-F	5	8				
137	KO-044	L	pri	42.6	44.4	48.6	31.5	F-J	5	11.1			A2	N
138	KO-045	L	vrm	258.9	-40.0	258.7	-24.9	AB	2	0				
139	KO-046	P	ovr	4.0	-41.5	170.2	44.2	B-G	6	14.4				
140	KO-046	L	vrm	215.8	-42.4	222.6	-30.5	AB	2	0				
141	KO-047	L	vrm	227.0	-12.8	227.8	0.2	AB	2	0				
142	KO-047	L	ovr	340.9	20.2	346.5	21.2	B-G	6	13.1				
143	KO-047	P	int	128.8	-3.5	130.6	-12.7	G-J	4	4.5				
144	KO-047	L	pri	139.2	39.2	130.3	31.2	J-N	5	18.4	x	319.2	A2	N

APPENDIX H

SQR FILE FOR KOCHKOR EAST (KSS) WITH RATINGS

#	Sample										180?
33	KSS-003	L	vrm	251.1	45.5	214.1	52.4	AB	2	0	
34	KSS-003	L	ovr	307.7	53.7	286.7	85.3	B-H	7	4	
35	KSS-003	P	pri	350.1	7.7	358.1	31.4	H-NP	8	13.1	
36	KSS-004	L	ovr	211.8	-13.3	220.4	-16.1	C-H	6	9.4	X
37	KSS-004	P	pri	276.2	64.0	186.5	72.3	I-O	7	17.2	X
38	KSS-005	L	vrm	258.4	70.1	171.1	64.9	AB	2	0	
39	KSS-005	L	ovr	29.4	62.3	81.4	53.2	B-G	6	7.9	
40	KSS-005	P	int	46.1	-4.4	43.0	-6.4	H-K	4	12	
41	KSS-005	P	pri	312.4	28.5	313.6	60.4	L-P	5	14.7	
42	KSS-006	L	ovr	73.1	65.0	102.9	40.7	A-F	6	7.6	
43	KSS-006	P	pri	135.4	44.9	134.2	12.9	G-KP	6	13.6	
44	KSS-007	L	ovr	199.3	-64.1	261.0	-58.0	B-G	6	8.7	X
45	KSS-007	P	pri	20.5	-24.3	11.0	-10.4	I-KMP	5	17.2	X
46	KSS-008	L	vrm	309.6	31.7	308.0	63.9	AB	2	0	
47	KSS-008	P	ovr	12.6	-33.7	0.4	-15.1	B-GP	7	17.1	
48	KSS-008	P	pri	71.5	20.1	76.9	2.2	KLNO	4	13.7	
49	KSS-009	L	pri	40.1	28.9	56.6	24.6	F-LQ	8	12.3	
50	KSS-009	P	ovr	204.7	55.3	174.7	37.8	BD-GS	6	26.4	
51	KSS-009	L	vrm	332.8	1.0	336.0	31.0	AB	2	0	
52	KSS-010	P	ovr	350.5	34.2	16.3	54.7	A-F	6	16.3	X
53	KSS-010	P	pri	251.5	48.0	210.8	54.1	H-L	5	5.2	X
54	KSS-011	L	vrm	354.0	-28.2	348.1	-2.3	AB	2	0	
55	KSS-011	L	ovr	178.4	80.2	142.4	50.8	B-G	6	4.8	
56	KSS-011	L	int	154.6	-8.1	160.7	-36.9	G-K	5	9.4	
57	KSS-011	L	pri	155.6	-17.0	165.4	-45.1	G-KP	6	9.9	
58	KSS-012	L	nrm	98.0	-9.0	90.2	-35.5	AB	2	0	
59	KSS-012	L	ovr	101.8	73.1	120.1	42.7	B-F	5	7.9	
60	KSS-012	L	pri	151.0	28.0	148.6	-2.5	G-P	10	17.5	
61	KSS-014	L	vrm	103.2	13.7	102.9	-15.0	AB	2	0	
62	KSS-014	L	ovr	351.4	67.9	86.3	69.6	B-F	5	4.6	
63	KSS-014	L	pri	76.3	64.3	103.8	39.2	F-IK	5	11.6	
64	KSS-015	L	ovr	304.2	54.4	261.2	84.8	A-H	8	11.4	
65	KSS-015	L	int	211.5	65.4	168.3	47.3	H-LQ	6	15.7	
66	KSS-015	P	pri	333.9	35.0	354.6	62.4	M-Q	5	11.7	
67	KSS-017	P	ovr	97.1	-17.0	85.4	-41.9	B-J	9	14.4	
68	KSS-017	L	vrm	213.5	36.0	194.6	26.3	AB	2	0	
69	KSS-017	L	pri	75.6	83.3	121.6	53.7	J-LOP	5	9.7	

70	KSS-018	P	ovr	43.8	-29.5	26.5	-26.1	A-I	9	15.8	
71	KSS-018	L	pri	137.9	52.1	135.5	20.3	I-MOP	7	12.1	
72	KSS-020	L	ovr	335.5	30.4	353.0	57.6	B-G	6	5.7	
73	KSS-020	L	vrm	296.4	-25.6	297.0	5.4	AB	2	0	
74	KSS-020	L	pri	274.8	50.2	225.6	67.8	H-Q	10	13.6	
75	KSS-021	L	vrm	199.0	9.0	199.0	-2.7	AB	2	0	
76	KSS-021	L	ovr	69.2	78.8	115.0	51.6	BCE-L	10	5.5	
77	KSS-021	L	pri	0.3	58.2	62.8	64.5	L-P	5	5.1	
78	KSS-022	L	ovr	324.5	39.9	342.3	70.0	A-E	5	9.1	X
79	KSS-022	L	pri	322.8	34.1	334.4	64.8	F-P	11	9.5	X
80	KSS-024	L	vrm	198.6	-0.9	202.5	-12.5	AB	2	0	
81	KSS-024	L	ovr	299.5	59.7	201.8	83.8	B-G	6	5.9	
82	KSS-024	L	pri	281.6	38.6	253.8	62.9	H-P	9	5.1	
83	KSS-026	P	ovr	63.4	-15.5	52.0	-25.0	A-D	4	1.2	
84	KSS-026	P	pri	334.3	34.1	354.2	61.5	D-GKMNP	8	15.2	
85	KSS-027	P	ovr	94.4	-22.5	258.9	45.8	A-F	6	9.3	
86	KSS-029	L	ovr	23.5	67.6	88.5	57.8	A-G	7	13.9	
87	KSS-029	P	pri	25.1	-23.0	15.6	-11.4	G-P	10	16.3	
88	KSS-030A	L	vrm	27.6	-7.9	25.5	0.2	AB	2	0	
89	KSS-030A	L	ovr	271.8	62.7	190.4	70.2	B-F	5	3.9	
90	KSS-030A	L	pri	322.9	44.6	345.0	74.7	F-OP	11	3.9	
91	KSS-031	L	vrm	63.1	1.1	61.6	-9.9	AB	2	0	
92	KSS-031	P	ovr	50.2	-44.0	20.1	-40.5	B-I	8	13.7	
93	KSS-031	P	pri	32.1	-36.3	13.2	-25.8	H-P	9	22.5	
94	KSS-032	L	vrm	338.1	32.0	357.7	58.2	AB	2	0	
95	KSS-032	L	ovr	92.2	62.9	110.6	34.5	B-H	7	7.9	
96	KSS-032	P	pri	59.0	-0.5	56.2	-9.8	I-O	7	8.3	
97	KSS-034	L	ovr	49.8	60.9	88.7	44.9	A-F	6	3.5	
98	KSS-034	L	pri	338.9	48.4	23.1	71.0	F-P	11	7.7	
99	KSS-035	L	vrm	268.7	-17.0	271.0	7.3	AB	2	0	
100	KSS-035	P	ovr	88.1	14.8	88.7	-9.5	B-EG	5	4.8	
101	KSS-035	P	pri	60.5	4.2	59.9	-6.5	FH-P	10	13.5	
102	KSS-037	L	ovr	241.6	79.6	150.8	60.2	A-H	8	12.6	
103	KSS-038	L	ovr	68.4	74.9	110.3	48.9	A-E	5	4.3	
104	KSS-038	L	pri	347.2	31.5	9.7	53.8	F-Q	12	7.7	

APPENDIX I

DAM SITE (KDS) FIELD DATA AND RATINGS WITH FOLD TEST

#	Sample										plastic	Geo Correct	RATING	N/R
41	KDS-029	L	ovr	22.6	74.9	169.8	41.5	B-F	5	8.2				
42	KDS-029	L	pri	5.9	30.2	107.7	82.7	G-MN	8	2.9			A2	N
43	KDS-030	L	pri	13.9	8.0	37.9	65.0	F-N	9	9.3			A2	N
44	KDS-030	L	ovr	112.1	59.3	149.5	12.7	A-E	5	3.6				
45	KDS-032	L	ovr	300.9	74.8	193.6	35.4	B-G	6	5				
46	KDS-032	L	pri	348.3	33.3	233.1	80.1	G-N	8	4.3			A2	N
47	KDS-032	L	vrm	92.1	23.0	110.4	6.9	AB	2	0				
48	KDS-033	L	ovr	315.5	45.4	228.8	52.3	A-G	7	6.2				
49	KDS-033	L	pri	333.2	11.5	298.4	61.5	G-N	8	2.4			A3	N
50	KDS-035	L	vrm	62.8	-27.8	58.5	9.1	AB	2	0				
51	KDS-035	L	ovr	354.9	39.1	190.8	78.7	B-F	5	6				
52	KDS-035	L	pri	15.9	9.6	43.8	65.0	F-N	9	4.2			A2	N
53	KDS-036	L	vrm	321.1	64.1	199.0	46.9	AB	2	0				
54	KDS-036	L	ovr	43.7	4.0	67.6	40.4	B-G	6	10				
55	KDS-036	L	pri	19.6	-7.4	31.6	48.9	G-N	8	5			A3	N
56	KDS-038	L	ovr	34.2	25.8	92.5	57.7	A-G	7	7.9				
57	KDS-038	L	pri	8.1	-26.7	8.9	34.5	G-N	8	6.6			A3	N
58	KDS-039	L	vrm	79.8	-0.4	82.9	6.4	AB	2	0				
59	KDS-039	L	ovr	48.9	13.7	82.0	40.7	B-G	6	7				
60	KDS-039	L	pri	12.0	-6.0	21.8	53.4	G-N	8	5.8			A3	N
61	KDS-041	L	vrm	162.7	53.0	170.5	-8.1	AB	2	0				
62	KDS-041	L	ovr	299.5	75.6	192.9	34.7	B-G	6	5.3				
63	KDS-041	L	int	3.8	45.8	164.9	71.7	G-J	4	5.3				
64	KDS-041	L	pri	5.8	1.3	15.0	62.3	J-N	5	4.9			A2	N

65	KDS-042	L	vrm	152.5	35.6	155.3	-22.1	AB	2	0				
66	KDS-042	L	ovr	349.0	79.4	180.1	38.4	B-G	6	2.9				
67	KDS-042	L	int	337.1	22.2	280.7	70.3	G-J	4	9.3				
68	KDS-042	L	pri	359.6	-21.2	360.0	40.8	J-N	5	8.7			A3	N
69	KDS-043	L	ovr	221.3	-13.3	257.0	-47.2	A-E	5	4.8	X	41.3		
70	KDS-043	L	int	211.9	-13.1	249.7	-55.1	E-I	5	11	X	31.9		
71	KDS-043	L	pri	180.5	-7.3	185.1	-69.3	JKMN	4	13.2	X	0.5	A3	N
72	KDS-044	L	ovr	30.2	62.6	155.7	49.4	A-E	5	11.4				
73	KDS-044	L	pri	350.0	52.3	189.6	65.0	FH-M	7	9.1			A1	N
74	KDS-045	P	ovr	319.9	-37.8	328.3	14.7	A-E	5	12.7				
75	KDS-045	L	pri	18.7	14.7	57.7	66.7	G-N	8	11.4			A2	N
76	KDS-047	L	ovr	32.0	48.1	134.6	56.9	B-G	6	10.7				
77	KDS-047	L	pri	354.9	-12.5	353.2	49.3	G-N	8	4.3			A3	N
78	KDS-048	L	vrm	80.7	-37.7	50.2	-11.6	AB	2	0				
79	KDS-048	L	ovr	15.8	66.5	167.0	49.9	B-G	6	4.3				
80	KDS-048	L	pri	1.4	-9.5	3.5	52.3	G-N	8	6.7			A3	N
81	KDS-049	L	vrm	129.2	-13.0	95.9	-42.2	AB	2	0	X	309.2		
82	KDS-049	L	ovr	206.7	-2.2	229.0	-52.4	B-E	4	7.5	X	206.7		
83	KDS-049	L	int	239.2	-4.8	258.2	-27.6	E-I	5	13.9	X	239.2		
84	KDS-049	L	pri	154.6	30.1	155.3	-27.8	I-N	6	15.1	X	334.6	A2	N
85	KDS-050	L	vrm	188.5	53.0	184.4	-8.5	AB	2	0				
86	KDS-050	L	ovr	1.2	52.0	173.2	66.0	B-G	6	2.2				
87	KDS-050	L	pri	338.4	19.8	288.4	70.4	G-LN	7	6.1			A2	N
88	KDS-051	L	ovr	29.2	70.4	164.1	44.1	A-G	7	4.4				
89	KDS-051	L	pri	2.7	28.5	96.4	85.8	G-N	8	6.5			A2	N
90	KDS-053	L	ovr	3.6	51.3	169.4	66.3	A-E	5	3.9				
91	KDS-053	L	int	355.6	14.7	348.2	76.5	E-I	5	22.5				
92	KDS-053	L	pri	352.5	-19.9	351.0	41.8	IK-N	5	8.6			A3	N

93	KDS-054	L	ovr	26.9	61.0	155.7	51.7	A-H	8	4				
94	KDS-054	L	pri	44.2	27.7	98.8	49.4	F-N	9	11.5			A2	N
95	KDS-055	L	pri	168.2	-30.7	68.1	-81.1	H-O	8	10.3	X	348.2	A3	N
96	KDS-055	L	vrm	114.6	-28.4	70.6	-34.2	BC	2	0	X	294.6		
97	KDS-055	L	ovr	257.6	-37.9	299.5	-24.5	C-H	6	5.2	X	77.6		
98	KDS-056	L	ovr	19.3	54.5	153.9	59.4	B-G	6	8.5				
99	KDS-056	L	pri	7.4	9.7	25.6	69.6	G-O	9	3.2			A2	N
100	KDS-057	L	vrm	97.2	-18.5	76.5	-16.8	AB	2	0				
101	KDS-057	L	ovr	56.1	60.9	145.6	39.7	B-G	6	7.3				
102	KDS-057	L	pri	28.8	14.1	68.5	58.2	G-N	8	3.9			A3	N
103	KDS-059	L	vrm	130.2	75.7	167.4	17.9	AB	2	0				
104	KDS-059	L	ovr	26.0	65.8	161.1	48.4	B-G	6	7.8				
105	KDS-059	P	pri	326.4	-32.2	329.2	22.7	GI-N	7	16.6			B1	N
	KDS-059	L	ps	348.9	55.8	188.8	61.5		2	0				
	KDS-059	L	pf	303.8	35.1	244.9	43.9		2	0				
10	KDS-058	L	vrm	96.4	19.8	110.1	1.6	AB	2	0				
11	KDS-058	L	ovr	2.8	64.0	174.4	53.9	B-H	7	16.1				
12	KDS-058	L	pri	195.2	37.6	192.6	-22.4	H-JLN-P	7	31.5			A3	N
21	KDS-068A	P	ovr	329.0	-1.7	310.2	49.2	A-F	6	4.2	X			
22	KDS-068A	P	int	55.9	15.5	88.0	35.3	F-J	5	7.6	X			
23	KDS-068A	L	pri	309.3	56.7	214.0	45.5	I-N	6	10.4	X	129.3	A2	N
13	KDS-060	L	ovr	23.4	66.1	162.6	48.9	A-E	5	6.9				
14	KDS-060	L	int	68.0	-21.9	59.2	6.0	E-G	3	5.5				
15	KDS-060	L	pri	350.3	24.5	292.7	82.3	G-O	9	10.1			A2	N
106	KDS-061	L	ovr	67.9	69.1	154.3	33.1	A-E	5	3				
107	KDS-061	L	pri	15.6	20.4	66.4	72.3	E-N	10	6.6			A2	N
108	KDS-062	L	ovr	329.0	68.1	193.1	46.4	A-G	7	6.2	X			
109	KDS-062	L	pri	327.7	20.1	277.2	61.4	G-M	7	8.8	X	147.7	A3	R

16	KDS-063	L	ovr	42.7	82.6	171.9	33.2	A-E	5	7.1		
17	KDS-063	L	int	357.4	69.0	178.2	49.1	E-H	4	11.3		
18	KDS-063	L	pri	19.9	45.0	138.2	65.6	G-Q	11	10.8	A1	N
110	KDS-064	L	ovr	87.4	60.4	145.1	24.2	A-E	5	6.9		
111	KDS-064	L	pri	47.2	31.7	105.4	47.5	F-N	9	10.2	A2	N
112	KDS-065	L	ovr	12.7	48.7	153.7	66.4	A-F	6	8.2		
113	KDS-065	L	int	33.7	8.5	65.1	51.0	G-J	4	9		
114	KDS-065	L	pri	27.9	-29.6	26.7	25.8	I-N	6	17.4	A3	N
19	KDS-066	P	ovr	28.6	41.7	124.7	61.9	A-F	6	6		
20	KDS-066	L	pri	220.4	30.4	216.0	-19.0	FGI-Q	11	8.4	A3	N

more fold test samples below

1	KDS-006	L	vrm	256.3	66.3	201.8	20.6	AB	2	0
2	KDS-006	L	ovr	46.9	49.4	131.8	47.3	B-H	7	5.9
3	KDS-006	L	pri	17.7	-21.4	21.2	37.0	IJL-P	7	11.6
4	KDS-008	L	vrm	36.0	-19.0	40.3	30.3	AB	2	0
5	KDS-008	L	ovr	285.1	65.5	206.0	32.3	B-G	6	10.7
6	KDS-008	L	pri	343.6	39.6	220.3	73.4	F-O	10	14.3
7	KDS-012	L	vrm	261.1	29.7	238.5	8.1	AB	2	0
8	KDS-012	L	ovr	19.8	68.1	166.1	47.8	B-H	7	4.4
9	KDS-012	L	pri	18.8	5.2	42.7	59.8	I-O	7	13

APPENDIX J

KARA SUU (KSU) FIELD DATA AND RATINGS

#	Sample						180?	Corrected geographic	RATING	N/R	
105	KU-116	L	ovr	213.4 -1.4 214.1 -20.1 A-H	8	6.4	X	33.4			1
106	KU-116	L	pri	61.7 -39.4 54.9 -23.8 I-P	8	10.2	X	241.7	A2	R	
107	KU-115	L	vrm	123.2 -20.8 115.7 -22.9 BC	2	0	X	303.2			
108	KU-115	L	ovr	228.7 -13.6 232.3 -30.5 C-I	7	10.1	X	48.7			
109	KU-115	L	pri	19.8 -5.7 19.7 13.3 IKMNP	5	12.9	X	199.8	A2	R	
110	KU-114	L	vrm	139.6 -13.5 134.0 -21.4 AB	2	0	X	319.6			2
111	KU-114	L	pri	27.6 -6.3 27.7 12.6 L-P	5	4.3	X	207.6	A2	R	
112	KU-113	L	pri	28.8 -1.1 29.2 17.8 K-P	6	8.6	X	208.8	A3	R	
113	KU-113	P	ovr	311.6 50.5 287.1 53.0 A-EHP	7	17.1	X	131.6			
114	KU-112	L	ovr	327.9 53.3 300.5 60.6 B-F	5	10.8	X	147.9			3
115	KU-112	L	pri	262.5 65.0 239.2 51.8 F-HJ-P	10	11.4	X	82.5	A2	N	
116	KU-111	L	vrm	266.7 -14.2 272.0 -21.9 AB	2	0	X	86.7			
117	KU-111	P	ovr	12.9 -11.5 13.1 7.4 B-H	7	5.8	X	192.9			
118	KU-111	L	pri	137.6 -75.2 70.5 -71.5 I-P	8	7.1	X	317.6	A1	R	
119	KU-110	P	ovr	22.5 -21.4 22.3 -2.5 A-G	7	12.9					4
120	KU-110	P	pri	66.6 -18.0 64.1 -3.9 HJ-P	8	14			B3	R	
	KU-110	L	pf	344.6 15.1 339.4 29.5	2	0					
	KU-110	L	pl	103.7 -41.7 88.8 -36.1	2	0					
121	KU-109	L	vrm	195.9 56.8 199.1 37.9 AB	2	0					
122	KU-109	L	ovr	349.3 62.3 309.7 74.3 B-L	11	7.6					
123	KU-109	P	pri	242.7 42.9 54.6 -27.6 L-P	5	5.9			B2	N	
	KU-109	L	pri	355.4 22.6 349.6 39	5	11.7			A2	N	
	KU-109	L									
124	KU-108	L	vrm	238.7 -49.5 259.3 -63.4 AB	2	0	X	58.7			

125	KU-108	L	ovr	149.2	14.0	151.4	2.3	B-G	6	4.3	X	329.2			
126	KU-108	L	pri	185.7	-21.4	182.0	-39.4	I-P	8	6.8	X	5.7	A3	N	
127	KU-107	L	vrm	293.3	56.6	266.9	52.7	AB	2	0					5
128	KU-107	L	ovr	26.8	29.1	28.0	48.0	B-J	9	8					
129	KU-107	L	pri	15.4	23.1	13.6	41.9	J-P	7	7.4			A2	N	
130	KU-106	L	vrm	186.3	-21.0	183.5	-37.9	AB	2	0					
131	KU-106	P	ovr	117.9	25.6	126.1	22.6	B-K	10	11.2					
132	KU-106	L	pri	339.0	43.3	321.3	55.0	K-P	6	9.3			A2	N	
133	KU-104	P	ovr	312.1	-41.7	325.9	-33.2	A-H	8	12.2					6
134	KU-104	L	pri	327.3	30.3	315.5	39.4	I-P	8	10.5			A2	N	
135	KU-103	L	ovr	358.0	74.1	258.8	81.9	A-H	8	6.6					
136	KU-101A	L	vrm	190.8	66.0	196.2	47.5	AB	2	0					7
137	KU-101A	L	ovr	6.0	53.8	350.3	71.3	B-H	7	6.2					
138	KU-101A	L	pri	338.4	43.2	320.7	54.7	I-P	8	6.5			A2	N	
139	KU-101	L	vrm	266.8	19.2	267.1	7.5	AB	2	0					
140	KU-101	L	ovr	339.2	60.2	302.2	69.7	B-J	9	8.6					
141	KU-101	L	pri	340.7	43.2	323.3	55.3	J-P	7	7.6			A1	N	
41	KU-009	L	vrm	200.7	42.9	199.8	24.2	AB	2	0					8
42	KU-009	L	ovr	341.1	57.3	309.4	67.7	B-G	6	11.4					
43	KU-009	L	pri	333.4	60.6	295.6	68.0	H-Q	10	4.4			A1	N	
44	KU-010	L	vrm	237.8	35.3	232.1	19.5	AB	2	0					
45	KU-010	P	ovr	118.8	39.3	133.0	35.1	B-L	11	6.8					
46	KU-010	L	pri	348.0	32.9	337.6	47.5	J-Q	8	5.5			A2	N	
47	KU-12	L	ovr	324.5	69.2	269.7	70.8	A-F	6	6.8					9
48	KU-12	L	pri	350.1	51.2	328.6	65.2	C-Q	15	11.7			A1	N	
49	KU-013	L	ovr	356.7	83.7	215.1	76.3	A-F	6	6.9					
50	KU-013	L	pri	8.5	55.0	354.1	72.8	F-KM-P	10	11.2			A1	N	

51	KU-15	P	ovr	311.9	-25.0	319.0	-17.6	A-F	6	10.5					10
52	KU-15	L	pri	347.7	17.5	342.2	32.5	F-Q	12	6.5			A2	N	
53	KU-16	L	ovr	21.7	53.4	20.5	72.3	A-G	7	13.7					
54	KU-16	P	pri	258.6	75.3	227.6	60.1	G-KM-OQ	9	21			B3	N	
55	KU-20	P	ovr	324.7	-13.9	326.9	-3.5	A-G	7	13.1					11
56	KU-20	L	pri	249.1	-33.5	261.5	-45.3	G-Q	11	3			A2	R	
57	KU-22	L	ovr	138.5	38.3	149.3	28.4	A-G	7	13.7					
58	KU-22	L	pri	265.3	-10.0	269.6	-18.2	G-Q	11	6.8			A3	R	
59	KU-24	L	ovr	212.2	-28.6	215.1	-47.7	B-F	5	10.8					12
60	KU-24	L	pri	192.7	-56.8	180.6	-75.1	G-Q	11	5.1			A1	R	
61	KU-25	L	ovr	353.4	36.6	342.9	52.3	A-E	5	7					
62	KU-25	L	pri	321.4	17.1	314.7	25.1	M-Q	5	6			A3	N	
63	KU-27	L	ovr	349.2	52.1	326.8	65.8	A-E	5	7.2					13
64	KU-27	L	pri	352.3	46.7	335.5	61.6	L-Q	6	11.1			A1	N	
65	KU-28	L	ovr	354.3	64.1	311.2	77.2	AF-M	9	9.4					
66	KU-28	L	pri	7.2	56.4	350.1	74.0	M-OSTV-	8	5.8			A1	N	
67	KU-30	P	ovr	69.2	-1.5	70.2	11.9	A-F	6	14.7					14
68	KU-30	L	pri	123.3	-50.4	100.1	-50.0	F-Q	12	11.4			A2	R	
69	KU-31	L	ovr	56.3	75.1	151.6	79.7	A-G	7	6					
70	KU-31	L	pri	149.4	-36.4	134.7	-45.8	G-LN	7	7.3			A2	R	
71	KU-50	L	ovr	102.1	4.9	104.1	8.1	A-H	8	19.7	X	282.1			15
72	KU-50	L	int	27.9	45.6	30.8	64.5	H-L	5	12.3	X	207.9			
73	KU-50	L	pri	265.0	36.4	255.2	26.0	M-Q	5	4.4	X	85	A3	N	
74	KU-52	P	ovr	131.1	49.8	328.5	-40.8	A-EH	6	11.6					
75	KU-52	L	int	176.1	-38.7	165.2	-54.8	H-L	5	3.9					
76	KU-52	L	pri	185.4	-34.6	179.0	-52.5	M-Q	5	7.4			A1	R	
77	KU-54	L	vrm	146.9	26.6	152.7	15.2	AB	2	0	X	326.9			16

78	KU-54	L	ovr	52.7	73.2	140.7	80.7	B-EGH	6	14.2	X	232.7			
79	KU-54	P	pri	92.5	-8.8	90.8	-1.9	H-MO-Q	9	13.4	X	272.5	B3	R	
80	KU-55	P	ovr	312.8	-15.7	316.7	-9.1	C-H	6	13.6					
81	KU-55	L	pri	191.9	-11.7	190.3	-30.4	H-Q	10	9.1			A2	R	
82	KU-57	L	ovr	276.9	73.3	238.9	61.4	B-H	7	10.3	X	96.9			17
83	KU-57	L	pri	344.4	72.5	267.7	78.0	H-Q	10	5.1	X	164.4	A2	N	
84	KU-58	L	ovr	177.3	39.6	181.9	22.2	A-EG	6	6.5					
85	KU-58	L	pri	183.1	-25.8	178.0	-43.4	F-Q	12	6.2			A2	R	
86	KU-60	L	pri	96.5	35.4	110.8	38.6	N-R	5	4.6	X	276.5	A3	N	18
87	KU-60	L	ovr	5.1	38.6	357.3	56.3	A-K	11	12.6	X	185.1			
88	KU-61	L	ovr	42.9	64.0	80.5	79.9	A-G	7	12					
89	KU-61	L	pri	178.5	-54.4	157.5	-70.3	H-JM-Q	8	9.9			A1	R	
90	KU-62	P	ovr	66.9	-21.4	63.8	-7.3	A-F	6	9.6	X	246.9			19
91	KU-62	L	pri	2.9	57.1	341.1	73.7	F-Q	12	4.2	X	182.9	A3	N	
92	KU-64	P	ovr	219.2	39.6	36.3	-21.4	B-H	7	17.8					
93	KU-64	L	pri	155.5	-36.9	141.2	-48.0	H-Q	10	7.3			A2	R	
94	KU-66	P	ovr	174.0	41.6	359.4	-24.7	A-F	6	14.5	X	354		?	20
95	KU-69	L	ovr	139.8	17.2	143.5	8.0	A-F	6	8.6	X	319.8			21
96	KU-69	L	pri	336.2	81.2	229.7	75.5	G-N	8	18.9	X	156.2	A2	N	
97	KU-70	P	ovr	66.9	-6.2	67.0	7.5	A-F	6	17.8					
98	KU-71	L	ovr	326.4	26.8	316.0	36.0	C-J	8	13.7	X	146.4			21
99	KU-71	L	pri	325.2	28.3	314.3	37.0	J-Q	8	6.7	X	145.2	A3	N	
100	KU-73	P	ovr	314.4	-35.2	325.9	-26.3	C-G	5	21.4					
101	KU-73	L	pri	162.0	-67.5	106.7	-75.4	H-NP-R	10	3.7			A1	R	
102	KU-74	L	ovr	290.0	15.0	285.3	13.3	B-EGH	6	18	X	110			23
103	KU-74	L	pri	317.3	38.1	301.4	43.5	JKM-OQ	6	19.7	X	137.3	A3	N	
104	KU-76	P	ovr	338.3	-32.7	344.5	-18.4	A-F	6	14					

105	KU-76	P	pri	63.3	-11.3	62.5	3.3	G-IL-NQ	7	17.8			A3	R	
106	KU-77	L	vrm	174.7	63.0	185.5	44.4	AB	2	0	X	354.7			24
107	KU-77	L	ovr	180.1	-49.9	164.0	-66.3	B-F	5	6	X	0.1			
108	KU-77	L	pri	191.8	-65.0	162.6	-82.8	G-Q	11	3.8	X	11.8	A2	R	
109	KU-79	L	ovr	348.9	51.8	326.4	65.3	B-DFH	5	16.3					
110	KU-79	L	pri	346.2	41.1	331.3	54.9	H-OQ	9	11.1			A2	N	
111	KU-150	L	ovr	180.0	-58.3	154.2	-74.2	B-G	6	7.4	X	0			25
112	KU-150	L	pri	128.8	-69.9	79.7	-66.7	I-NQ	7	13.6	X	308.8	A2	R	
113	KU-152	L	ovr	19.5	28.1	18.5	47.1	B-F	5	6.5					
114	KU-152	L	pri	3.6	-15.4	4.3	2.6	G-Q	11	8.3			A2	N	
115	KU-153	P	ovr	253.2	56.7	237.9	42.6	A-F	6	13	X	73.2			
116	KU-155	L	ovr	1.3	40.5	351.4	57.7	A-F	6	7.5					
117	KU-155	L	pri	343.2	30.6	332.8	44.2	F-NPQ	11	8.8			A2	N	
118	KU-156	L	vrm	154.9	20.6	158.9	6.8	AB	2	0	X	334.9			
119	KU-156	L	ovr	186.3	-41.0	178.3	-58.9	B-G	6	5.4	X	6.3			
120	KU-156	L	pri	179.3	-50.6	162.5	-67.0	G-Q	11	5.1	X	359.3	A3	R	
121	KU-158	L	ovr	6.1	50.0	353.7	67.6	A-E	5	9.1					
122	KU-158	L	pri	355.4	37.4	344.9	53.5	M-Q	5	8.5			A2	N	
123	KU-160	L	ovr	173.8	-19.4	168.8	-35.6	A-E	5	5.3	X	353.8			
124	KU-160	L	pri	171.7	-52.4	149.7	-66.8	M-Q	5	6	X	351.7	A3	R	
125	KU-162	P	ovr	236.5	44.1	49.6	-27.7	A-F	6	13.6	X	56.5			
126	KU-162	P	pri	262.2	74.9	229.8	60.5	L-Q	6	17.8	X	82.2	A2	N	
127	KU-164	L	vrm	274.6	34.5	263.9	26.4	AB	2	0					
128	KU-164	L	ovr	8.1	33.6	2.7	51.8	B-G	6	8.2					
129	KU-164	L	pri	335.8	33.3	323.3	44.7	G-Q	11	10.2			A2	N	
130	KU-165	L	vrm	71.8	44.8	92.3	55.3	AB	2	0	X	251.8			
131	KU-165	L	ovr	118.5	7.1	120.5	4.8	B-F	5	9.7	X	298.5			

13 2	KU- 165	L	pri	137.8 G-Q	-7.5	134.2	-15.0	1 1	6.9	X	317.8	A3	N

APPENDIX K

SOURCES FOR MATERIAL INCLUDED IN COMPARISONS AND PHYLOGENETIC ANALYSIS

Institutional Abbreviations—NMNH, Smithsonian Natural History Museum, Washington D.C., U.S.A.; UONMCH, University of Oregon Museum of Natural and Cultural History, Eugene, Oregon, U.S.A., MGUH, Uppsala Museum, Uppsala Sweden.

Sources for the taxa used in morphological comparisons and the phylogenetic analysis. Underlined taxa included in the phylogenetic analysis. If bold, data taken directly from reference and not the fossil material

Taxon	Collection/Institution	Reference
<u>Persiatherium huadeensis</u>		**Pandolfi, 2015, Lu, 2013**
<u>Aceratherium depereti</u>		**Pandolfi, 2015**
<u>Aceratherium incisivum</u>		**Pandolfi, 2015**
<u>Aceratherium porpani</u>		**Pandolfi, 2015**
<u>Acerorhinus fugensis</u>		**Pandolfi, 2005**
<u>Acerorhinus hezhengensis</u>		**Pandolfi, 2015, Lu, 2013**
<u>Acerorhinus lufengensis</u>		**Pandolfi, 2015**
<u>Acerorhinus palaeosinensis</u>		**Pandolfi, 2015, Ringström, 1924, Lu, 2013**
<u>Acerorhinus tsaidamensis</u>		**Pandolfi, 2015, Lu, 2013**
<u>Acerorhinus yuanmouensis</u>		**Pandolfi, 2015, Lu, 2013**
<u>Acerorhinus zernowi</u>		**Pandolfi, 2015, Antoine et al., 2003**
<u>Alicornops complanatum</u>		**Pandolfi, 2015, Antoine et al., 2003**
Alicornops laogouense		**Pandolfi, 2015**
<u>Alicornops simorrense</u>		**Pandolfi, 2015**
<u>Aphelops malacorhinus</u>	NMNH	Prothero, 2009
<u>Aphelops megalodus</u>	NMNH	Prothero, 2009
<u>Aphelops mutilus</u>	NMNH	Prothero, 2009
<u>Brachypotherium brachypus</u>		**Pandolfi, 2015, Guérin, 1980**
Brachypotherium goldfussi		**Pandolfi, 2015, Guérin, 1980**
<u>Bugtirhinus praecursor</u>		**Pandolfi, 2015, Antoine et al., 2010**
<u>Ceratotherium simum</u>	MNCH	Pandolfi, 2015, Guérin, 1966
<u>Ceratotherium neumayri</u>		**Pandolfi, 2015**

Chilotherium anderssoni	MGUH	Pandolfi, 2015, Ringström, 1924, Deng, 2006
Chilotherium habereri	MGUH	Pandolfi, 2015, Schlosser, 1903, Ringström, 1924
Chilotherium kiliasi		**Pandolfi, 2015**
Chilotherium kowalevskii		**Pandolfi, 2015**
Chilotherium licenti		
Chilotherium persiae		**Pandolfi, 2015**
Chilotherium primigenium		**Deng, 2006**
Chilotherium samium		**Pandolfi, 2015**
Chilotherium schlosseri	MGUH	Pandolfi, 2015
Chilotherium wimani	MGUH	Pandolfi, 2015, Deng, 2006, Ringström, 1924
Diceratherium aginense		**Pandolfi, 2015, Antoine et al., 2010**
Diceratherium armatum		**Pandolfi, 2015, Antoine et al., 2010, Prothero, 2009**
Dicerorhinus sumatrensis		**Pandolfi, 2015, Guérin, 1980, Antoine et al., 2010**
Diceros bicornis		**Pandolfi, 2015, Guérin, 1980, Antoine et al., 2010**
Dihoplus pikermiensis		**Pandolfi, 2015**
Dihoplus schleirmacheri		**Pandolfi, 2015, Guérin, 1980**
Gaindatherium browni		**Pandolfi, 2015, Antoine et al., 2010**
Hispanotherium beonense		**Pandolfi, 2015, Antione, 2002, Antoine et al., 2010**
Hispanotherium matritense		**Pandolfi, 2015**
Hoploaceratherium tetradactylum		**Pandolfi, 2015, Guérin, 1980**
Iranotherium morgani		**Pandolfi, 2015, Antoine, 2002**
Lartetotherium sansaniense		**Pandolfi, 2015, Guérin, 1980, Antoine, 2002**
Menoceras arikarense	NMNH	Pandolfi, 2015, Prothero, 2009, Antoine et al., 2010
Plesiaceratherium gracile		**Pandolfi, 2015, Lu, 2013**
Plesiaceratherium mirallesi		**Pandolfi, 2015, Antoine et al., 2010**
Protoceratherium minutum		**Pandolfi, 2015, Antoine et al., 2010**

Rhinoceros sondaicus		**Pandolfi, 2015, Guérin, 1980, Antoine et al., 2010**
Rhinoceros unicornis		**Pandolfi, 2015, Guérin, 1980, Antoine et al., 2010**
Ronzotherium filholi		**Pandolfi, 2015, Antoine et al., 2010**
Shansirhinus ringstroemi		**Pandolfi, 2015, Deng, 2005, 2006**
Subchilotherium intermedium		**Pandolfi, 2015**
Subhyracodon occidentalis	NMNH	Pandolfi, 2015, Prothero, 2009, Antoine et al., 2010
Trigonias osborni	NMNH	Pandolfi, 2015, Prothero, 2009, Antoine et al., 2010
Teleoceras fossiger	NMNH	Prothero, 2009
Teleoceras major	NMNH, MNCH	Prothero, 2009

APPENDIX L

PHYLOGENETIC CHARACTERS AND DESCRIPTIONS

List and description of the 214 characters included in the phylogenetic analysis as used in by Pandolfi (2015), with characters modified in most cases from Lu (2012) and Antoine (2002)

Skull

1. Nasal: lateral apophysis = 0, absent; 1, present

   -Posterior end of the nasal is significantly wider that anterior end, on the order of twice as broad. Nasal constricts suddenly, leaving the nasals with two lateral bulges.

2. Nasal: dorsal profile: 0, straight; 1, undulated; 2, dorsally arched; 3, upturn

   -Profile of the nasal bone is primarily referring to the anterior portion of the nasal bone where it is not in contact with other facial bones. Starting just behind the nasal opening, the dorsal most profile of the nasal bone is (0) roughly straight, (1) dished before turning ventrally in the anterior most portion, (2) a smooth curve, with the highest point mid nasal bone, or (3) dished with the anterior most portion pointing dorsally.

3. Nasal: anterior end: 0, at the level of DP1 or after DP1: 1, before the DP1 without over the premaxillae; 2, before premaxillae

   -Anterior most tip of nasal bone, when viewed laterally, is (0) even or posterior to the first deciduous premolar, (1) anterior to the first deciduous premolar but posterior to the anterior most projection of the premaxillae, or (2) projects anterior to the anterior most projection of the premaxillae.

4. Maxillary: foramen infraorbitalis = 0 above premolars; 1, above molars

   - When viewed laterally, the entirety to majority of the infraorbital foramen is situated above the premolars (0), or the entirety or majority of the infraorbital foramen is dorsal to the molar teeth (1), if the occlusal surface of the upper dentition is aligned flat as a plane.

5. Infraorbital foramen: 0, behind the nasal notch; 1, below the nasal notch

-When viewed laterally, the posterior most opening of the external naras opening, ventral to the projecting portion of the nasal bones. The infraorbital foramen is situated ventral to the afore described feature (1), or with the anterior most edge of the infraorbital foramen situated posterior to the posterior most edge of the nasal notch opening.

6. Infraorbital foramen: 0, one; 1, two–three

-Generally clumped closely together is there are more than one (1), otherwise, the single standard infraorbital foramen.

7. Nasal notch = 0, above P1–3; 1, above P4–M1

The posterior most portion of the nasal notch, when the skull is leveled so that the upper tooth row forms a plane, is dorsal to the P1-3 (0) or is dorsal to the P4-M1 (1)

8. Nasal notch: 0, U–shaped; 1, V–shaped

The posterior portion of the nasal notch, as is "pointing" posteriorly, forms a broad U-shape (0), or narrows to more of a point in a V-shape (1)

9. Nasal notch: distance to the orbit/length of the skull: 0, long (>17%); 1, short (≤17%)

-From the most posterior point of the nasal notch opening measured directly posterior (with the upper tooth row flat for a plane) measured to the most anterior portion of the opening of the orbit. This first measurement is then compared to the length of the skull, with the skull again leveled so that the upper tooth row is flat. The anterior most portion may be the nasals or the premaxilla.

10. Nasal septum = 0, never ossified; 1, ossified (even sometimes)

-This feature is most typified in woolly rhinos, in the broad ossification of the nasal septum extending from the posterior of the nasal notch, far anterior, leaving opening on either side with a boney median.

11. Nasal septum: ossified = 0, partially; 1, totally

-ossification extends to some median point between the most posterior opening of the nasal notch to the anterior tip of the nasal bone (0), or extends fully to the anterior tip of the nasal bone (1). If character 10 was a 0 than this character is a -.

12. Nasal/lacrymal: contact = 0, long; 1, punctual or absent

-The contact between the lacrimal bone and the posterior portion of the nasal bone connects unevenly or over a very short distance of roughly ~1cm (1), or the contact between the two bones is longer and continuous, and is greater than 1cm of contact.

13. Orbit: anterior border = 0, above P4–M2; 1, above M3; 2, behind M3

-With the skull aligned with the upper dentition as a plane, the anterior most border of the orbit is directly dorsal to the P4-M2 (0), M3 (1), or posterior to the M3 (2).

14. Lacrymal: processus lacrymalis = 0, present; 1, absent

-The lacrimal process in rhinos is anterior in the orbit, just above the median anterior-posterior division of the orbit to slightly more dorsal. The process usually projects posterior-laterally. If the process is present (0), if process is absent (1).

15. Frontal: processus postorbitalis = 0, present; 1, absent

-The post orbital process projects ventrally from the frontal bone forming the rear of the orbit. No rhinocerotid taxa form a complete post orbital bar, however some taxa pocess a significant process. Any degree of process is coded as the process being present (0) in this case, while a total absence is (1).

16. Maxillary: anterior base of the processus zygomaticus maxillari = 0, high; 1, low

-Where the zygomatic arch joins into the maxillary bone, does the suture extend the connection of the maxillary bone all the way to the orbit (0) or terminate before reaching the orbit (1).

17. Zygomatic arch = 0, low; 1, high; 2, very high

-The median portion of the Zygomatic arch dips ventrally towards the tooth row (0), is relatively flat lying, without any portion extending ventrally (1), or extends dorsally in the medial most portion (2).

18. Zygomatic arches: dorsoventral depth: 0, shallow (<75mm); 1, deep (≥75mm)

-in the median to anterior portion of the zygomatic arch, when viewed laterally, the dorsoventral depth is shallow(1) or deep(1).

19. Zygomatic arches: depression at the external surface of the anterior part: 0, absent; 1, present

-A concave portion of the anterior most edge of the zygomatic arch is present (0) as compared to the entire anterior portion of the arch structure is convex (1).

20. Zygomatic ach: constriction of the ventral edge anterior to the temporal condyle: 0, present; 1, absent

-The anterior most portion of the zygomatic arch, where it curves medially, constricts on the ventral edge where the edge moves dorsally (0). If no constriction is present (1).

21. Zygomatic arches: process on the posterior end of the dorsal edge: 0, present; 1, absent

-When present (0) this is generally a small cone-shaped protrusion on the posterior most dorsal surface of the zygomatic arch. If not present (1) the dorsal margin of the zygomatic arch maintains a smooth profile. See supplemental figure Character 21.

22. Zygomatic arch: processus postorbitalis = 0, present; 1, absent

-Again, while no included taxa form a post orbital bar, the post orbital process is the ventral portion, where part of the zygomatic bone extends dorsally. This is most commonly in the form of a small cone shaped structure in the medial most portion of the zygomatic arch (0). If not present (1) the medial portion of the zygomatic arch maintains a smooth dorsal profile. See also supplementary figure Character 23 for an example from Chilotherium licenti.

23. Zygomatic arch: processus postorbitalis = 0, on jugal; 1, on squamosal

-If a post orbital process is present (0 on character 22), it is more anterior and forms on the jugal (zygomatic) bone (0) or is more posterior and forms on the squamosal bone (1). See supplemental figure Character 23.

24. Jugal/squamosal: suture = 0, smooth; 1, rough

-In the portion of the zygomatic arch where the jugal and squamosal bone suture, does the suture form a smooth extended “S” shape (0), or does it have a rougher, more goniatic, suture (1).

25. Skull: dorsal profile = 0, flat; 1, concave; 2, very concave

-If the skull is viewed laterally, the profile from the posterior most portion of the occipital bone to the anterior most portion of the nasal bone forms roughly a straight line (0), is concave with the nasals and occipital slightly more dorsal than the median portion of the skull (1), or the nasals and occipital are so raised compared to the median portion of the profile that the skull is dish shaped (2). See supplemental figure for an example of Character 24 in state 2.

26. Sphenoid: foramen sphenorbitale and f. rotundum = 0, distinct; 1, fused

-When viewed looking at the ventral surface of the skull, the sphenoid bone has 1-2 foramen. If these foramen merge across the median axis on the palate, then the character state is (1), whereas if two distinct foramen persist then (0). As this bone is extremely thin, this feature is not preserved in most specimens to an extent that allows the character to be coded.

27. Squamosal: area between temporal and nuchal crests = 0, flat; 1, depression

-When viewing the skull laterally, the nuchal crest connects to the temporal crest at the posteriodorsal most point. If this area outlines by the afore mentioned features form a depression than (1), whereas if the crest rise above an area that is flat in the central portion and then steeply rises into the crests (0).

28. External auditory pseudo–meatus = 0, open; 1, partially closed; 2, closed

-The external auditory meatus is formed from two bones closing to form a tube shape. In many rhinos this is still two separate bones, with each bone forming a lunate shape when viewed laterally, connected on the dorsal side (0). If the ventral opening, when viewed laterally, is showing contact between the two bones, it is considered partially closed (1). Both sides must be fused forming a tube (2) to be considered closed. See Supplementary figure Character 28 for an example of character state 2 from Chilotherium habereri.

29. Occipital side = 0, inclined forward; 1, vertical; 2, inclined backward

-When viewed laterally, with the molar portion of the tooth row leveled, the posterior most visible portion of the occipital bone is inclined forward (0), vertical (1), or backwards (2). For an example of character state 2 see Chilotherium primigens in the Supplemental Figures Character 29.

*This character was removed for later analyses. This character seems to variable within species, when larger sample sizes are examined (such as Subhyracodon and Teleoceras) and can also be hard to separate from diagenic alteration.

30. Occipital: ventral end of the paraoccipital process relative to the postglenoid process: 0,

under; 1, above; 2, nearly equal

-The paraoccipital process and the post glenoid process together form two finger-like projections ventrally, when viewed laterally. When the skull is leveled relative to the molar portion of the tooth row, the two processes may be level in maximum extent (2), or have the posterior of the two processes, the paraoccipital extend farther ventrally than the post glenoid process (0), or the postglenoid process extend ventrally to the paraoccipital process (1).

31. Occipital: ventral end of the paraoccipital processes: 0, inclined anteriorly; 1, inclined posteriorly; 2, straight

-The paraoccipital process, the posterior of the two ventrally projecting processes, when the skull is leveled relative to the molar portion of the tooth row, projects forward (0), is vertical (1), or projects posteriorly (2).

32. 20 Occipital: nuchal tubercle = 0, little developed; 1, developed; 2, very developed

-A projecting tubercle off of the nuchal crest on the occipital bone when viewed from the posterior. If absent (0), or a slight thickening of the profile of the crest (1), if a pronounced cone-shaped protrusion (2). See Supplemental Figure Character 32 for an example of a state 2 as shown in Chilotherium primigens.

33. Skull: back of teeth row = 0, in the posterior half; 1, restricted to the anterior half

-If the skull, viewed in lateral view, is leveled given the occlusal surface of the molars, the posterior edge of M3 is before the anteroposterior midpoint of the skull (1), or is posterior to the midpoint of the skull (0).

34. Pterygoid: posterior margin = 0 nearly horizontal; 1, nearly vertical

-The pterygoid bone, where it projects posterior to the M3, points out posteriorly when viewed laterally (0), or curves upwards sharply posterior to the M3 (1).

35. Skull = 0, dolichocephalic; 1, brachycephalic

-Brachycephalic, defined as a foreshortened skull compared to the norm, is herein defines as a skull that is broad compared to the overall length, when comparing the maximum width across the posterior edge of the zygomatic arches. Teleoceras fossiger would be an example of a brachycephalic skull, whereas Subhyracodon copei would be an example of dolichocephalic.

36. Skull: narrowing of dorsal surface anterior the orbit: 0, gradual; 1, abrupt

-The skull narrows, angled at roughly around 45 degrees, in toward the median line when viewed from above (1), as compared to the skull continuing posteriorly at roughly the same thickness to a slight narrowing (0). See the two supplemental figures, Character 36A is Chilotherium primigens (state 1) and Character 36B Chilotherium licenti (state 0).

37. Skull: widest part of the dorsal surface: 0, at level of postorbital process area; 1, at level of supraorbital process

-The postorbital process area sits just posterior to the orbit, regardless of is the taxon possesses postorbital processes or not. The supraorbital process sits in the front third of the orbit region. The skull of Chilotherium primigens has red bars drawn on both sites, with the supraorbital process site being the widest (1) (Supplemental Figure Character 37).

38. Nasal bones: rostral end = 0, narrow; 1, broad; 2, very broad

-The rostral, or anterior, end of the nasal bones end in a narrow point (0), is relatively blunt and rounded on the anterior end (1), or is thickened and almost hammer-like (2).

39. Nasal bones = 0, totally separated; 1, anteriorly separated; 2, fused

-At the anterior portion of the nasal bones are the separate (0), touching but with a distinct separation at the anterior tip (1), or fully fused together (2).

40. Nasal bones = 0, long; 1, short; 2, very long

-Long nasals are generally also narrow. Short nasals tend to form more a triangular shape than the long or very long nasals, which poses roughly parallel lateral outlines.

41. Median nasal horn = 0, absent; 1, present

-While the horn is not preserved, the rugose texture of the nasal bone indicates presence of a horn. A median nasal horn span the suture in the nasal bone.

42. Median nasal horn = 0, small; 1, developed

-Developed refers to the diameter of the rugose area relative to the size of the skull.

43. Paired nasal horns = 0, absent; 1, present

-As seen in Menoceras, two distinct areas of rugosity on either side of the suture in the median of the nasal bone.

44. Paired nasal horns = 0, terminal bumps; 1, lateral crests

45. Frontal horn = 0, absent; 1, present

-A more posterior horn, in contact with the frontal bone and not just the nasal bones.

46. Frontal horn = 0, small; 1, huge

47. Orbit: lateral projection = 0, absent; 1, present

-When viewed from dorsally, the orbits project out laterally noticeably away from the skull (1). In taxa lacking this trait, the exact position of the orbits is not visible from a dorsal view. (0)

48. Zygomatic width/frontal width = 0, less than 1.5; 1, more than 1.5

-When measured from a dorsal view, the width across the widest portion of the zygomatic arches is 1.5 times or less the width of the frontal bone at the same position (0). Shown in Supplemental Figure Character 48 on Chilotherium sp. nov. character state 1.

49. Frontal–parietal = 0, sagittal crest; 1, close frontoparietal crests; 2, distant crests

-A sagittal crest (0) in a single structural feature running along the median of the skull. Close frontoparietal crests are nearly fused into one structure, but have a crack or slot between the two parallel ridges (1). Distinct crest have a flattened area between the distinct crests, which may or may not be directly parallel to each other or slightly concave towards the median line (2).

50. Occipital crest: transverse expansion: 0, narrow; 1, wide

-The occipital crest, Or the most central portion of the nuchal crest connecting the sagittal crest may narrowly connect to the posterior most portion of the sagittal crest (0) or have a broad connection (1).

51. Parietal crest: dorsal surface: 0, concave; 1, prominent

-The parietal crest, or posterior portion of the sagittal crest, when viewed in profile is slightly curved downwards (0) or is strongly pronounced and either level or projecting slightly upwards (1). The structure most form a notable crest, and not just be an upturning of the entire posterior of the skull.

52. Occipital crest = 0, concave; 1, straight; 2, forked

-When viewed from the posterior, the occipital crest forms the dorsal most outline of the skull. If this is shallowly concave, with a general U-shaped curve, then (0). If the profile is straight across (1), and if it forms a steeply sided fork ending in a V-shape as the base, then (2).

53. Maxillary: processus zygomaticus maxillari, anterior tip = 0, progressive; 1, brutal

-Where the zygomatic arch connects into the maxillary bone is a small cone-shaped bump. If this process is smooth and angled somewhat anteriorly, it is progressive (0), whereas is its roughened and almost rugose in texture, while projecting primarily laterally, it is brutal (1).

54. Vomer = 0, acute; 1, rounded

-If the vomer projects as a very thin ridge and narrows quickly, it is acute (0), if it tapers more gradually into the palate, than it is rounded (1).

55. Squamosal: articular tubercle = 0, smooth; 1 high

-The articular tubercle, on the posterior ventral most surface of the zygomatic arch, may either be low in profile and smooth (0), or project out noticeably from the rest of the zygomatic (1).

56. Squamosal: transversal profile of articular tubercle = 0, straight; 1, concave

-When viewed from the ventral surface, the articular tubercle is deeply grooved with a concave surface (1), or presents more as a flat shelf, with no internal groove (0).

57. Squamosal: foramen postglenoideum = 0, distant from the processus postglenoidalis; 1, close to it

-When viewing the skull from the ventral surface, the postglenoid foramen is situated posterior to the glenoid fossa. It can either be relatively lateral near the postglenoid process (1), or displaced more medially, away from the postglenoid process (0).

58. Squamosal: processus postglenoidalis = 0, flat; 1, convex; 2, dihedron

-When viewing the anterior and ventral surfaces of the postglenoid process, it can form a small plateau, with a level ventral surface (0), a small hook shape with the hook opening towards the anterior (1), Or have steeply sloping sides with distinct ridges making a dihedron shape when viewed ventrally (2).

59. Basioccipital: foramen nervi hypoglossi = 0, in the middle of the fossa; 1 shift antero-externally

-The hypoglossal canal sits just inside or just externally of the foramen magnum.

60. Basioccipital: sagittal crest on the basilar process = 0, absent; 1, present

-Looking directly at the foramen magnum, the basilar process sits directly ventral to the opening. A sagittal crest is usually a small ridge initiating within a centimeter of the foramen magnum and extending anteriorly along the basilar process when present (1). When absent, the whole basilar process is smooth and convex in profile (0).

61. Squamosal: posterior groove on the processus zygomaticus = 0, absent; 1, present

-The posterior edge of the zygomatic process has a mediolateral groove (1), or presents are a straight vertical surface to a convex surface when viewed laterally (0).

62. Squamosal–occipital: processus posttympanicus and processus paraoccipitalis = 0,

fused; 1, distant

-The post tympanic process is present in basal rhinocerotids, as well as the teleoceracid lineages. It forms a thin wing-like projection when not connected to the paraoccipital process (1).

63. Squamosal: processus posttympanicus = 0, well developed; 1, little developed; 2, huge

-only if present in the last character can this character be well developed or huge.

64. Occipital: processus paraoccipitalis = 0, well developed; 1, little developed

-The process just anterior to the lateral margin of the occipital condyles. Well developed (0) it is very robust, as opposed to the more finger-like nature of a little developed paraoccipital process (1).

65. Nuchal face: outline: 0, bell–shaped; 1, trapezoidal; 2, square

-Viewing the skull from the posterior, the main face of the back of the skull, outlines by the nuchal crests, form a bell shape (0), a trapezoid with the smaller limb across the top (1), or a square (2).

66. Magnum foramen: dorsal incision: 0, absent; 1, present

-The dorsal incision, when present, is a small notch extending dorsally from the otherwise ovate foramen magnum. In some literature, this is referred to as being “onion shaped”.

67. Occipital: foramen magnum = 0, circular; 1, subtriangular

-The foramen magnum can be either circular (0) or somewhat triangular, with rounded edges and the ventral portion being wider that the narrow dorsal portion (1).

68. Basioccipital: median ridge on the condyle = 0, absent; 1, present

-the most median edge of the occipital condyle forms a ridge before opening to the foramen magnum.

69. Basioccipital: medial truncation on the condyle = 0, absent; 1, present

-The condyle truncates abruptly before the opening to the foramen magnum (1), or the surface of the condyle smoothly wraps anteriorly into the foramen magnum (0).

70. Basioccipital: medial truncation on the condyle = 0, present at juvenile stage; 1, still present at adult stage

-If last character was a 1, then character 70 can be coded as a (1) even without juvenile material available. If no juvenile material is available, and last character was a (0), then this character is left (?)

Mandible

71. Symphysis = 0, very upraised; 1, upraised; 2, nearly horizontal

-Very upraised, is when the posterior/dorsal surface of the symphysis is almost facing directly posterior (0), upraised is when the posterior/dorsal surface forms a distinct slope, increasing in height anteriorly (1), and nearly horizontal is when the symphysis projects anteriorly almost as a shelf (2).

72. Symphysis = 0, spindly; 1, massive; 2, very massive

-Spindly is a very narrow anteroposterior connection (0), whereas massive is a much thicker connection, and very massive is a symphysis that extends far beyond the tooth row and is around 50% of tooth row length or greater.

73. Symphysis: ventral surface: 0, flat; 1, concave

74. Symphysis: constriction before the lower cheek teeth row: 0, absent; 1, present

-When viewed from above, the bone of the mandible forms a “chromosome shaped” X, with the limbs of the X being the tooth row and then extending out on the mandibular symphysis to tusks.

75. Symphysis: crest along the diastema: 0, slender; 1, stout

-stout is defined as both vertical and horizontal robustisity.

76. Symphysis: posterior margin = 0, in front of p2; 1, level of p2–4

- When viewed from above, the posterior most edge of the symphysis is either in front of the teeth of behind the teeth.

77. Foramen mentale = 0, in front of p2; 1, level of p2-4

78. Corpus mandibulae: lingual groove = 0, present; 1, absent

79. Corpus mandibulae: lingual groove = 0, still present at adult stage; 1, present at juvenile stage only

80. Corpus mandibulae: base = 0, straight; 1, convex; 2, very convex

-Basically, how strongly curved is the base of the jaw? An example of character state 2 would be Aphelops megalodus

81. Mandible: orientation of row of lower cheek teeth: 0, not parallel to long axis of mandible; 1, parallel to long axis of mandible

-When viewed from dorsally, does the tooth row follow the line of the mandible or not?

82. Ramus = 0, vertical; 1, inclined forward; 2, inclined backward

-Is the anterior most edge of the ascending ramus, when viewed laterally, vertical (0), or inclined in either direction?

83. Ramus: processus coronoideus = 0, well developed; 1, little developed

-When little developed, the dorsal most portion of the coronoid process comes to a sharp tip, rather than a blunt and rounded feature in (0)

84. Foramen mandibulare = 0, below the teeth neck; 1, above the teeth neck

Teeth

85. Compared length of the premolars/molars rows = 0, (100 x LP3–4/LM1–3) > 50; 1, 42 < (100 x LP3–4/LM1–3) < 50; 2, (100 x LP3–4/LM1–3) < 42

86. Cheekteeth: enamel foldings = 0, absent; 1, weak; 2, developed; 3, intense

87. Cheekteeth: cement = 0, absent; 1, present

88. Cheekteeth: cement = 0, weak or variable; 1, abundant

89. Cheekteeth: shape of enamel = 0, wrinkled; 1, wrinkled and corrugated; 2, corrugated and arborescent

-Corrugated is the extention of “wrinkles” most of the crown height of the tooth.

Arborescent is complicated branching patterns in the textured enamel of the crowns. Most apparent on the labial surface typically.

90. Cheekteeth: crown = 0, low; 1, high

91. Cheekteeth: crown = 0, high; 1, partial hypsodonty; 2, subhypsodonty; 3, hypsodonty

92. Cheekteeth: roots = 0, distinct; 1, joined; 2, fused

-Often related to the degree of hypsodonty, more hypsodont teeth form less distinct roots. Roots that are distinct also typically angle out from the enamel dentine juncture to an extent.

93. I1 = 0, present; 1, absent

94. I1: shape of the crown (cross section) = 0, almond; 1, oval; 2, half moon

95. I2 = 0, present; 1, absent

96. I3 = 0, present; 1, absent

97. C1 = 0, present; 1, absent

98. i1 = 0, present; 1, absent

99. i1: crown = 0, developed, with a pronounced neck; 1, reduced

100. i2 = 0, present; 1, absent

-If present, usually the protruding tusk in the lower dentition.

101. i2: shape = 0, incisor–like; 1, tusk–like

-Earlier rhinos retained more incisors, and were more likely to have canines present. In most of the “tusked” rhinocerotids, the tusks are formed by the i2. If the i2 is greatly enlarged AND projects at a different angle than i1, it would be considered tusk-like (1).

102. i2: orientation = 0, parallel; 1, divergent

-If tusks are present, do they project forwards in a continuation of the tooth row angle (0), or do they angle laterally (1).

103. i2: upturning of the internal edge: 0, absent; 1, present

-Forms a flange on the median edge of the tusk (1), or tusk is ovate or conical in cross section (0).

104. i3 = 0, present; 1, absent

105. c1 = 0, present; 1, absent

106. Upper cheek teeth: lingual rim of row of cheek teeth: 0, arched; 1, always straight

107. Upper cheek teeth: branch of the crochet and crista: 0, always absent; 1, occasionally present; 2, always present

108. Upper cheek teeth: protocone constricted: 0, anteroposteriorly; 1, just anteriorly

109. Upper cheek teeth: expansion of the lingual cusps: 0, absent; 1, present

110. Upper cheek teeth: crista: 0, one; 1, always doubled

111. Upper premolars: V-shaped incision on the lingual cingulum around the entrance of the median valley: 0, absent; 1, present

112. Upper premolars: labial cingulum = 0, always present; 1, usually present; 2, usually absent; 3, always absent

113. P2–4: crochet = 0, always absent; 1, usually present; 2, always present

114. P2-4: crochet = 0, always simple; 1, usually simple; 2, usually multiple

115. P2–4: metaloph constriction = 0, absent; 1, present

116. P2–4: lingual cingulum = 0, always present; 1, usually present; 2, usually absent; 3, always absent

117. P2–4: lingual cingulum = 0, continuous; 1, reduced

118. P2-4: postfossette = 0, narrow; 1, wide; 2, posterior wall

119. P2-3: antecrochet = 0, always absent; 1, usually absent; 2, usually present; 3, always present

120. P1 (in adults) = 0, always present; 1, usually present; 2, always absent

121. P1: antero–lingual cingulum = 0, present; 1, absent

122. P2 = 0, present; 1, absent

123. P2: protocone and hypocone = 0, fused; 1, lingual bridge; 2, separated; 3, lingual wall

124. P2: metaloph = 0, hypocone posterior to metacone; 1, transverse; hypocone anterior to metacone

125. P2: lingual groove = 0, present; 1, absent

126. P2: protocone = 0, equal or stronger than the hypocone; 1, less strong than the hypocone

127. P2: protoloph = 0, present; 1, absent

128. P2: protoloph = 0, joined to the ectoloph; 1, interrupted

129. P3–4: medifossette = 0, always absent; 1, usually absent; 2, usually present; 3, always present

130. P3–4: constriction of the protocone = 0, always absent; 1, usually absent; 2, usually present; 3, always present

131. P3–4: protocone and hypocone = 0, fused; 1, lingual bridge; 2, separated; 3, lingual wall

132. P3–4: metaloph = 0, transverse; 1, hypocone posterior to metacone; 2, hypocone anterior to metacone

133. P3: protoloph = 0, joined to the ectoloph; 1, interrupted

134. P3: crista = 0, always absent; 1, usually absent; 2, usually present; 3, always present

135. P3: pseudometaloph = 0, always absent; 1, sometimes present

136. P4: antecrochet = 0, always absent; 1, usually absent; 2, usually present; 3, always present

137. P4: hypocone and metacone = 0, joined; 1, separated

138. Upper molars: labial cingulum = 0, always present; 1, usually present; 2, usually absent; 3, always absent

139. Upper molars: antecrochet = 0, always absent; 1, usually absent; 2, usually present; 3, always present

140. Upper molars: base of the antecrochet spread toward the entrance of the median valley: 0, absent; 1, present

141. Upper molars: crochet = 0, always absent; 1, usually absent; 2, usually present; 3, always present

142. Upper molars: crista = 0, always absent; 1, usually absent; 2, usually present; 3, always present

143. Upper molars: medifossette = 0, always absent; 1, usually absent; 2, usually present

144. Upper molars: lingual cingulum = 0, always present; 1, usually present; 2, usually absent; 3, always absent

145. M1–2: constriction of the protocone = 0, always absent; 1, usually absent; 2, usually present; 3, always present

146. M1–2: constriction of the protocone = 0, weak; 1, strong

147. M1–2: paracone fold = 0, present; 1, absent

148. M1–2: paracone fold = 0, strong; 1, weak

149. M1–2: metacone fold = 0, present; 1, absent

150. M1–2: metastyle = 0, short; 1, long

151. M1–2: metaloph = 0, long; 1, short

152. M1–2: posterior part of the ectoloph = 0, straight; 1, concave

153. M1–2: cristella = 0, always absent; 1, usually present; 2, always present

154. M1–2: posterior cingulum = 0, continuous; 1, low and reduced

155. M1: metaloph = 0, continuous; 1, hypocone isolated

156. M1: antecrochet-hypocone = 0, always separated; 1, sometimes joined; 2, always joined

157. M1: postfossette = 0, present; 1, usually absent

158. M2: protocone, lingual groove = 0, always absent; 1, usually absent; 2, always present

159. M2: metaloph = 0, continuous; 1, hypocone isolated

160. M2: mesostyle = 0, absent; 1, present

161. M2: mesostyle = 0, weak; 2, strong

162. M2: antecrochet and hypocone = 0, separated; 1, joined

163. M3: ectoloph and metaloph = 0, distinct; 1, fused (ectometaloph)

164. M3: shape = 0, quadrangular; 1, triangular

165. M3: constriction of the protocone = 0, always absent; 1, usually absent; 2, always present

166. M3: protocone = 0, trefoil–shape; 1, indented

167. M3: protoloph = 0, transverse; 1, lingually elongated

168. M3: posterior groove on the ectometaloph = 0, present; 1, absent

169. p2-3: vertical external rugosities = 0, absent; 1, present

170. Lower cheekteeth: external groove = 0, developed; 1, smooth, U-shaped; 2, angular, V-shaped

171. Lower cheekteeth: external groove = 0, vanishing before the neck; 1, developed until the neck

172. Lower cheekteeth: paralophid: 0, nearly reach the lingual rim; 1, away from the lingual rim

173. Lower cheekteeth: occlusal outline of the trigonid basin: 0, U-shaped; 1, V-shaped

174. Lower cheekteeth: trigonid = 0, angular; 1, rounded

175. Lower cheekteeth: trigonid = 0, obtuse or right dihedron; 1, acute dihedron

176. Lower cheekteeth: metaconid = 0, joined to the metalophid; 1, constricted

177. Lower cheekteeth: entoconid = 0, joined to the hypolophid; 1, constricted

178. Lower premolars: lingual opening of the posterior valley = 0, U-shape; 1, narrow, V-shape

179. Lower premolars: lingual cingulum = 0, always present; 1, usually present; 2, usually absent; 3, always absent

180. Lower premolars: lingual cingulum = 0, reduced; 1, continuous

181. Lower premolars: labial cingulum = 0, present; 1, absent

182. Lower premolars: labial cingulum = 0, continuous; 1, reduced

183. d1/p1 (in adults) = 0, always present; 1, usually present; 2, usually absent; 3, always absent

184. d1: 0, always two-rooted; 1, usually two-rooted; 2, always one-rooted

185. p2 = 0, always present; 1, usually present; 2, always absent

186. p2: paralophid = 0, isolated, spur-like; 1, curved, without constriction

187. p2: paraconid = 0, developed; 1, reduced

188. p2: posterior valley = 0, lingually open; 1, usually closed; 2, always closed

189. Lower molars: lingual cingulum = 0, always present; 1, usually present; 2, usually absent; 3, always absent

190. Lower molars: lingual cingulum = 0, reduced; 1, continuous

191. Lower molars: labial cingulum = 0, always present; 1, usually present; 2, usually absent; 3, always absent

192. Lower molars: labial cingulum = 0, continuous; 1, reduced

193. Lower molars: hypolophid = 0, transverse; 1, oblique; 2, almost sagittal

194. m2-3: lingual groove of the entoconid = 0, absent; 1, present

195. dI1 = 0, present; 1, absent

196. dI2 = 0, present; 1, absent

197. D2: mesostyle = 0, present; 1, absent

198. D3-4: mesostyle = 0, absent; 1, present

199. D2: lingual wall = 0, absent; 1, present

200. D2: secondary folds = 0, absent; 1, present

201. D2: mesoloph = 0, absent; 1, present

202. di1 = 0, present; 1, absent

203. di2 = 0, present; 1, absent

204. Lower milk teeth: constriction of the metaconid = 0, present; 1, absent

205. Lower milk teeth: constriction of the entoconid = 0, absent; 1, present

206. Lower milk teeth: protoconid fold = 0, present; 1, absent

207. d1 (in juveniles) = 0, present; 1, absent

208. d2-3: vertical external roughnesses = 0, absent; 1, present

209. d2-3: ectolophid fold = 0, present; 1, absent

210. d2: anterior groove on the ectolophid = 0, absent; 1, present

211. d2: paralophid = 0, simple; 1, double

212. d2: posterior valley = 0, always open; 1, usually open; 2, usually closed; 3, always closed

213. d3: paralophid = 0, double; 1, simple

214. d3: lingual groove on the entoconid = 0, always absent; 1, usually absent; 2, always present

REFERENCES CITED

Abdrakhmatov, K., H.B. Havenith, D. Delvaux, D. Jongmans, & P. Trefois. 2003. Probabilistic PGA and arias intensity maps of Kyrgyzstan (Central Asia). Journal of Seismology, 7(2): 203-220.

Abdrakhmatov, K., R. Weldon, S. Thompson, D. Burbank, C. Rubin, M. Miller, and P. Molnar. 2001. Onset, style and current rate of shortening in the central Tien Shan, Kyrgyz Republic. Russian Geology and Geophysics, 42(10); 1585-1609.

Abdrakhmatov, K., S.A. Aldazhanov, B.H. Hager, M.W. Hamburger, T.A. Herring, K.B. Kalabaev, V.I. Makarov, P. Molnar,S.V. Panasyuk, M.T. Prilepin, R.E. Reilinger, I.S. Sadybakasov, B.J. Souter, Y.A. Trapeznikov, V.Y. Tsurkov, and A.V. Zubovich. 1996. Relatively recent construction of the Tien Shan inferred from GPS measurements of present-day crustal deformation rates. Nature, 384; 450–453.

Abdrakhmatov, K.Ye. 1988. Quaternary tectonics of the Chu Basin. Ilim, Frunze (Bishkek), p. 1-118. (in Russian)

Abrajevitch, A. 2008. Magnetic memory of rocks: the Kazakhstan orocline and climatic record of the Indian monsoon. Doctoral dissertation, The University of Michigan.

Andersson, K., and L. Werdelin. 2005. Carnivora from the Late Miocene of Lantian, China. Vertebrata Pal Asiatica 43(4); 256-271.

Antoine, P.O. 2002. Phylogénie et evolution des Elasmotheriina (Mammalia, Rhinocerotidae). Mémoires du Muséum National d'Histore Naturelle 188, 1-359.

Antoine, P.O., Downing, K.F., Crochet, J.Y., Duranthon, F, Flynn, L.J., Marivaux, L., Métais, G., Rajpar, A.R., and Roohi, G. 2010. A revision of Aceratherium blanfordi Lydekker, 1884 (Mammalia, Rhinocerotidae) from the Early Miocene of Pakistan: Postcranials as a key. Zoological Journal of the Linnean Society 160; 130-194.

Antoine, P.O., Duranthon, K.F., and Welcomme, J.L. 2003. Alicornops (Mammalia, Rhinocerotidae) dans le Miocène supérieur des collines Bugti (Balouchistan, Pakistan): implications phylogénétiques. Geodiversitas 25; 575-603.

Aslan, A., and A.K. Behrensmeyer. 1996. Taphonomy and time resolution of bone assemblages in a contemporary fluvial system: the East Fork river, Wyoming. PALAIOS 11; 411-421.

Averianov, A.O., A.A. Bakirov, T. Martin. 2007. First definitive stegosaur from the Middle Jurassic of Kyrgyzstan. Paläontologische Zeitschrift, 81(4): 440-446.

Averianov, A.O. and M. Godinot. 2005. Ceratomorphs (Mammalia, Perissodactyla) from the early Eocene Andarak 2 locality in Kyrgyzstan. Geodiversitas, 27(2); 221-237.

Averianov, A. and M. Godinot. 1998. A report on the Eocene Andarak mammal fauna of Kyrgyzstan. In Dawn of the Age of Mammals, Beard and Dawson, eds. Bulletin of Carnegie Museum of Natural History 34; 210-219.

Averianov, A. and I. Danilov. 1996. Agamid lizards (Reptilia, Sauria, Agamidae) from the Early Eocene of Kyrgyzstan.

Azanza, B., G.E. Rössner, E. Ortiz-Jaureguizar. 2013. The early Turolian (late Miocene) Cervidae (Artiodactyla, Mammalia) from the fossil site of Dorn-Dürkheim 1 (Germany) and implications on the origin of crown cervids. Palaeobiodiversity and Palaeoenvironments 93(2); 217-258.

Badgley, C. 1986. Taphonomy of mammalian fossil remains from Siwalik rocks of Pakistan. Paleobiology 12(2); 119-142.

Barry, J.C., M.E. Morgan, L.J. Flynn, D. Pilbeam, A.K. Behrensmeyer, S.M. Raza, I.A. Khan, C. Badgley, J. Hicks, and J. Kelley. 2002. Faunal and environmental change in the late Miocene Siwaliks of northern Pakistan. Paleobiology 28(sp3); 1-71.

Batsch, A.J.G.K. 1788. Versuch einer Anleitung zur Kenntniß und Geschichte der Thiere und Mineralien: Allgemeine Geschichte der Natur, besondre der Säugthiere, Vögel, Amphibien und Fische, Volume 1. Akademische Buchhandlung, pp. 528.

Bayshashov, B.U. 1982. A new rhinoceros species of the genus Chilotherium from Pavlodar. In Mezozoic and Cenozoic Vertebrate Fauna and Flora of North-Eastern and Southern Kazakhstan. Academy Natural Kazakhstan, Alma-Ata (Almaty); 8; 72-83, 1Pl.

Behrensmeyer, A.K., S.M. Kidwell, and R.A. Gastaldo. 2000. Taphonomy and Paleobiology. Paleobiology, 26(4); 103-147.

Behrensmeyer, A.K. 1991. Terrestrial vertebrate accumulations. Taphonomy: releasing the data locked in the fossil record, in P.A. Allison and D.E.G. Briggs (eds.), Topics in Geobiology, v.9, Plenum Press, New York, p. 291-335.

Behrensmeyer, A.K., and A.P. Hill. 1980. Fossils in the making; Vertebrate taphonomy and paleoecology. The University of Chicago Press, Chicago IL.

Behrensmeyer, A.K. 1978. Taphonomic and ecological information from bone weathering. Paleobiology 4(2); 150-162.

Belyaeva, E.I. 1962. First record of a tapiromorph in the Eocene of Middle Asia. Byuleten' Moskovskogo Obschestva Ispytatelei Prirody, Otdel Geologicheskii 37(5); 142-145 (in Russian).

Belyaeva, E.I. 1948. Katalog Mestonakhozhdenii Tretichnykh Nazemnykh Mlekopitayushchikh na Territorii SSSR [Catalogue of the Localities of Finds of Tertiary Terrestrial Mammals on USSR Territory] (in Russian). Trudy Paleontologicheskogo Instituta AN SSSR. 1948; 36-114.

Berger, J., S. Dulamtseren, S. Cain, D. Enkkhbileg, P. Lichtman, Z. Namshir, G. Wingard, and R. Reading. 2001. Back-casting sociality in extinct species: new perspectives using mass death assemblages and sex ratios. Proceedings of the Royal Society of London 268; 131-139.

Bernor, R.L., Z. Qiu, and L.C. Hayek. 1990. Systematic revision of Chinese *Hipparion* species described by Sefve, 1927. American Museum Novitates 2984; 60 pp.

Beziehung auf die Gattung Castor. Mémoires de l'Academie impériale des sciences de Saint-Pétersbourg, sixième série Sciences Mathematiques, Physiques et Naturelles, seconde partie, Sciences Naturelles 7; 127-365.

Blob, R.W. and A.R. Fiorillo. 1996. The significance of vertebrate microfossil size and shape distributions for faunal abundance reconstructions: a Late Cretaceous example. Paleobiology 22; 422-435.

Boaz, N.T. and A.K. Behrensmeyer. 1976. Hominid taphonomy: transport of human skeletal parts in an artificial fluviatile environment. American Journal of Physical Anthropology 45; 53-60.

Böhme, W. 2003. Checklist of the living monitor lizards of the world (family Varanidae). Zoologische verhandelingen / uitgegeven door het Rijksmuseum van Natuurlijke Historie te Leiden (Ministerie van Cultuur, Recreatie en Maatschappelijk Werk) 341; 1-43.

Bowditch, T.E. 1821. An analysis of the natural classification of Mammalia for the use of students and travelers. John Smith, Paris, France, 115 pp.

Brandt, J.F. 1855. Untersuchungen über die Craniologischen Entwickelungsstufen ung die davon herzuleitenden Verwandtschaften und Classification der Nager der Jetztwelt mit besonderer Beziehung auf die Gattung Castor. Mémoires de l'Academie impériale des sciences de Saint-Pétersbourg, sixieme série Sciences Mathmatiques, Physiques et Naturelles, seconde partie, Sciences Naturelles 7; 127-365.

Breda, M. 2001. The holotype of Cervalces gallicus (Azzaroli, 1952) from Sénèze (Haute-Loire, France) with nomenclature implications and taxonomical-phylogenetic accounts. Rivista Italiana di Paleontologia e Stratigrafia 107(3); 439-449.

Burbank, D.W., J.K. McLean, M. Bullen, K.Y. Abdrakhmatov, and M.M. Miller. 1999. Partitioning of intermontane basins by thrust-related folding, Tien Shan, Kyrgyzstan. Basin Research 11; 75-92.

Burgette, R.J., R.J. Weldon, K.Ye. Abdrakhmatov, C. Ormukov, L.A. Owen, and S.C. Thompson. 2017. Timing and process of river and lake terrace formation in the Kyrgyz Tien Shan. Quaternary Science Reviews 159; 15-34.

Calede, J.J. 2016. Comparative taphonomy of the mammalian remains from the Cabbage Patch beds of western Montana (Renova Formation, Arikareean): contrasting depositional environments and specimen preservation. PALAIOS 31;497-515.

Cande, S.C. and D.V. Kent. 1995. Revised calibration of the geomagnetic polarity timescale for the Late Cretaceous and Cenozoic. Journal of Geophysical Research, Solid Earth 100(B4); 6093-6095.

Cardoso, H.F.V., A. Santos, R. Dias, C. Garcia, M. Pinto, C. Sérgio, and T. Magalhães. 2010. Establishing a minimum postmortem interval of human remains in an advanced state of skeletonization using the growth rate of bryophytes and plant roots. International Journal of Legal Medicine 124(5); 451-456.

Chainey, A., W.F.F. McLaughlin, E.B. Davis, S.S.B. Hopkins. (in prep) New methods for geometric and statistical differentiation of *Gazella* horn cores, with comments on new material from Kyrgyzstan.

Chediya, O.K. 1986. Morphology and neotectonics of the Tien Shan. Ilim, Frunze (Bishkek), p. 313. (in Russian)

Chen, S., T. Deng, S. Hou, Q. Shi, and L. Pang. 2010. Sexual dimorphism in perissodactyl rhinocerotid Chilotherium wimani from the late Miocene of the Linxia Basin (Gansu, China). Acta Palaeontologica Polonica 55(4); 587-597.

Chinsamy, A. 1997. Assessing the biology of fossil vertebrate through bone histology. Palaeontologis Africana 33; 25-39.

Christol, J. de. 1832. Description of *Hipparion*. Annales Science I'Industrie du midi de la France; 180-181.

CIA World Fact Book: Kyrgyzstan (https://www.cia.gov/library/publications/the-world-factbook/geos/kg.html) Accessed, November 17, 2017.

Coombs, M.C. and W.P. Coombs. 1997. Analysis of the geology, fauna, and taphonomy of Morava Ranch Quarry, early Miocene of northwest Nebraska. PALAIOS 12;165-187.

Danilov, I.G., A.O. Averianov, P.P. Skutchas, and A.S. Rezvyi. 2006. “Kirgizemys (Testudines, ‘Macrobaenidae’): new material from the lower Cretaceous of Buryatia (Russia) and taxonomic revision” in: Danilov I.G. and Parham J.F. (eds.), Fossil Turtle Research, Vol. 1, Russian Journal of Herpetology, 13(Supplimental), pp. 46-62.

Deng, T., X. Wang, M. Fortelius, Q. Li, Y. Wang, Z.J. Tseng, G.T. Takeuchi, J.E. Saylor, L.K. Säilä, G. Xie. 2011. Out of Tibet: Pliocene woolly rhino suggests high-plateau origin of ice age megaherbivores. Science, 333:1285-1288.

Deng, T. 2006. Neogene rhinoceroses of the Linxia Basin (Gansu, China). CFS Courier Forschungsinstitut Senckenberg 256; 43-56.

Deng T. 2006. Paleoecological comparison between late Miocene localities of China and Greece based on *Hipparion* faunas. Geodiversitas 28(3); 499-516.

Deng, T. 2005. New discovery of Iranotherium morgani (Perissodactyla, Rhinocerotidae) from the Late Miocene of the Linxia Basin in Gansu, China, and its sexual dimorphism. Journal of Vertebrate Paleontology 25; 442-450.

Deng, T. 2002. Limb bones of Chilotherium wimani (Perissodactyla, Rhinocerotidae) from the Late Miocene of the Linxia Basin in Gansu, China. Vertebrata PalAsiatica 40(4); 305-316.

Deng, T. 2001. New material of Chilotherium wimani (Perissodactyla, Rhinocerotidae) from the Late Miocene of Fugu, Shaanxi. Vertebrata Palasiatica 39; 129-138.

Deng, T., X. Wang, M. Fortelius, Q. Li, Y. Wang, Z.J. Tseng, G.T. Takeuchi, J.E. Saylor, L.K. Säilä, G. Xie. 2011. Out of Tibet: Pliocene woolly rhino suggests high-plateau origin of ice age megaherbivores. Science, 333:1285-1288.

Ding, Z.L., S.F. Xiong, J.M. Sun, S.L. Yang, Z.Y. Gu, and T.S. Liu. 1999. Pedostratigraphy and paleomagnetism of a ~7.0 Ma eolian loess-red clay sequence at Lingtai, Loess Plateau, north-central China and the implications for paleomonsoon evolution. Palaeogeography, Palaeoclimatology, Palaeoecology 152(1-2); 49-66.

Dollo, L. 1885. Rhinocéros vivants et fossils. Revue des Questions Scientifiques 17:293-299.

Dong, W. 1993. “The fossil records of deer in China” in Deer of China. N. Ohtaishi and H.-I. Sheng, editors. Elsevier Science Publishers B. V. pg. 95-102.

Dudley, J.P., G.C. Craig, D.ST.C. Gibson, G. Haynes, and J. Klimowicz. 2001. Drought mortality of bush elephants in Hwange National Park, Zimbabwe. African Journal of Ecology 39(2); 187-194.

Erfurt, J., A.O. Averianov, J. Buchantschenko, A.B. Fortuna. 1999. Rediscovery of the Eocene mammal site Toru Ajgyr (Kyrgyzstan). Hallesches Jahrbuch Geowissenschaften 21; 107-127.

Faith, J.T., and A.K. Behrensmeyer. 2006. Changing patterns of carnivore modification in a landscape bone assemblage, Amboseli Park, Kenya. Journal of Archaeological Sciences 33; 1718-1733.

Famoso, N.A., and D. Pagnac. 2011. A comparison of the Clarendonian equid assemblages from the Mission Pit, South Dakota and Ashfall Fossil Beds, Nebraska. Transactions of the Nebraska Academy of Sciences 32; 98-107.

Fischer von Waldheim, G. 1817. Adversaria zoological. Mémories de la Société Impériale des Naturalistes de l'Université Impériale de Moscou 5; 368-428.

Flora, H., W.N.F. McLaughlin, S.S.B. Hopkins, E.B. Davis. (in prep for Journal of Vertebrate Paleontology). A description of lagomorph material from Kyrgyzstan, with the first occurrence of leporids.

Flynn, L.J., A.J. Winkler, M. Erbaeva, N. Alexeeva, U. Anders, C. Angelone, S. Čermák, F.A. Fladerer, B. Kraatz, L.A. Ruedas, I. Ruf, Y. Tomida, K. Veitschegger, and Z. Zhang. 2013. The Leporid Datum: a late Miocene biotic marker. Mammal Review 44(3-4); 164-176.

Fortelius, M., K. Hessig, G. Sarac, and S. Sen. 2003. Rhinocerotidae (Perissodactyla). In M. Fortelius, J.W. Kappelman, S. Sen, and R.L. Bernor (eds). Geology and paleontology of the Miocene Sinap Formation, Turkey. Columbia University Press. pp.282-307.

Geyer, G., J.S. Peel, M. Streng, and S. Voigt. 2014. A remarkable Amgan (Middle Cambrian, Stage 5) fauna from the Sauk Tanga, Madygen region, Kyrgyzstan. Bulletin of Geosciences, 89(2): 375-400.

Global Seismic Hazard Assessment Program. 1999. GSHAP Region 8, Eastern Asia. (http://static.seismo.ethz.ch/GSHAP/eastasia/) Accessed January 2018.

Goloboff, P.A., and S.A. Catalano. 2016. TNT version 1.5, including a full implementation of phylogenetic morphometrics. Cladistics 32(3); 221-238.

Gray, J.E. 1821. On the natural arrangement of vertebrose animals. London Medical Repository 15:296-310.

Gubanov, A.P., R.B. Blodgett, V.N. Lytochkin. Early Devonian (Pragian) gastropods from Kyrgyzstan (Central Asia). Journal of Paleontology 69(3); 431-440.

Guérin, C. 1980. Les rhinoceros (Mammalia, Perissodactyla) du Miocène terminal au Pleistocène supérieur en Europe occidentale: comparaison avec les espèces actuelles. Documents du Laboratoire de Géologie de la Faculté des Sciences de Lyon 79; 1-1182.

Güleç, E.S., A. Sevim, C. Pehlevan, F. Kaya. 2007. A new great ape from the late Miocene of Turkey. Anthropological Science 115(2); 153-158.

Halvorson, S.J. & J.P. Hamilton. 2007. Vulnerability and the erosion of seismic culture in mountainous Central Asia. Mountain Research and Development, 27(4); 322-330.

Hanson, C.B. 1980. Fluvial taphonomic processes: models and experiments. In Fossils in the Making, A.K. Behrensmeyer and A.P. Hill eds. University of Chicago Press, Chicago IL, 156-181.

Haynes, G. 1988. Mass deaths and serial predation: Comparative taphonomic studies of modern large mammal death sites. Journal of Archaeological Science 15(3); 219-235.

Hessig, K. 1999. Family Rhinocerotidae; pp. 175-188 in G.E. Rössner and K. Heissig (eds.), The Miocene Land Mammals of Europe. Pfeil, Munich.

Heissig, K. 1996. The stratigraphic range of fossil rhinoceroses in the late Neogene of Europe and the eastern Mediterranean. In: Bernor, Fahlbusch, & Mittman (eds) The Evolution of Western Eurasian Neogene Mammal Faunas. Columbia University Press, New York. 339-347 pp.

Hunt Jr., R.M. 1990. Taphonomy and sedimentology of Arikaree (Lower Miocene) fluvial, eolian, and lacustrine paleoenvironments, Nebraska and Wyoming: A paleobiota entombed in fine-grained volcaniclastic rocks. Special Paper of the Geological Society of America 244; 69-111.

Hutchins, M. and M.D. Kreger. 2006. Rhinoceros behavior: implications for captive management and conservation. International Zoo Yearbook, 40(1); 150-173.

Kaiser, T.M., D.W.H. Müller, M. Fortelius, E. Schulz, D. Codron, M. Clauss. 2013. Hypsodonty and tooth facet development in relation to diet and habitat in herbivorous ungulates: implications for understanding tooth wear. Mammal Review 43(1); 34-46.

Kirschbaum, D.B., R. Adler, Y. Hong, S. Hill, A. Lerner-Lam. 2010. A global landslide catalog for hazard applications: method, result, and limitations. Natural Hazards, 52(3); 561-575.

Kirschvink, J.L. 1980. The least-squares line and plane and the analysis of the paleomagnetic data: examples from Siberia and Morocco. Geophysical Journal of the Royal Astronomical Society 62; 699-718.

Kostopoulos, D.S. 2009. The late Miocene mammal faunas of the Mytilinii basin, Samos Island, Greece: new collection. 2. Giraffidae. Beiträge zur Paläontologie 31; 345-389.

Koufos, G.D. 2003. Late Miocene mammal events and biostratigraphy in the Eastern Mediterranean. Natuurhistorisch Museum Rotterdam 10(1); 343-372.

Kuznetsov, V.D., K.K. Karabalaev, and I.M. Ibragimov. 1964. The fossil land tortoise from Kyrgyzstan. Materials on the geology of the Tien Shan. Ilim Publishing house, Frunze, pp. 135-146 (in Russian).

Kyrgyz National Census "Национальный состав населения (оценка на начало года, человек)". stat.kg. (http://www.stat.kg/ru/opendata/category/312/) Accessed, November 17, 2017.

Laurenti, J.N. 1768. Specimen medicum, exhibens synopsin Reptilium emendatam cum experimentis circa venena et antidota Reptilium Austriacorum. 214 pp. J.T. de Trattern, Wien.

Laurie, A. 1982. Behavioral ecology of the Greater one-horned rhinoceros (Rhinoceros unicornis). Journal of Zoology (196)3; 307-341.

Levy, D., R. Giustetto, and A. Hoser. 2012. Structure of magnetite (Fe_3O_4) above the Curie temperature: a cation ordering study. Physics and Chemistry of Minerals 39(2); 169-176.

Linnaeus, C. 1758. Systema naturae per regna tria naturae, secundum classis, ordines, genera, species cum characteribus, differentiis, sunonyms locis, 10th revides edition, Volume 1. Laurentii Salvii, Stockholm, 824 pp.

Lloveras, L., M. Moreno-García, and J. Nadal. 2012. Accessing the variability in taphonomic studies of modern leporid remains from Eagle Owl (*Bubo bubo*) nest assemblages: the importance of age of prey. Journal of Archaeological Science 39; 3754-3764.

Lu, X. 2013. A juvenile skull of Acerorhinus yuanmouensis (Mammalia: Rhinocerotidae) from the Late Miocene hominid fauna of the Yuanmou Basin (Yuannan, China). Geobios 46; 539-548.

Macaulay, E.A., E.R. Sobel, A. Mikolaichuk, M. Wack, S.A. Gilder, A. Mulch, A.B. Fortuna, S. Hynek, and F. Apayarov. 2016. The sedimentary record of the Issyk Kul basin, Kyrgyzstan: climatic and tectonic inferences. Basin Research 28; 57-80.

Maldonado, V., L.G.M. Monteiro, A. Rotti, C. Pereira, H.I. de Araújo-Júnior, and L. dos Santos Avilla. 2016. Taphonomic aspects of deer (Mammalia, Cetartiodactyla, Cervidae) remains from a Quaternary cave deposit in Northern Brazil. Journal of Sedimentary Environments 1(2); 234-248.

Makarov, V.I. 1990. Late Cenozoic orogens, their structure and geodynamics. Scientific report for Doctor of Geological and Minerological Sciences, Geological Institute Russian Academy of Science, p.1-57. (in Russian)

Makorov, V.I. 1977. Neotectonic structures of the central Tien Shan. Order of the Red Banner Geology Institute, Akad. Sci., Moscow, Vol. 307, p. 1-171. (in Russian)

Martin, T., and A.O. Averianov. 2004. A new docodont (Mammalia) from the Middle Jurassic of Kyrgyzstan, Central Asia. Journal of Vertebrate Paleontology 24(1): 195-201.

Merrem, B. 1820. Versuch eines systems der Amphibien, Vol. 8. J.C. Krieger, Marburg, xv + 191 pp.

Miao, Y., M. Herrmann, F. Wu, X. Yan, and S. Yang. 2012. What controlled Mid-Late Miocene long-term aridification of Central Asia?-Global cooling or Tibetan Plateau uplift: a review. Earth Science Review 112; 155-172.

Mihlbachler, M.C. 2005. Linking sexual dimorphism and sociality in rhinoceroses: insights from Teleoceras proterum and Aphelops malacorhinus from the Late Miocene of Florida. Bulletin of the Florida Museum of Natural History 45(4); 495-520.

Mikolaichuk, A.V., F.Kh. Apayarov, M.F. Buchroithner, Z.I. Chernavskaja, L.I. Skrinnik, M.D. Ghes, A.V. Neyevin, and T.A. Charimov. 2008. Geological Map of Khan Tengri Massif, Explanatory Note. ISTC Project No. #KR-920, Bishkek, Kyrgyzstan.

Molnar, P. 2005. Mio-pliocene growth of the Tibetan plateau and evolution of east Asian climate. Palaeontologia Electronica 8(1); 2A:23p.

Moore, J.R. and D.B. Norman. 2009. Quantitatively evaluating the sources of taphonomic biasing of skeletal element abundances in fossil assemblages. PALAIOS 24;591-602.

Nakaya, Hideo. 1994. Faunal change of Late Miocene Africa and Eurasia: Mammalian fauna from the Namurungule Formation, Samburu Hills, Northern Kenya. African Study Monographs, Suppl. 20;1-112.

Nikonorov, V.V., J.V. Karaev, F.I. Borisov, T.S. Zamaletdinov, T.V. Larina, V.I. Tolsky. 2017 Mineral resources map of Kyrgyz Republic. Computer version compiled by T.E. Nogaev, N.A. Polovinskaja.

The NOW Community [2017]. New and Old Worlds Database of Fossil Mammals (NOW). Licensed under CC BY 4.0. Release [4.0], retrieved [September-December 2017] from http://www.helsinki.fi/science/now/.

Oppel, M. 1811. Die Ordnungen, Familien und Gattungen der Reptilien als Prodrom einer Naturgeschichte derselben. Joseph Lindauer, Munich, 87 pp.

Owen, R. 1845. Odontography or a treatise on the comparative anatomy of the teeth, their physiological relations, mode of development, and microscopic structure, in the vertebrate animals: 665 S.; London (Ballièete).

Owen, R. M. 1848. Description of teeth and proportion of jaws of two extinct Anthracotherioid quadrupeds (Hyopotamus vectianus and Hyopotamus bovinus) discovered by the Marchioness of Hastings in the Eocene deposits on the N.W. coast of the Isle of Wight: with an attempt to develop Cuvier's idea of the classification of pachyderms by the number of their toes. Quarterly Journal of the Geological Society of London 4; 103-141.

Paleobiology Database, data downloaded in December, 2017, using the following parameters: time interval = Neogene, region = Central Asia, Kyrgyzstan.

Palmqvist P., B. Martinez-Navarro, and A. Arribas. 1996. Prey selection by terrestrial carnivores in a lower Pleistocene paleocommunity. Paleobiology 22; 514-534.

Pandolfi, L. 2015. Persiatherium rodleri, gen. et. sp. nov. (Mammalia, Rhinocerotidae) from the Upper Miocene of Maragheh (Northwestern Iran). Journal of Vertebrate Paleontology 36(1); e1040118.

Parker, T.J. and W.A. Haswell. 1910. A text-book of zoology: Volume 2. Macmillan and co., limited, London, United Kingdom. 714 pp.

Paulson, K. 2013. Generation of structural relief by fault propagation folding, Tien Shan, Kyrgyzstan. Master's thesis, University of Oregon, Eugene, Oregon.

Petronio, C., T. Krakhmalnaya, L. Bellucci, G. Di Stefana. 2007. Remarks on some Eurasian pliocervines: Characteristics, evolution, and relationships with the tribe Cervini. Geobios 40;113-130.

Pitra, C., J. Fickel, E. Meijaard, and P.C. Groves. 2004. Evolution and phylogeny of old world deer. Molecular Phylogenetics and Evolution 33; 880-895.

Prothero, D.R. 2005. The evolution of North American rhinoceroses. Cambridge University Press, Cambridge, United Kingdom. 218 pp.

Purdue, J.R. 1983. Epiphyseal closure in white-tailed deer. The Journal of Wildlife Management 47(4); 1207-1213.

Qiu, Z., W. Huang, and Z. Guo. 1987. Chinese hipparionines from the Yushe Basin. Palaeontologica Sinica, series C 175(25); 1-250.

Qiu, Z.X., J.Y. Xie, and D.F. Yan. 1987. A new chilothere skull from Hezheng, Gansu, China, with special reference to the Chinese "Diceratherium". Scientia Sinica, Series B 30; 545-552.

Quade, J., T.E. Cerling, and J.R. Bowman. 1989. Development of Asian monsoon revealed by marked ecological shift during the latest Miocene in northern Pakistan. Nature 342; 163-166.

Rage, J-C. and S. Bailon. 2005. Amphibians and squamate reptiles from the late early Miocene (MN 4) of Béon 1 (Montréal-du-Gers, southwestern France). Geodiversitas 27(3); 413-441.

Retallack, G.J. 2008. Soils of the past; An introduction to paleopedology. Wiley. 403 pp.

Ringström, T. 1924. Nashorner der Hipparion-fauna Nord-Chinas. Palaeontologia Sinica C 1(4) (4); 1-159.

Ríos, M., I.M. Sánchez, and Jorge Morales. 2017. A new giraffid (Mammalia, Ruminantia, Pecora) from the late Miocene of Spain, and the evolution of the sivathere-samothere lineage. PLoS ONE 12(11); e0185378.

Ríos, M., M. Danowitz, and N. Solounias. 2016. First comprehensive morphological analysis on the metapodials of Giraffidae. Palaeontologia Electronica 19.3.50A;1-39.

Robson, S., W.N.F. McLaughlin, J. Tseng, S.S.B. Hopkins. (in prep) A new species of hyenid from the Kochkor Basin, Kyrgyzstan.

Rowley, D.B. 1996. Age of initiation of collision between India and Asia: A review of stratigraphic data. Earth and Planetary Science Letters 145(1-4); 1-13.

Sadybakasov, I. 1990. Neotectonics of high Asia. Nauka, Moscow, pp. 1-176. (in Russian)

Sánchez, I.M., J.L. Cantalapiedra, M. Ríos, V. Quiralte. 2015. Systematics and Evolution of the Miocene Three-Horned Palaeomerycid Ruminants (Mammalia, Cetartiodactyla). PLoS ONE 10(12): e0143034.

Schlosser, M. 1903. Die fossilen Säugethiere Chinas nebst einer Odontographie der recenten Antilopen. Abh Bayer Akad Wiss 22;1-221.

Sen S. 1990. Hipparion datum and its chronologic evidence in the Mediterranean area. In: Lindsay E.H., Fahlbusch V., Mein P. (eds) European Neogene Mammal Chronology. NATO ASI Series (Series A: Life Sciences), vol 180. Springer, Boston, MA.

Shannon, L.M., R.H. Boyko, M. Castelhano, E. Corey, J.J. Hayward, C. McLean, M.E. White, M.A. Said, B.A. Anita, N.I. Bondjengo, J. Calero, A. Galov, M. Hedimbi, B. Imam, R. Khalap, D. Lally, A. Masta, K.C. Oliveira, L. Pérez, J. Randall, N.M. Tam, F.J. Trujillo-Cornejo, C. Valeriano, N.B. Sutter, R.J. Todhunter, C.D. Bustamante, & A.R. Boyko. 2015. Genetic structure in village dogs reveals a Central Asian domestication origin. Proceedings of the National Academy of Sciences of the United States of America, 112(44); 13639-13644.

Shipman, P. 1981. Life history of a fossil; An introduction to taphonomy and paleoecology. Harvard University Press, Cambridge, MA.

Shotwell, J.A. 1955. An approach to the paleoecology of mammals. Ecology 36(2);327-337.

Shrader, A.M. and N. Owen-Smith. 2002. The role of companionship in the dispersal of white rhinoceroses (Ceratotherium simum). Behavioral Ecology and Sociobiology 52(3); 255-261.

Silver, I.A. 1963. 26 The aging of domestic animals. Science in Archaeology: a comprehensive survey of progress and research. 250 pp.

Smith, D.R. 1995. Environmental security and shared water resources in Post-Soviet Central Asia. Post-Soviet Geography 36(6); 351-370.

Sobel, E.R., M. Oskin, D. Burbank, and A. Mikolaichuk. 2006. Exhumation of basement-cored uplifts: Example of the Kyrgyz Range quantified with apatite fission track thermochronology. Tectonics 25(2); 1-17.

Sobel, E.R., and T.A. Dumitru. 1997. Thrusting and exhumation around the margins of the western Tarim Basin during the India-Asia collision. Journal of Geophysical Research 102; 5043-5063.

Sotnikova, M.V., A.E. Dodonov, and A.V. Pen'kov. 1997. Upper Cenozoic bio-magnetic stratigraphy of Central Asian mammalian localities. Palaeogeography, Palaeoclimatology, Palaeoecology 133; 243-258.

Southern Asia (Political) map. 2004. Perry-Castañeda Library Map Collection, The University of Texas at Austin, University of Texas Libraries. Accessed September 2014.

Stilson, K.T., S.S.B. Hopkins, and E.B. Davis. 2016. Osteopathology in Rhinocerotidae from 50 million years to the present. PLOS ONE 11(8): e0160793.

Tapio, M., N. Marzanov, M. Ozerov, M. Cinkulov, G. Gonzarenko, T. Kiselyova, M. Murawski, H. Viinalass, J. Kantanen. 2006. Sheep mitochondrial DNA variation in European, Caucasian, and Central Asian areas. Molecular Biology and Evolution, 23(9); 1776-1783.

Tarasov, S.A. 1970. Cenozoic geology and neotectonics of the Tien Shan (in Russian): Frunze (Bishkek), Ilim, 211 p.

Thompson, S.C., R.J. Weldon, C.M. Rubin, K. Abdrakhmatov, P. Molnar, G.W. Berger. 2002. Late Quaternary slip rates across the central Tien Shan, Kyrgyzstan, central Asia. Journal of Geophysical Research 107(B9); 2203.

Turner, A., M. Antón, and L. Werdelin. 2008. Taxonomy and evolutionary patterns in the fossil Hyaenidae of Europe. Geobios 41(5); 677-687.

Valli, A.M.F. 2005. Taphonomy of the late Miocene mammal locality of Akkaşdaği, Turkey. In Sen S. (ed.), Geology, mammals and environments at Akkaşdaği, late Miocene of Central Anatolia. Geodiversitas 27(4); 793-808.

Van Valkenburgh, B. 1988. Trophic diversity in past and present guilds of large predatory mammals. Paleobiology 14(2); 155-173.

Vislobokova, I., M. Sotnikova, and A. Dodonov. 2003. Bio-events and diversity of the Late Miocene-Pliocene mammal faunas of Russia and adjacent areas. In: Distribution and Migration of Tertiary Mammal in Eurasia, DEINSEA 10; 563-574.

Voorhies, M.R. 1969. Taphonomy and population dynamics of an early Pliocene vertebrate fauna, Knox County, Nebraska. Rocky Mountain Geology 8;1-69.

Wack, M.R., S.A. Gilder, E.A. Macaulay, E.R. Sobel, J. Charreau, A. Mikolaichuk. 2014. Cenozoic magnetostratigraphy and magnetic properties of the southern Issyk-Kul basin, Kyrgyzstan. Tectonophysics 629; 14-26.

Wang, Y., T. Deng, and D. Biasatti. 2006. Ancient diets indicate significant uplift of southern Tibet after ca. 7 Ma. Geology 34(6); 309-312.

Weldon, R.J. 1986. The late Cenozoic geology of Cajon Pass: Implications for tectonics and sedimentation along the San Andreas fault, Ph.D. thesis, 400 pp., California Institute of Technology, Pasadena, California.

Zabelina, I.V., I.Y. Koulakov, and M.M. Buslov. 2013. Deep mechanisms in the Kyrgyz Tien Shan orogeny (from results of seismic tomography). Russian Geology and Geophysics, 54(7); 695-706.

Zdansky, O. 1925. Fossil Hirsche Chinas. Palaeontologia Sinica C 2; 1-94.

Zhang, Z-Q. and R. Yang. 2016. Morphology and taxonomy of *Gazella* (Bovidae, Artiodactyla) from the Late Miocene Bahe Formation, Lantian, Shaanxi Province, China. Vertebrata PalAsiatica 54(1);1-20.

Zhu, Y., L. Zhou, D. Mo, A., Kaakinen, Z. Zhang, and M. Fortelius. 2008. A new magnetostratigraphic framework for late Neogene Hipparion Red Clay in the eastern Loess Plateau of China. Palaeogeography, Palaeoclimatology, Palaeoecology 268(1-2); 47-57.